UNIVERSITY OF SOUTHAMPTON

THEORETICAL STUDIES AND STRUCTURAL ANALYSIS OF MODELS OF SURFACE ORGANOMETALLIC CENTRES

A Thesis submitted for the Degree of Doctor of Philosophy

by

Rohana bt Adnan

PhD degree
Dept. of Chemistry
University of Southampton
August 2000

UNIVERSITY OF SOUTHAMPTON

ABSTRACTS

FACULTY OF SCIENCE

CHEMISTRY

Doctor of Philosophy

THEORETICAL STUDIES AND STRUCTURAL ANALYSIS OF MODELS OF SURFACE ORGANOMETALLIC CENTRES

by Rohana binti Adnan

Theoretical calculations utilizing the density functional theory (DFT) method are presented here from the point of view of their applicability in modelling catalytic rhodium gem dicarbonyl, $Rh(CO)_2$, species on silica surfaces. The surface rhodium gem dicarbonyl were modelled by $[Rh(CO)_2(OSiH_3)]$, $[Rh(CO)_2(OHSiH_3)]^+$, $[Rh(CO)_2(ClSiH_3)]^+$, $[Rh(CO)_2(Cl)(OSiH_3)]^-$, $[Rh(CO)_2(Cl)(OHSiH_3)]$, $[Rh(CO)_2(Cl)(ClSiH_3)]$. In all model structures the rhodium atoms are assumed to have the oxidation state of +1.

The geometries were optimized using the hybrid B3LYP exchange-correlational functional and effective core potential basis set of Hay and Wadt, LanL2DZ was used on the Rh atoms while the 6-31G** basis set was applied on the rest of the system. We also presented the DFT-B3LYP predictions of their vibrational frequencies, charge distribution, and HOMO-LUMO energy gaps. The result shows Rh-O distance within the suggested experimental range for both O^{-2} and OH^- ligands. Combination of geometry optimization, frequency calculation and HOMO-LUMO energy gap, shows $[Rh(CO)_2(Cl)(ClSiH_3)]$ to best model the surface $Rh^1(CO)_2$ with $[Rh(CO)_2(Cl)(OHSiH_3)]$ being the other closest possibility.

The flexibility of octasilsesquioxanes, $R'_nR_mSi_8O_{12}$ (m=8-n, n=0,1,2) and their incompletely condensed polyhedral oligosilsesquioxanes, $R_8Si_8O_{12}$ which are of great interest due to their striking structural similarity with silica polymorphs, is analyzed using crystal data extracted from the Cambridge Crystallographic Database (CSD). The results are represented as histograms and scattergrams. Linear correlation between Si..Si nonbonding distances and Si-O-Si bond angle was observed in both systems while no obvious structural difference was detected for different R group in Si_8 cages. In all, the silica cage system shows a remarkable flexibility in adapting large subsituents and behaving very similarly to the SiO_2 framework. No obvious correlation between ^{29}Si NMR chemical shifts and various geometric parameters of this system was found.

Finally, a theoretical study was performed adopting the B3LYP/6-31G** method to analyze the suitability of a hypothetical incompletely condensed polyhedral oligosilsesquioxanes; $H_7Si_8O_9OH$, $H_7Si_7O_9(OH)_2(OCH_3)$ and $H_7Si_7O_9(OH)_3$ to model surface hydroxyl and methoxy groups. The result shows that this hypothetical model is able to differentiate between isolated and hydrogen bonding ν(OH) bands. The hydrogen bonding is confirmed by short O..O distances, XH…H (X=C, O) angles greater than 90°, very intense ν(OH) bands at 3650 cm^{-1} region and shift to higher wavenumber for the $\nu(CH)_3$ band.

To my husband,
To our parents

To my children,

.....And that be dutiful to your parents. If one of them or both of them attain old age in your life, say not to them a word of disrespect, nor shout at them but address them with honor. And lower unto them the wing of submission and humility ... The Qur'an 17:23-24

Contents.

	Abstract	i
	Contents	iv
	Acknowledgements	viii
	Abbreviations	ix

Chapter One : Introduction

1.0	**Introduction**	2
1.1	**Catalyst**	2
1.1.1	Homogeneous catalysis	2
1.1.2	Heterogeneous catalysis	2
1.1.3	Homogeneous vs. Heterogeneous catalysis	3
1.1.4	Hybrid catalysts	3
1.2	**Nature of Oxide Surface**	4
1.2.1	Introduction	4
1.2.2	Silica	4
1.3	**Surface Organometallic Chemistry**	7
1.3.1	Introduction	7
1.3.2	Reactions of Organometallic Complexes with Oxides Surfaces	8
1.3.3	Reactions of Organometallic Complexes with Silica	8
1.4	**Surface Rhodium Carbonyl species**	11
1.4.1	Introduction	11
1.4.2	The rhodium gem dicarbonyl species	12
1.5	**Polyhedral Oligosilsesquioxanes**	13
1.5.1	Models for Silica Surfaces	13
1.5.2	Synthesis and Characterisation Techniques	16
1.5.3	Structure and Bonding	18
1.6	**Theoretical Chemistry**	20
1.6.1	Introduction	20

1.6.2 Molecular Modelling, Computational and Theoretical Chemistry 21
1.7 Crystallographic Structural Databases 22
1.7.1 Introduction 22
1.7.2 Cambridge Structural Database (CSD) 23
1.8 Scope and the aim of the thesis 25
1.9 References 25

Chapter Two : Theory and Method

2.0 Introduction 35
2.1 Molecular Orbital Theory 36
2.2 Molecular Orbital Approach 37
2.2.1 Hartree Fock Approximations 38
2.2.2 Linear Combination of Atomic Orbitals (LCAO) 38
2.2.3 Variational Principle 39
2.2.4 Hartree Fock- Closed Shell system 39
2.2.5 Open Shell system 40
2.2.6 Molecular Orbital Calculation 42
2.3 Basis set 43
2.3.1 Slater and Gaussian basis set 43
2.3.2 Classification of basis set 44
2.3.3 Pseudo potential basis set 45
2.4 Theoretical Method 46
2.4.1 Ab initio 47
2.4.2 Semi empirical 47
2.4.3 Hartree Fock 47
2.4.4 Correlated Method 48
2.4.5 Density Functional Theory 48
2.5 Useful properties calculation 52
2.5.1 Single point calculation 52
2.5.2 Geometry optimization 52

2.5.3 Mulliken population analysis 53
2.5.4 Vibrational frequencies 54
2.5.4.1 Introduction 54
2.5.4.2 The Simple Harmonic Oscillator 58
2.5.4.3 Calculation of Harmonic Vibrational Frequencies 60
2.5.4.4 Harmonic and Anharmonicity 61
2.5.5. Zero point Energy calculation 62
2.6 References 62

Chapter Three : DFT calculation on rhodium *gem* dicarbonyl

3.0 Introduction 67
3.1 Theoretical approach 67
3.2 Model systems 68
3.3 Aim 70
3.4 Computational details 70
3.4.1 Calibration 70
3.4.2 Supported rhodium *gem* dicarbonyl 71
3.5 Results and Discussion 72
3.5.1 Calibration results 72
3.5.2 Models of supported rhodium *gem* dicarbonyl 81
3.5.2.1 Geometrical parameters 81
3.5.2.2 Vibrational frequencies 89
3.5.2.3 Properties of adsorbed CO 91
3.5.2.4 HOMO-LUMO energy analysis 92
3.5.2.5 Reliable Predictions on Limited Model? 94
3.6 Further work 94
3.7 Conclusion 95
3.8 References 95

Chapter Four : Systematic Analysis of Silica cage system

4.0 Introduction 101

4.1 Detail of Analysis 102

4.1.1 Crystals data analysis 102

4.1.2 ^{29}Si NMR Correlation studies 113

4.2 Results and Discussion 117

4.2.1 Si-O bond 117

4.2.2 Bond angle 119

4.2.3 Data set with R factor 0.05 122

4.2.4 Si..Si nonbonding distances 124

4.2.5 Openness of silsesquioxane cages 126

4.2.6 NMR chemical shift/geometric parameter correlations studies 127

4.3 Conclusion 131

4.4 References 131

Chapter Five: POSS as the model for silica surface

5.0 Introduction 138

5.1 Computational Detail 141

5.2 Result and Discussion 143

5.2.1 Calibration result 143

5.2.2 Potential energy surface study 148

5.2.3 Optimized geometric parameters 155

5.2.4 Hydrogen bonded system 156

5.2.5 Charge distribution/transfer 159

5.2.6 Vibrational frequency analysis 160

5.2.6.1 ν(OH) bands 160

5.2.6.2 ν($SiOCH_3$) bands 161

5.2.7 The method 163

5.3 Conclusion 163

5.4 References 164

Acknowledgements

Alhamdulillah, I would like first to thank my best friend and husband, Md. Harashid Haron, firstly for being here not only to support me but also to look after our children when I'm at school and at night when I got to study or sleep. Secondly for the constant encouragement, support, lectures etc. There is actually no word to completely describe how much, Jazakallah khairan katsiraa.

Second, I am very thankful to have two such excellent supervisors, Prof. John Evans and Prof. Mike Hursthouse. To Prof. JE, for his patience in reading this thesis, advice, help and most importantly, kindness. To Prof. MH, for the Dell computer, advice and stimulating discussion.

Then, I would like to thanks all the wonderful computational chemists or should I say the theoretical chemists I got to know during this period of study. First and foremost, I would like to thank Dr. Edmond Lee and Dr. Oliver Wartshaw for teaching me Gaussian and believing in me and supporting me when I'm at my low when I think I can't do it, I'll better pack my things and go home!.. Also to Julie at Kings College for helps with Columbus. Douglas Fox (Director of Gaussian Technical Support) who helped me most with Gaussian problem from the first exercise till the end of this work.

In addition to that I would like to acknowledge the use of Gibbs Power Challenge for Gaussian94 calculations which was made available through Prof. John Dyke.

I also wish to acknowledge the use of the EPSRC's Chemical Database Service at Daresbury. Scholarships from Universiti Sains Malaysia(USM) and support from Prof. Idiris Salleh, Head of Chemistry Dept, USM are also fully acknowledged.

Last but not least, I would like to thanks all the people in the Chemistry department, especially from the John Evans group. Also many thanks to Dr. Tony Genge who usually is the person to ask when things go wrong around here. To Dr. Roslina Sidek, PhD in Electrical Engineering (1999), a mother of two, for inspiration. No one understands it better than a mother!

Abbreviations

DFT	Density Functional Theory
DFT-B3LYP	Becke-three hybrid-Lee-Yang-Parr density functional
DFT-BLYP	Becke-Lee-Yang-Parr density functional
DZ	Double zeta
DZP	Double zeta plus polarization
ECP	Effective core potential
EXAFS	Extended X-rays Absorption Fine Structure
FTIR	Fourier transform infrared spectroscopy
GTO	Gaussian type orbital
HF	Hartree Fock
HOMO	Highest occupied molecular orbital
KS	Kohn-Sham
LCAO	Linear Combination of Atomic Orbitals
LUMO	Lowest unoccupied molecular orbital
MO	Molecular orbital
MP2	Moller-Pleset second order pertubation theory
PES	Potential energy surface
POSS	Polyhedral oligosilsesquioxanes
PM3	Parametrization Model 3 (semiempirical method version 3 of MNDO)
RAIRS	Reflection-Absorption Infrared Spectroscopy
RHF	Restricted Hartree Fock
SCF	Self consistent field
STO	Slater type orbital
SV	Split valence
TM	Transition Metal
TPD	Temperature Programmed Desorption
TZ	Triple zeta
UHF	Unrestricted Hartree Fock
ZPE	Zero point energy

Basis set description

STO-3G	Minimal basis set
3-21G	Gaussian standard split valence
6-31G	Gaussian standard valence double zeta, ζ
6-31G**,6-31G(d,p)	Valence double ζ plus d functions on nonhydrogen atoms and p functions on hydrogen
DZ	Double ζ
DZP	Double ζ plus d functions on non-hydrogen atoms and p functions on hydrogen
DZVP	valence Double ζ plus d and p functions
DZP/TZ(O)	Triple ζ on oxygen and double ζ on the remaining atoms plus d unctions on non-hydrogen atoms plus p functions on hydrogen atoms

Chapter 1

Introduction

Chapter One : Introduction

1.0 Introduction

This thesis describes an investigation into rhodium *gem* dicarbonyl species using theoretical methods and an exploration for a suitable silica surface model based on silsesquioxane system. This chapter will give an introduction to why such systems are considered.

1.1 Catalyst

A catalyst can be defined as a substance which increases the rate at which chemical reaction reaches equilibrium by lowering the activation energy, without itself being consumed in the process. Often a catalyst will selectively or preferentially enhance one reaction pathway at the expense of the others, and hence can be used to control the selectivity of a reaction to a desired product.

1.1.1 Homogeneous catalysis

In a homogeneous catalytic system the catalyst and the reactant are in the same phase, most often in solution. A homogeneous system will normally consist of sequential chemical reactions involving discrete transition metal complexes, derived from a well-defined starting complex, in a closed catalytic cycle. Intermediates may be short lived and exist only in very low concentrations but can be characterised by spectroscopic techniques.

1.1.2 Heterogeneous catalysis

In a heterogeneous catalytic system, the reactants and the catalyst are in different phases, usually involving a solid catalyst and a gaseous reactant. Heterogeneous catalysts play important roles in industry and are used in a range of chemical processes from hydrocarbon reforming and oxidation to olefin polymerisation and metathesis. The importance of heterogeneous silica supported transition metal catalysts has provided impetus for understanding the surface chemistry of this species at a molecular level. Despite recent dramatic improvements

in surface science techniques, detailed mechanistic study of silica supported species as well as other metal oxides, are still not very tangible, resulting in uncertainty in the nature of the active species involved in catalysis.

1.1.3 Homogeneous vs. Heterogeneous catalysis

In general, the advantages of heterogeneous catalysis over homogeneous catalysis are a higher activity, easier product separation and robustness of the catalyst, although catalyst leaching may be a problem. Homogeneous catalysts also offer some advantages, including that they tend to be more uniform, with the potential of easy and controlled modification that may lead to controlled selectivity. In addition to that, homogeneous catalysts are normally well defined molecular structures, so tailor made catalysts are possible, in principle.

The disadvantages of homogeneous catalysts include lack of stability under extreme conditions and difficulty in separation of products from catalysts compared to the heterogeneous catalysts. However, as the homogeneous catalysts are easier to study and to understand, to gain an insight into understanding a heterogeneous catalyst, development of homogeneous catalysts that models the heterogeneous catalyst is advantageous in creating the opportunities to enhance control over selectivity, activity and catalyst lifetime.

1.1.4 Hybrid catalysts

Hybrid catalysts combine the practical benefit of heterogeneous catalysts with the advantages of homogeneous catalysts i.e. selectivity, efficiency, reproducibility and controlled design. These so called hybrid catalysts usually consist of transition metal compounds attached to a solid support, without substantial change in their structure.

1.2 Nature of Oxide Surface

1.2.1 Introduction

An oxide surface is generally thought to consist of Brønsted or Lewis base (O^{2-}), Brønsted acid (^{-}OH) as well as Lewis acid (M^{n+}) sites. The most commonly used oxide surfaces in surface organometallic chemistry are silica, alumina, titania and magnesia.

1.2.2 Silica

Silica powders and gels are widely used in industry as fillers, catalysts, catalyst supports, adsorbents, chromatographic agents and so on. There are two forms of silica: gels and sils, each with a difference in their morphology. Gels are highly porous materials and are less suitable for use in surface organometallic chemistry. There is doubt over the accessibility of large organometallic compounds to pores, in fact size distributions for these supports would have to be known. In addition to that, some metal cations can be present as contaminants from the hydrolysis procedures in their production. Sils are essentially nonporous and derive their high surface area from small particle size (5-40 nm diameter). Generally sils are also higher in purity, with some residual chloride emanating from the $SiCl_4$ precursor, being the most likely contaminant.

Silica is usually prepared either by acid precipitation from metal silicate solutions, especially sodium silicate, or by hydrolysis of silicon compounds, such as silicon tetrachloride, in liquid or vapour phase.[1] The formation of silica by hydrolysis in the liquid phase has been summarised by Carman[2] and Iler[3] in the following reaction scheme.

1st stage;

Hydrolysis to $Si(OH)_4$ → polymerisation → Colloidal particles of SiO_2

2nd stage;

a). Dilute solution → Aggregation → Weak gel or precipitate

b). Concentrated solution → Aggregation → strong, firm gel

Silica surfaces are usually covered with a layer of hydroxyl groups and H_2O which can be largely removed by drying at high temperature. The degree of hydroxylation of the surface of silica has been studied by infra red spectroscopy,[4] and high resolution ^{29}Si NMR which derives surface selectivity by the cross-polarisation of protons to the silicon spins.[5]

Silica surfaces contain a variety of terminal silanol group some of which are isolated single [SiOH] or geminal [$Si(OH)_2$], whereas others are either of the above type involved in hydrogen bonding or are perturbed due to inter particle contact.[6] IR spectroscopy however does not distinguish or discriminate between isolated and geminal species.[7] The isolated SiOH groups are characterised by a sharp band at 3750 cm^{-1}, while the hydrogen bonded SiOH groups are distinguished by a broad band at around 3650 cm^{-1}.

The loss of the physically adsorbed water present under ambient conditions is the predominant dehydration process at temperatures below 150°C, but is incomplete below 300°C. At temperature above 150°C the condensation of surface hydroxyls is the principle route to the elimination of water. At a moderate drying temperature, adsorbed water, silanol groups and siloxane linkages provide possible reactive sites to an organometallic complex. Some hydroxyl content is still evident even after drying at 1100°C, the silanol groups themselves will have different spatial distributions.

X-ray work on silica suggests that the structure most closely resembles that of β-crystobalite. Most prevalent descriptions of the silica surface are thus based upon an assumed similarity to the various crystallographic faces of this form of silica.

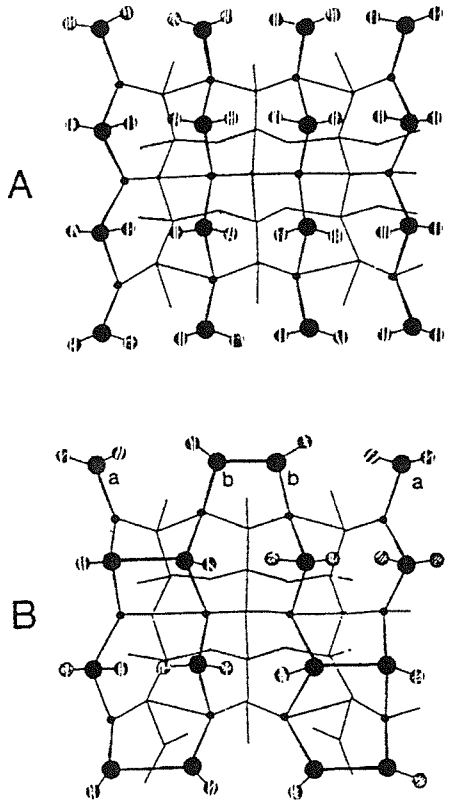

Figure 1.1: Surface geometry β-crystobalite (100) face including the mechanism of dehydration suggested by Peri and Hensley.[8] (A) completely hydrated (B), following partial dehydration. In site B, b sites are "vicinal pair" formed from the condensation of adjacent geminal hydroxyl sites, a. (Shaded circles) Hydroxyls groups; (●) surface silanol silicons; (•) cross polarizable lattice-type silicons.

Considering the silica surface in more detail, on an ideal (111) crystal face of β-crystobalite the silanols are ~ 5Å apart and virtually isolated. Vicinal pairs separated by 3.3 Å occur on the (110) face. There is also evidence of *gem* silanediols which may represent 10-20% of the total silanol population depending upon the pre-treatment used. A surface model that predicts the existence of paired hydroxyl groups at all levels of dehydration was proposed by Peri and Hensley [Figure 1.1].[8] In this work, the surface is assumed to be similar to the (100) face of β-crystobalite.

Each surface silicon is connected to a geminal pair of hydroxyl groups, the paired group are located in rows. This spatial distribution is important for the adsorption sites, for example, water is chemisorbed preferentially on neighbouring silanol pairs whereas amines bind to isolated groups.[4] When the silica is pure these silanol groups act as weak Brønsted[9] acid sites but Lewis acidity is not evident.

1.3 Surface Organometallic Chemistry

1.3.1 Introduction

The reactivity of organometallic compounds supported on the surface of inorganic oxides has been subjected to an increasingly intensive study over the last twenty years.[10] The study of these organometallic compounds supported on inorganic oxides has shown similarity to both homogeneous and heterogeneous catalytic systems. Heterogeneous reactions may involve surface organometallic fragments as the reaction intermediates. It is intended that the study of these well-defined surface organometallic species will lead to a better understanding of the basic steps of heterogeneous catalyst reaction mechanisms and hence the catalytic reactivity.[11]

The advantage of surface supported catalysts over homogeneous systems is that the readily formed unsaturated intermediates are stabilised by the surface which acts as a large, co-ordinating and rigid ligand to trap them.[12] Despite their similarities with heterogeneous systems, the reactivity, the distribution of the support material and the relatively uniform structure of supported organometallic may be considered to make them homogeneous in nature.[13] Studies have shown similarities between the chemistry of surface organometallic complexes and that of homogeneous analogues.[11] For this reason, supported organometallic systems can be considered as hybrid catalysts.

Since isolation of the active sites can help prevent some undesirable side reactions, this will lead to an improved selectivity of this type of catalysts. In addition to that, some supported organometallic complexes have been shown to be highly effective at even low temperature.

Well-defined organometallic surface complexes can undergo reactions with the support in which the support acts as a real ligand. Its effect is to dilute the organometallic species and to reduce their mobility, allowing in some cases the obtention and stabilization of extremely electron deficient metal hydrides.[14] Knowledge of surface structures allows a good understanding of the reactions occurring on the various substrates, so modelling the catalytic cycles, step by step is possible.[14] Furthermore, the knowledge is also important in designing new catalysts.

on the various substrates, so modelling the catalytic cycles, step by step is possible.[14] Furthermore, the knowledge is also important in designing new catalysts.

1.3.2 Reactions of Organometallic Complexes with Oxides Surfaces

The metal-support interaction is a topic of a great importance in the research involving supported transition metal catalysts. The nature of the support has been shown to affect the behaviour of the catalyst. This is illustrated for example by the CO hydrogenation reaction over nickel[15,16] where Ni/TiO_2 catalysts are more active in methanation than Ni/Al_2O_3 or Ni/SiO_2 catalysts. Furthermore, methanation proceeds more rapidly on Ru/SiO_2 than on Ru/Al_2O_3,[17] while the opposite has been reported for the water gas shift reaction for Pt/Al_2O_3 or Pt/SiO_2.[18]

Reactions between an organometallic compound and an oxide surface can generally be defined as examples of well known organometallic reaction mechanisms such as oxidative oxidation, nucleophilic or electrophilic attack at either the ligands or the metal centre, ligand dissociations or associations, electrophilic cleavage of metal-carbon bonds, acid base reactions or redox interactions.[13] The various types of surface functionalities involve hydroxyl groups, protons, and acid base centres.[13]

1.3.3 Reactions of Organometallic Complexes with Silica

Heterogeneous silica supported transition metal compounds play an increasingly important role as catalysts in the petrochemical industry.[19] The potential commercial importance of such catalysts has stimulated an intense interest in the chemical processes which occur on the surface of the catalyst. Although advances in surface characterisation techniques such NMR, IR and EXAFS, have allowed great strides toward understanding the chemical reaction that occur on the surface, detailed mechanistic studies are still inherently difficult due to the very complicated atomic structure on the surface.

The reaction of $Rh(\eta^3\text{-}C_3H_5)_3$ with oxides, especially, silica, alumina, titania, magnesia and zeolites is an example of a well-studied organometallic reaction mechanism. On silica (in toulene solution), this is thought to consist of electrophilic cleavage of a Rh-allyl bond by a silanol group, releasing one equivalent of propene.[20]

$$[Si]\text{-}OH + Rh(\eta^3\text{-}C_3H_5)_3 \rightarrow [Si]\text{-}O\text{-}Rh(\eta^3\text{-}C_3H_5)_2 + C_3H_6$$

The formation of a chemical bond between rhodium and silica via an oxygen, of the grafted species was concluded on the basis of Raman spectroscopy.[20] The spectrum shows bands at 447, 481 and 505 cm^{-1} attributed to the ν(Rh-O) vibrations. Dufour et al.[11] studied the reaction of $Rh(\eta^3\text{-}C_3H_5)_3$ with variously treated silicas and the same stoichiometry of this reaction was observed regardless of the degree of hydroxylation or porosity of the silica sample.

On silica, the formation of a complex with a coordinated hydroxyl group was observed. Dufour and co-workers[21] performed molecular modelling of the surface complex, using bond lengths and bond angles identical to those in the model compound of $[Rh(\mu\text{-}OH)(\eta^3\text{-}C_3H_5)_2]_2$. The silica surface was modelled using the (100) and (111) faces of β-cristobalite. In summary, three microenvironments were proposed for **1** on the silica surface, [Figure 1.2], based on the known structure analogue of $Rh(\eta^3\text{-}C_3H_5)_2$, IR evidence[22] and theoretical calculations.[23]

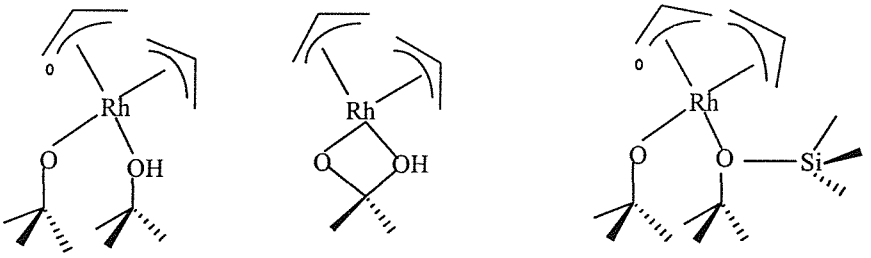

1a **1b** **1c**

Figure 1.2: Three proposed fragments of $Rh(\eta^3\text{-}C_3H_5)_2$ thought to exist on silica.

Disagreements on the stoichiometry of the reaction have shown the need for a variety of techniques to be employed for accurate identification of the surface organometallic species.[24,25]

The reaction of tetraneopentyl zirconium with the hydroxyl groups of silica has also been fully characterised. [26] The spectroscopic data of this system is summarised in Figure 1.3. Molecular modelling studies show that such a structure can be achieved on the silica surface with the oxygen atoms being at a reasonable distance from the zirconium. [27]

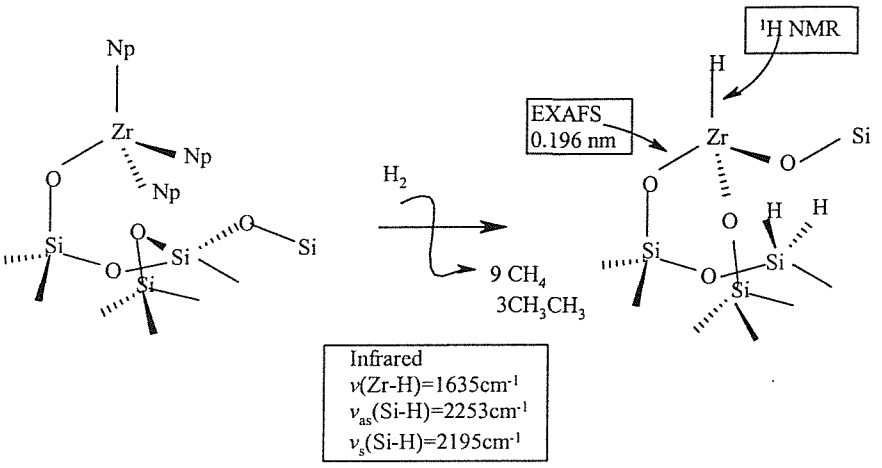

Figure 1.3: Reaction of tetraneopentyl zirconium with hydroxyl groups of silica

A concept which involves the calculation of the number of electrons surrounding the metal in a complex has been very useful. In the cases of $Rh(\eta^3\text{-}C_3H_5)_3$ with silica for example, if the rhodium is co-ordinated by a single bond to the siloxide site, it would have a co-ordination sphere of only 16 electrons. Alternatively, it could react with two oxygen atoms, adopting an 18 electrons configuration on the surface, Figure 1.4.

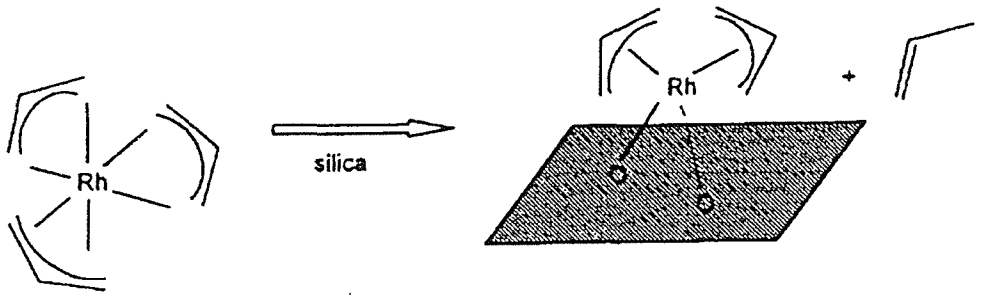

Figure 1.4: Proposed scheme for the reaction of $Rh(\eta^3\text{-}C_3H_5)_3$ with silica.

The determination of the structure of a grafted organometallic complex, at a molecular and atomic level, is known as a key step for the understanding of the rules governing the stability and the reactivity of these species. Obviously, the combination of various tools i.e. EXAFS, NMR, infrared spectroscopy and molecular modelling can be used to shed some light on the nature of the chemical bond between the metal atom of the organometallic fragment and the surface.

1.4 Surface Rhodium Carbonyl species

1.4.1 Introduction

Rhodium is industrially used as a homogeneous catalyst for processes such as in the production of acetic acid from methanol. It is also used as a heterogeneous catalyst in the synthesis of nitric acid from ammonia and as a part of the three way automotive exhaust catalyst (with platinum and ceria), for the removal of carbon monoxide, nitric oxide and hydrocarbons from exhaust gases. Rhodium particles on metal oxide supports catalyse a number of reactions important to industrial processes including the hydrogenation and oxidation of carbon monoxide, [28,29] the reduction of nitric oxide,[30] carbon-carbon bond formation and the water–gas shift reaction.

Surface rhodium carbonyls may result from the reaction of rhodium carbonyl compounds with metal oxide, the adsorption of CO onto metal oxide supported metal particles or the exchange of hydrocarbon ligands for CO. Infrared spectroscopy is a particularly useful tool for investigating the chemistry of carbonyl compounds as the frequencies of the υ(C-O) bands are very intense and highly sensitive to the electronic environment, due to the degree of back donation from metal occupied d orbitals to the π^* orbital of the CO, and intermolecular interactions, allowing useful information about electronic characteristic of the metal and the bonding of the CO to be obtained. The sensitivity of the υ(CO) band, the ease and its adaptability for making in situ measurement, have led to CO being widely employed as a probe molecule to study metal particle morphology.

In principal there are three types of carbonyl species formed by the adsorption of CO on supported rhodium:

- Linear rhodium carbonyls, the frequency of which shift to a higher wavenumber on increasing coverage (i.e. 2050 $cm^{-1} \rightarrow$ 2080 cm^{-1})
- CO bridging between two rhodiums with a frequency at about 1850 cm^{-1} (1840 cm^{-1} to 1920 cm^{-1}, depending on coverage)
- The gem dicarbonyl species, $Rh^{I}(CO)_2$ with two CO molecules on one isolated rhodium atom.[31]

The relative distribution of these three species is shown to be dependent on the metal loading[32], reduction conditions[33], the organometallic precursor[34,35] and the support.[36,37]

1.4.2 The rhodium gem dicarbonyl species

The rhodium gem dicarbonyl species is characterised by two infrared bands at around 2100 cm^{-1} and 2030 cm^{-1}. In the past, this has been characterised by the fact that it displays no shifts in frequency with increasing coverage and is thought to exist as an isolated Rh^I site.[38, 39] However, it has been shown recently that a small shift in wavenumber up to 9 cm^{-1} may be observed with increasing coverage.[40] Isotopic substitution by Yates and Kolansinki have confirmed this species to be a non-linear C_{2v} species, as the expected numbers of bands were observed and the frequencies matched the calculated values within experimental error.[38,,41]

Generation of $Rh^I(CO)_2$ on oxide support can be achieved by

i). adsorption of CO on the oxidized or reduced Rh[42]

ii). exposure of supported $Rh_6(CO)_{16}$ and $Rh_4(CO)_{12}$ to oxygen [43]

iii). reaction of supported rhodium salt such as chlorides and nitrates with CO and H_2. [44]

Initial proposals suggested that the $Rh^I(CO)_2$ was formed via dissociation of CO, resulting the oxidation of Rh^0 to Rh^I by oxygen adatoms.[45,46] Subsequent studies however, showed that the gem dicarbonyl is formed at a lower temperature than those required for CO dissociation. [47,48] The currently favoured mechanism involved the consumption of isolated OH groups[49] and the species can be regenerated following reaction with water. [50, 51]

More recently, Evans *et. al*[40] reported that the rhodium gem dicarbonyl species, $Rh(CO)_2$ can be formed by dissociative adsorption of $Rh_2(CO)_4Cl_2$ on both single crystal $TiO_2(110)$ and powders TiO_2 surfaces at 300K. This species has been characterised by TPD, XPS, and RAIRS techniques, using CO as the probe adsorbate molecule. The gem dicarbonyl species is believed to be stable to 450K above which temperature a phase change occurs. In spite of the extensive work done in this field, arguments over the chemical bonding of the species to the surface, the adsorption state and the function and the existence of Cl in the system continue.

Authors are divided concerning the existence of Rh-Cl bond. Koningsberger and co-workers[52] concluded that the species formed is $(CO)_2Rh(O_{surf})_3$, where the oxygen is from the support with the Rh-O distance of 2.18 Å. Johnston *et al*[53] however, argued that the data are more accurately described by the proximity of

chlorine rather than oxygen and deduced the Rh-Cl distance as 2.33 Å, which is very similar to that in the crystalline compound of $(CO)_4Rh_2Cl_2$.[54]

The importance of residual chlorine is widely recognised and this has been emphasised by Bond *et al.*[55] Using EXAFS results, Johnston et al.[53] had suggested that the presence of chlorine ion may be the stabilising factor for the Rh^I entities and compared with the work with halogen free condition of Frederick et al. who reported that the species is unstable *in vacuo* at 298K.[56]

Based on series of work on titania, using EXAFS data, Evans[57] concluded that the rhodium centres is like that of **A**. Thermolysis of **A** under mild condition appears to maintain the Rh-Cl bond but not above 525K.

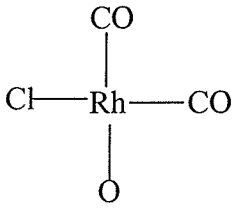

A

However, depending on the nature of the surface, the nature of the reactions will differ considerably. Again, factors such as strong or weak metal and support surface interaction and purity of the oxide sample,[58] in addition to methods of pre-treatment, often have been found to be the determining factor for explaining differences in results between in various laboratories. [13,59] The reaction can occur not only with the hydroxyl groups but also with more or less strained M-O-M bridges resulting from dehydroxylation process or even with the M=O double bonds with certain metals in high oxidation state.[60]

1.5 Polyhedral Oligosilsesquioxanes

1.5.1 Models for Silica Surfaces

Polyhedral silsesquioxanes (POSS) represent a rather versatile class of three-dimensional organosilicon oligomers which are of considerable theoretical and practical interest. They are composed of a polyhedral silicon-oxygen skeleton containing intermittent siloxane chains which bear organic or inorganic substituents.[61]

The molecules of this compound have the general formula of $(XSiO_{1.5})_n$ where X = organic or inorganic groups and $n \geq 4$.

Sil-ses-quioxane, (sometimes also written as silasesquioxane) denotes that each silicon atoms is connected to three oxygen atoms, $\{SiO_3\}$. The prefix 'oligo' is often used to indicate a small number or silsesquioxane in the link while prefixes such as 'octa', 'penta', etc. are used to indicate the specific number of these link.[62, 63] They have been used as building block units for the synthesis of new materials, such as dry resist in microelectronics,[64] alternative precursors for the generation of low-dielectric-constants materials,[65] and precursors for ceramics. [66, 67, 68, 69]

Octasilsesquioxanes, the most intensively studied silsesquioxanes, are cube-shaped molecules consisting of a core and eight reactive sites, which, in principle, all can be functionalized differently.[70] The interest in these compounds derives from the fact that their Si_8O_{12} core is analogous to the T_8O_{12} fragment (T_8 usually the mixture of Al, Si, P and Co(II)) found in zeolites such as Linde A and others.[71] However in the case of octasilsesquioxanes only one type (Si) of tetrahedral atoms are present. The relation between the T_8O_{12} fragment and the zeolite A structure is shown in Figure 1.5.

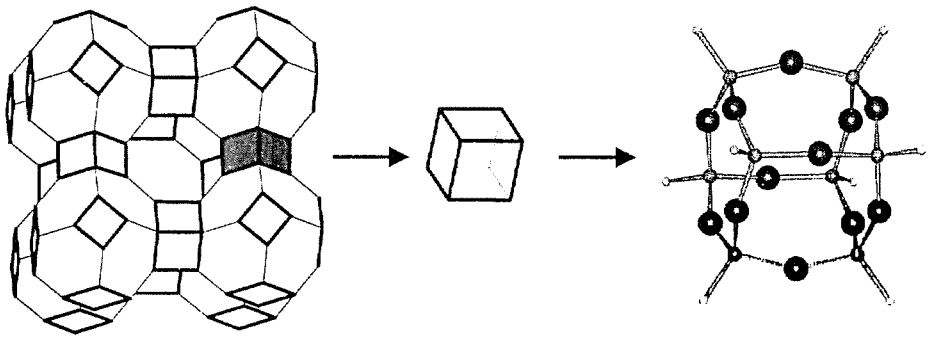

Figure 1.5: Relation between the structure of Zeolite A, T_8O_{12} fragment and the $R_8Si_8O_{12}$

Incompletely condensed polyhedral oligosilsesquioxanes (POSS) such as **1-3**, in Figure 1.6 are suitable molecular models for heterogeneous catalysts since, firstly they possess sufficient degree of oligomerisation as to be relevant models for highly siliceous materials and secondly because they retain reactive Si-OH functionality which allows for their exploitation as ligands in a variety of main group and transition metal complexes.[72] Since POSS such as **1-3**, possess an extensive Si-O framework, their electronic properties should be more similar to silica and siliceous solids than that of conventional models such as siloxide ligands, e.g. $(C_6H_5)_3SiO$-.

Employment of the correlation between Hammett substituent parameters and ^{13}C chemical shifts suggests that the electron withdrawing tendency of the Si_8O_{12} framework,[73] is more similar to $-CF_3$ group rather than R_3Si derivatives which is electron donating in nature.[74]

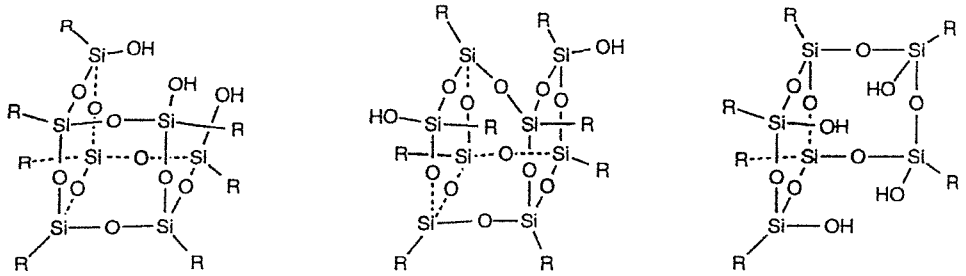

1b R = *c*-C_5H_9
1a R = *c*-C_6H_{11}
1c R = *c*-C_7H_{13}

2 R = *c*-C_6H_{11}

3 R = *c*-C_7H_{13}

Figure 1.6: Examples of some incompletely condensed polyhedral oligosilasesquioxanes (POSS)

Conventional models fail in their ability to mimic the co-ordination geometry of supposed silica supported species. Usually a metal dictates the arrangement of ligands within its co-ordination sphere. Subtle changes in this arrangement can have a profound influence on chemical reactivity.

Incompletely condensed POSS dictate the co-ordination geometry of metal complexes much more effectively and show great similarity to alleged silica surface sites. This is demonstrated by trisilanol, **1(a-c)**. The term trisilanol is used in a loose sense to denote the compound which contain three [SiOH] groups such as the incompletely condensed silsesquioxanes prepared by Feher and co-workers.[72]

A single crystal X-ray diffraction study[72] shows the structure was similar to that of the octahedral face of β-crystobalite[75](111) and the idealised (001) rhombohedral face of β-trydimite[76](0001), [Fig. 7]. These crystalline forms of silica are often implicated as representing the surface structure of surface silica.[77]

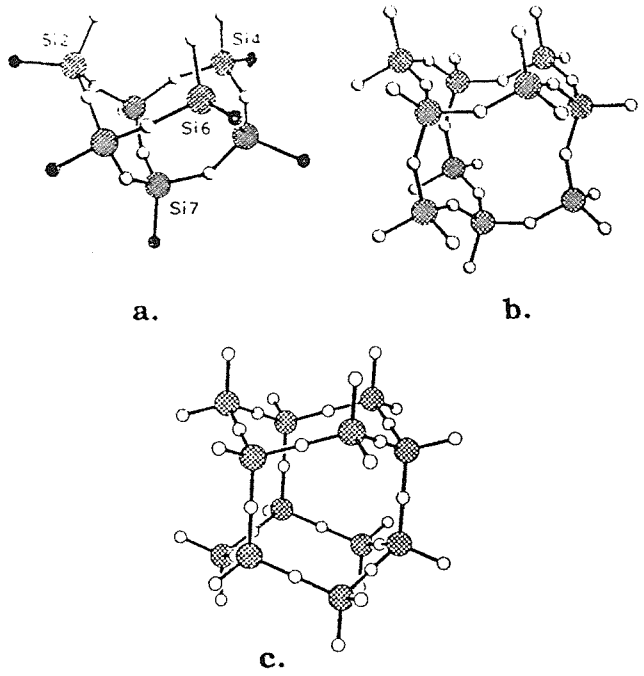

Figure 1.7: ORTEP plots (side views) of a). the trisilanol **1a** and b). the idealized (111) face of of β-crystobalite and c). idealized (0001) rhombohedral face of β-tridymite. Unshaded atoms are oxygens, cross hatched atoms are silicon while the shaded atoms are the ipso-carbons or cyclohexyl groups which are pendant to each silicon in trisilanol **1a**

As a result of their similarities, both geometric and electronic to silica supported complexes, transition metal complexes of POSSs are believed to be an exceptional model system for heterogeneous silica supported catalysts.

1.5.2 Synthesis and Characterisation Techniques

POSS can be synthesised by hydrolytic condensation of $RSiCl_3$ molecules. Many factors affected these reactions including solvent, temperature, pH and nature of R group.[78] Most often the products are contumacious mixtures, except for those species which precipitate from polar or strongly acidic mediums.

Brown and Vogt described the synthesis of the trisilanol, **1a**, which is quite useful and has been the focal point of much chemistry, by hydrolytic condensation of *c*-$C_6H_{11}SiCl_3$ in aqueous acetone.[79] The synthesis of heteroatom- and transition metal-containing silsesquioxanes has relied on three general methodologies: (a). the reaction of silanols such as **1a-3a** with metal alkyl complexes (Eqn. 1) (*b*). the metathesis of **1a-3a** for less acidic alkoxide or amide ligands (Eqn 2) (c). the base assisted (e.g. Et_3N) reactions with **1a-3a** with active metal halide complexes (Eqn 3).

(1)

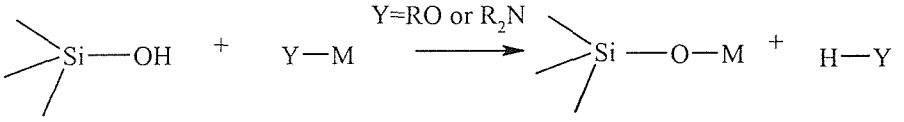

(2)

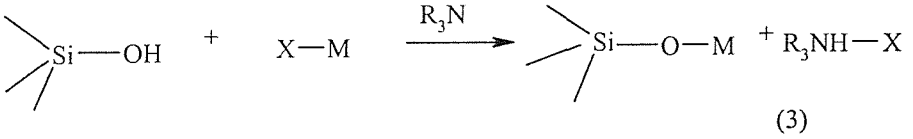

(3)

These three reactions can be used to synthesize a wide range of interesting metallasilsesquioxanes but each with has its limitations. For example, the protonolysis of metal alkyl complexes (Eqn. 1) only works well with the reactive alkyl complexes of electropositive metals e.g. Ti, Zr, V and Ga but fails with the less reactive M-C bonds of the late transition metals i.e. $CpPt(CH_3)_3$ and Me_3ReO_2.

Amine assisted metathesis of Si-OH (Eqn. 2) has been proven to be most effective and has been used in many "corner capping" reactions of trisilanol, **1**, using a wide variety of reagents, but reactive metal halides complexes, such as $O{=}VCl_3$,[80] $CpZrCl_3$,[81] $CpTiCl_3$, $TiCl_3(NMe_3)_2$,[82] PCl_3 , $SbCl_3$[83] and $AlCl_3$.[64] This procedure is exemplified by equation (Eqn. 4) below.

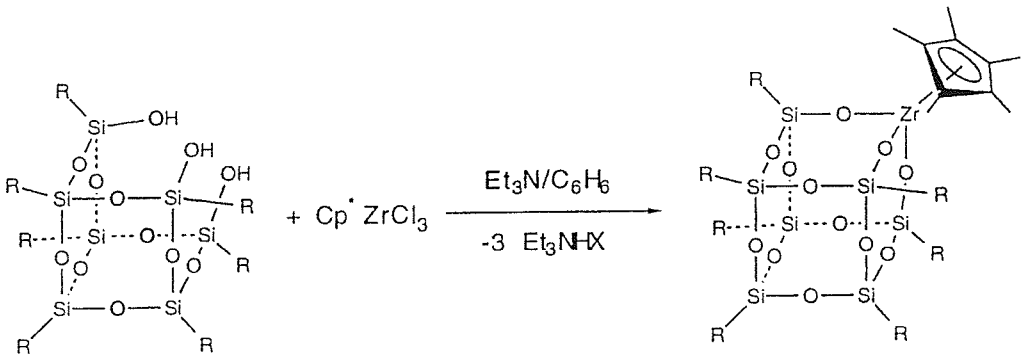

(4)

The reaction of incompletely condensed POSS, **1** with $SbMe_5$ are particular notable because they are selective for exactly one methyl group in the antimony reagent, Eqn.5.

(5)

Silsesquioxanes have been successfully viewed as model compounds for zeolites and silica surfaces and some of them have been thoroughly investigated and identified by different spectroscopic techniques, i.e. X-ray or neutron diffraction and vibrational spectroscopy and ^{1}H, ^{13}C and ^{29}Si NMR spectroscopy. [61,63]

1.5.3 Structure and Bonding

The unique nature of the Si-O-Si fragment in the silica cages system is the main focus of this study. Due to the flexible nature of the Si-O-Si backbone, fragments as diverse as "CpZr" (Zr covalent radius =1.45 Å) and "P" (P covalent radius =1.06 Å) [84] are easily accommodated by the silsesquioxane framework. The Si-O bond distances are believed to be inflexible and span in a narrow range. The Si-O-Si angles on the other hand, span a very large range, from 135° to 180°, with a theoretically calculated energetic minimum at 150°. [85]

The dynamic behaviour shown by many of these complexes is supplementary evidence for the flexibility of the cage frameworks in heteroatom and transition metal

derivatives of POSS. As an example of this flexibility, the Si atoms closest to the binding cavity in incompletely condensed POSS derivatives may be separated, i.e. Si..Si distances of the open cages, by as little as 4.2 Å as found in **4** or as much as 5.5 Å in **5**.[64] These values may be compared to the observed siloxyl group Si..Si distance in **1a** of 4.9 Å and β-cristobalite, which is 5.04 Å.[75]

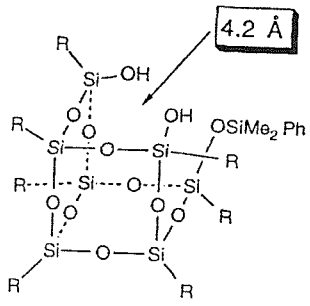

4

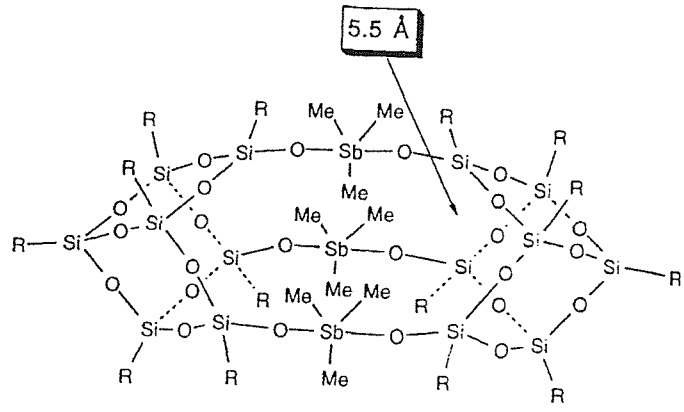

5

The ability of the ligand to dictate unusual coordination geometry was another exciting feature of POSS. It was anticipated that trivalent ions, such as V^{III} and Al^{III} would react trisilanol, **1**, to form complexes with a low co-ordination number (due to the steric bulk of the aliphatic periphery) and a pyramidalised geometry (due to the unique nature of binding cavity). On the contrary, the flexibility of the cage famework had enabled these ions, to attain higher co-ordination number through dimerisation, for example structure **6** and **7**, Figure 1.8.[86]

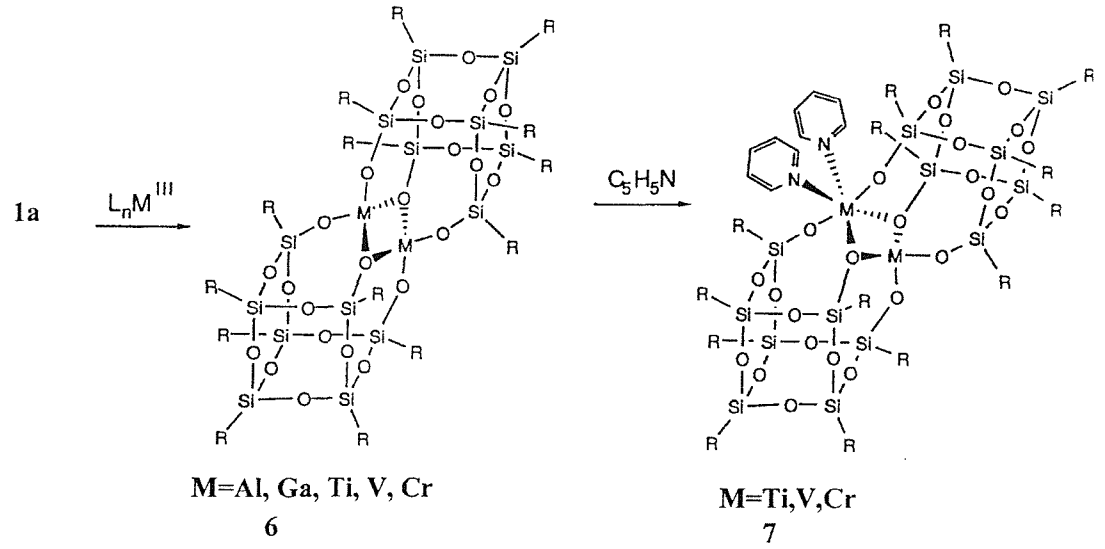

Figure 1.8: Examples of how higher co-ordination numbers are attained through dimerisation

Another dynamic behaviour of the cage framework, is its ability to exist as a mixture of monomer and dimer, see structure **8** and **9** for example, Figure 1.9. The disparity between structure **8** and **9** necessitates significant structural changes to affect their interconversion, reflecting the ease with which the skeletal deformation of the silsesquioxane frameworks occurs in these complexes.

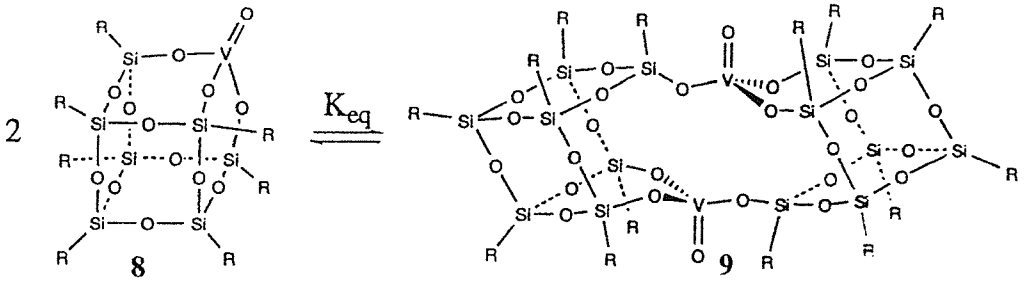

Figure 1.9: Sample of monomer and dimer existing together

1.6 Theoretical Chemistry

1.6.1 Introduction

Catalysis may well be one of the most practical of the many sub disciplines of science. The gasoline burned in internal combustion engines, the precursors for a variety of plastics, polymers, fertilizers, edible oils, pharmaceutical and medicinal products, dyestuffs, food additives, cosmetics, pollution control both in automotives and stationary plants all involve the use of catalysts.

As with much science, experiment has preceded theory in catalysts. Many of the catalysts referred to in the present, have been in industrial use for a considerable length of time, but an understanding of the theory of their catalytic activity is not complete. The application of quantum mechanics in the field of catalyst was slow. It is evident that the surface of a heterogeneous catalyst is one of its important features. However, theoretical techniques are most conveniently applied to isolated molecules as applications to surfaces are more complex.

1.6.2 Molecular Modelling, Computational and Theoretical Chemistry

There is much confusion over the meaning of the terms "molecular modelling", "computational chemistry" and "theoretical chemistry".

Theoretical chemistry is often considered synonymous with quantum mechanics. Computational chemistry encompasses a variety of mathematical methods which fall into two broad categories: molecular mechanics and quantum mechanics. Molecular mechanics applies the laws of classical physics to molecular nuclei without explicit consideration of electrons. Quantum mechanics relies on the Schrödinger equation to describe a molecule with explicit treatment of electronic structure. Generally, quantum mechanical methods can be subdivided into two classes: ab initio and semi empirical, making a total of three generally accepted classes, as shown below, Figure 1.10.

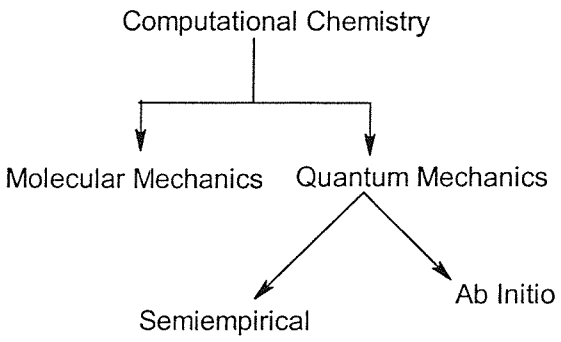

Figure 1.10: Computational Chemistry

While a number of different definition has been proposed for *computational chemistry*, perhaps the definitions proposed Lipkowitz and Boyd as "those aspects of

chemical research that are expedited or rendered practical by computers" is the most inclusive.[87]

1.7 Crystallographic Structural Databases

1.7.1 Introduction

Experimental information about the structures of molecules can often be extremely helpful for forming theories of conformational analysis and helping to predict the structures of molecules for which no experimental information is available. The most currently available technique for determining the three dimensional structure of molecules is X-ray crystallography. The international crystallographic community has established centres where crystallographic data is collected and then distributed in electronic form.

Two particularly important databases for the molecular modeller are the Cambridge Structural Database (CSD)[88,89,90] which contains crystal structures of organic and organometallic molecules and the Protein Databank (PDB)[91] which contains structures of proteins and DNA fragments. Other databases which are also available, are the Inorganic Crystal Structure Database (ICSD) for inorganic compounds and complexes[92] and the Nucleic Acid Database for structures of nucleic acids.[93]

The most common use of the crystallographic database is to avoid duplication of effort, both on the part of experimentalists and journals. As the number of structures continues to increase, this simple but important check, has already saved significant amount of data-collection time and computational resources as well as valuable refereeing and editorial time for journals that wish to decline duplicate structure determinations.[94]

A simple use of a database is for extracting information about a particular molecule or groups of molecules. One may wish to retrieve the crystal structure for a particular molecule for example, for computational chemistry purpose, and this may be specified by a variety of ways, such as by name, molecular formula or by literature citation, or by creating a two-dimensional representation of the molecules and using a substructure search to search the database.

Crystallographic databases have also been used to develop an understanding of the factors that influence the conformations of molecules and of the ways the molecules interact with each other. For example the CSD, has been comprehensively used to characterise how the lengths of the chemical bonds depend upon atomic numbers, hybridisation and environment of the atoms involved.[95] Analysis of intermolecular hydrogen bonding have revealed distinct distance and angular preferences[96,97]. Substructure search for molecules contain particular fragment, in order to investigate the conformation(s) that the fragment adopts, is among the major use of the CSD.

1.7.2 Cambridge Structural Database (CSD)

The Cambridge Structural Database (CSD) maintains a database relating to the structure of organics, organometallics and metal complexes determined by X-ray and neutron diffraction. The CSD software system is supported and developed on an ongoing basis by CCDC(Cambridge Crystallographic Data Centre) staff in Cambridge. [98] The current database (Nov.1999) comprises structural information for over 200,000 organic and metal organic compounds, analysed using X-ray or neutron diffraction techniques.[99]

Table 1.1: Summary of information content of the CSD

File Name	Information Content
BIB Bibliographic File[100]	Compound name; synonym (or trivial name; qualifying phrase(s) indicating, for example neutron study, low temperature work, molecular formula, author list, chemical classes, literature reference
CONN Chemical Connectivity[101]	Compact coded representation of the chemical structural diagram in terms of atoms and bond properties for each residue in the crystal unit
DATA Structural Data File	Unit-cell parameters; space group; symmetry, atomic co-ordinates of crystal chemical unit; published bond lengths; accuracy indicator(R factors); textual comment related to errors located, corrections applied and details of disorder.

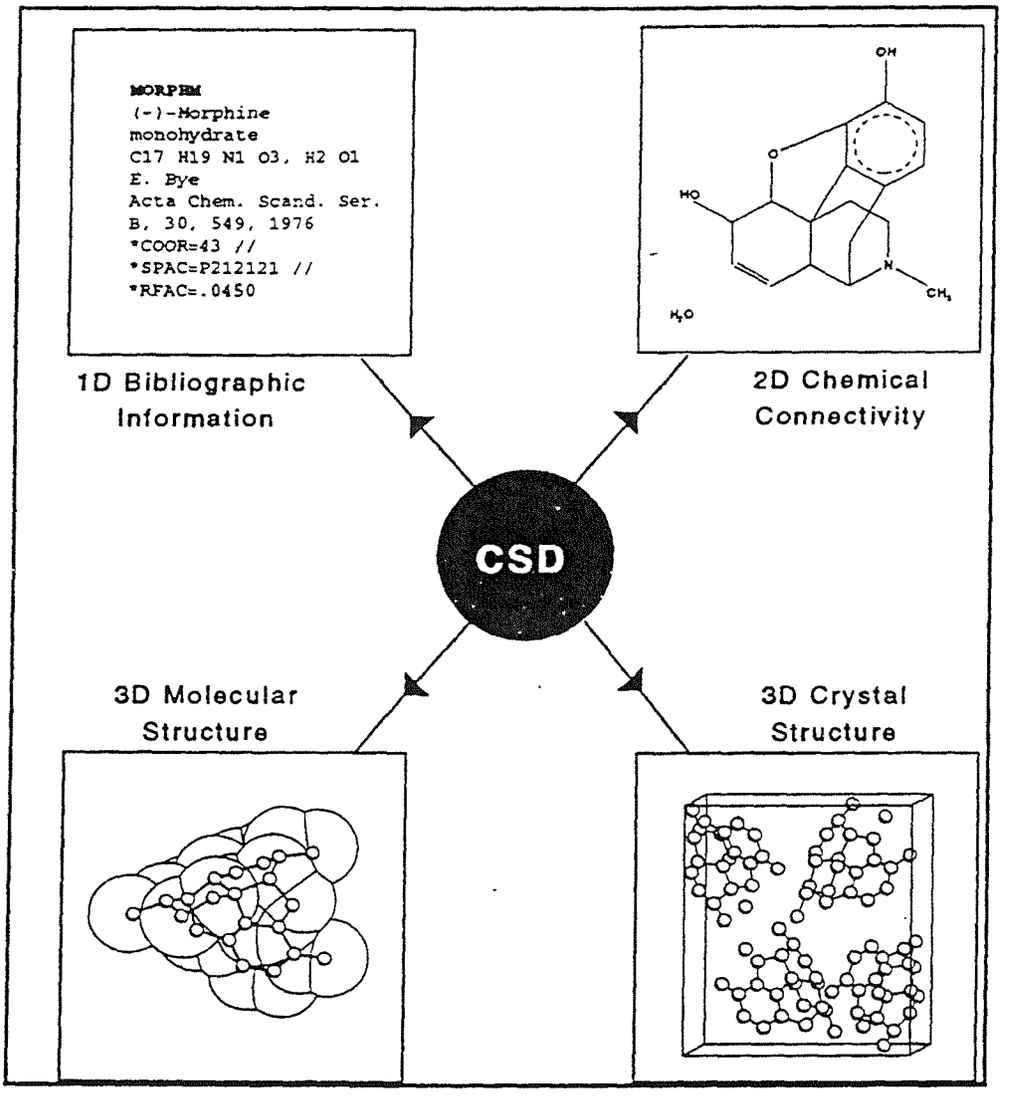

Figure 1.11: Information content of entries in the Cambridge Structural Database.

The database comprises of three important files a). bibliographic information (BIB) b). chemical connectivity information (CONN) c). crystallographic data (DATA) files, conveniently categorised in terms of their "dimensionality", 1D, 2D and 3D informations, respectively. Table 1.1 and Figure 1.11, summarises the information content from each of these files. Example of the typical work making use of this facility was illustrated by the work of Murray-Rust & Motherwell[102] and Murray-Rust & Bland.[103]

1.8 Scope and the aim of the thesis

This thesis has been organised into five chapters. Chapter Two gives insight into the basic of theory and method of computational chemistry. Chapter Three presents a theoretical studies of rhodium gem dicarbonyl species supported on silica using Density Functional theory.

Specifically, the objectives of the work in Chapter Three are to determine the molecular environment of the rhodium gem dicarbonyl, i.e., the oxygen atom co-ordinated to the rhodium, the presence of chlorine atom and also to study the ν(CO) shifts in these systems using Density Functional Theory (DFT) method on a simple silica surface model.

The remaining two chapters are devoted to silsesquioxanes. Chapter Four gives a systematic structural analysis based on crystal data from CSD and correlation studies of ^{29}Si NMR chemical shift with geometric parameters such as Si-O distances, Si-O-Si bond angles and Si..Si nonbonding distances.

Finally Chapter Five involves a theoretical study of hypothetical incompletely condensed POSSs. In this chapter, we study the isolated and hydrogen bonded hydroxyl groups and $SiOCH_3$ groups using a hypothetical trisilanol as the model for silica surface.

1.9 References

1. J. A. Hockey, *Chem. Ind.*, 1965, 57.

2. P. C. Carman, *Trans Faraday Soc.*, 1940, **36**,964.

3. R. K. Iler, *The Colloid Chemistry of Silica and Silicates*, 1955, New York, Cornell University Press.

4. M. L. Hair, *Silanes, Surfaces and Interfaces*, Ed. D. E. Leyden, Gordon and Breach, The Netherlands, 1986, and references therein.

5. J. Evans, *Surface Organometallic Chemistry: Molecular Approaches to Surface Catalysis*, Kluwer Academic Publishers, 1988, p 47-73 and references therein.

6. B. A. Morrow, *Stud. Surf. Sci. Catal.*, 1990, **57A**, A161.

7. P. Hoffman, H. Knözinger, *Surf. Sci.*, 1987, **188**, 181.

8. J. B. Peri and A. L .Hensley Jr., *J. Phys. Chem.*, 1968, **72**, 2926.

10. R. Buffon, M. Leconte, A. Choplin and J. M. Bassett, *J. Chem. Soc., Dalton Trans.*, 1994, 1723.

11. P. Dufour, S. L. Scott, C. C. Santini, F. Lefebvre and J. M. Basset, *Inorg. Chem.*, 1994, **33**, 2509.

12. S. L. Scott, and J. M. Basset, *J. Mol. Catal.*, 1994, **86**, 5.

13. S. L. Scott, J. M. Basset, A. Chopin, M. Leconte, F. Quignard, C. Santini, and A. Theolier, *Elementary Steps in Heterogeneous Catalysis*, Ed. R. W. Joyner and R. A. van Santen, Kluwer Academic, 1993, p 39-49.

14. J .M. Basset, F. Lefebvre and C. Santini, *Coord. Chem. Rev.*, 1998, **178-180**, 1703.

15. M. A. Vannice, *J. Catal.*, 1975, **37**, 449. b). M. A. Vannice and R. L. Garten, *J. Catal.*, 1980, **66**, 242.

16. R. Burch and A. R. Flambard, *J. Chem. Soc., Chem. Commun.*, 1981, 123.

17. E. Zagli and J. L. Falconer, *J. Catal.*, 1981, **69**, 1.

18. D. C. Grenoble, M. M. Estadt and D. F. Ollis, *J. Catal.*, 1981, **67**, 90.

19. Y. I. Yermakov, B. N. Kuznetsov, V. A. Zakharov, *Catalysis by Supported Complexes*, Elsevier, New York, 1981.

20. J. Schwartz, *Acc. Chem. Res.*, 1985, **18**, 302.

21. I. Tanaka, N. Jin-No, T. Kushida, N. Tsutui, T. Ashida, H. Suzuki, H. Sakurai, Y. Moro-Oka, T. Ikawa, *Bull. Chem. Soc. Jpn.*, 1983, **56**, 657.

22. P. Dufour, C. Houtman, C. C. Santini, C. Nédez, J. M. Basset, L. Y. Hsu, S. G. Shore, *J. Am. Chem. Soc.*, 1992, **114**, 4248.

23. J. F. Hallet, and R. Hoffman, *J. Am. Chem. Soc.*, 1989, **111**, 3548.

24. Y. Iwasawa and H. Sato, *Chem. Lett.*, 1985, 507.

25. H. C. Foley, S. J. DeCanio, K. D. Tau, K. J. Chao, J. H. Uneferko, C. Dybowski and B. C. Gates, *J. Am. Chem. Soc.*, 1983, **105**, 3074.

26. J. Corker, F. Lefebvre, C. Lecuyer, V. Dufaud, F. Quignard, A. Choplin, J. Evans and J. M. Basset, *Inorg. Chem.*, 1992, **21**, 928.

27. J. M. Basset, F. Lefebvre and C. Santini, *Coord. Chem. Rev.*, 1998, **178-180**, 1703.

28. L. Guczi in *Studies in Surface Science and Catalysis*, 1991, 64.

29. F. Solymosi, I. Tombacz, and M. Kocsis, *J. Phys. Chem.*, 1990, **94**, 4617.

30. F. Solymosi and J. Sarkany, *Appl. Surf. Sci.*, 1979, **3**, 68.

31. A. C. Yang and C. W. Garland, *J. Phys. Chem.*, 1957, **61**, 1504;

32. V. E. Henrich and G. Dresselhaus and H. J. Zeiger, *Phys. Rev. Lett.*, 1972, **36**, 1335.

33. G. A. Hyde, R. Rudham, C. H. Rochester, *J. Chem. Soc., Faraday Trans*,1983, **79**, 2405.

34. S. D. Worley, C. A. Rice, G. A. Mattson, C. W. Curtis, J. A. Guin, A. R. Tarrer, *J. Phys. Chem.*, 1982, **76**, 20.

35. G. M. Nuñez, A. R. Patrigani, A. J. Rouco, *J. Catal.*, 1986, **98**, 554.

36. S. D. Worley, C. A. Rice, G. A. Mattson, C. W. Curtis, J. A. Guin, A. R. Tarrer, *J. Phys. Chem.*, 1982, **86**, 2714.

37. T. Ioannides and X. Verykios, *J. Catal.*, 1993, **140**, 353.

38. J. T. Yates and K. Kolansinki, *J. Chem. Phys.*, 1983, **79**, 1026.

39. S. Trautmann and M. Baerns, *J. Catal.*, 1994, **150**, 335.

40. J. Evans, B. E. Hayden, J. F. W. Mosselmans and A. Murray, *Surf. Sci.*, 1994, **301**,61.

41. H. P. Wang, and J. T. Yates, *J. Chem. Phys.*, 1984, **89**, 79.

42. P. Basu, D. Panayotov, and J. T. Yates Jr., *J. Am. Chem. Soc.*, 1988, **110**, 2074.

43. A. K. Smith, F. Hughes, A. Theolier, J. M. Basset, A. K. Smith, G. M. Zanderighi, and R. Ugo, *J. Organomet. Chem.*, 1978, **153**, 73.

44. M. P. Keyes and K. L. Watters, *J. Catal.*, 1986, **100**, 477; C. A. Rice, S. D. Worley, S. W. Curtis, J. A. Guin and A. R. Tarrer, *J. Chem. Phys.*, 1981, **74**, 6487.

45. Z. L. Zhang, A. Kladi and X. E. Verykios, *J. Mol. Catal.*, 1994, **89**, 229.

46. M. Primet, *J. Chem. Soc., Faraday Trans. I*, 1978, **74**, 2570.

47. H. F. J. van't Blik, J. B. A. D. van Zon, T. Huizinga, J. C. Vis, D. C. Koningsberger and R. Prins, *J. Phys. Chem.*, 1985, **107**, 3139.

48. J. T. Yates Jr., E. D. Williams and W. Weinberg, *Surf. Sci.*, 1980, **91**, 562.

49. P. Basu, D. Panayotov and J. T. Yates Jr., *J.Phys.Chem*, 1987, **91**, 3133.; P. Basu, D. Panayotov and J. T. Yates Jr., *J. Am. Chem.Soc.*,1988, **110**, 2074.

51. D. A. Buchanan, M. E. Hernandez, F. Solymosi and J. M. White, *J. Catal.*, 1990, **125**, 456.

52. H. F. J. van't Blik, J. B. A. D. van Zon, T. Huizinga, J. C. Vis, D. C. Koningsberger and R. Prins, *J. Mol. Catal.*, 1984, **25**, 379; H. F. J. van't Blik, J. B. A. D. van Zon, T. Huizinga, J. C. Vis, D. C. Koningsberger and R. Prins, *J. Phys. Chem.*, 1983, **87**, 2264; H. F. J. van't Blik, J. B. A. D. van Zon, T. Huizinga, D. C. Koningsberger and D. E. Sayers, *J. Chem Phys.*, 1985, **82**, 5742.

53. P. Johnston, R. W. Joyner, P. D. A. Pudney, E. S. Shpiro and B. P. Williams, *Faraday Discuss. Chem. Soc.*, 1990, **89**, 91.

54. L. F. Dahl, C. Martell, and D. L. Wampler, *J. Am. Chem. Soc.*,1961, **83**, 1761.

55. G. C. Bond, R. R. Rajaram, and R. Burch, *Appl. Catal.*, 1986, **27**, 379.

56. G. C. Frederick, G. Apai, and T. N. Rhodin, *J. Am. Chem. Soc.*, 1987, **109**, 4797.

57. J. Evans, *Chem. Soc. Rev.*, 1997, 11.

58. S. D. Worley, C. A. Rice, G. A. Mattson, C. W. Curtis, J. A. Guin and A. R. Tarrer, *J. Phys. Chem.*, 1982, **86**, 2712;

59. P. Dufour, C. Houtman, C. C. Santini, C. Nedez, J. M. Basset, L. Y. Hsu and S. G. Shore, *J. Am. Chem. Soc.*, 1992, **114**, 4248.

60. J. M. Basset, F. Lefebvre and C. Santini, *Coord. Chem. Rev.*, 1998, **178-180**, 1703.

61. M. G. Voronkov and V. I. Lavrent'yev, *Top. Curr. Chem.*, 1982, **102**, 199.

62. R. H. Baney, *Chem. Rev.*, 1995, **95**, 1409.

63. P. G. Harrison, *J. Organometal. Chem.*, 1997, **542**, 141.

64. A. Schmidt, S. Babin, K. Böhmer, and H. W. P. Koops, *Microelectron. Eng.*, 1997, **35**, 129.

65. N. P. Hacker, *MRS Bull.*, 1997, **22**, 33.

66. D. A. Loy and K. J. Shea, *Chem. Rev.*, 1995, **95**, 1431.

67. P. G. Harrison and R. Kannenggiesser, *Chem. Commun.*, 1996, 415.

68. F. J. Feher, and T. A. Budzichowski, *Polyhedron*, 1995, **14**, 3239.

69. M. Wiebcke, D. Hoebel, *J. Chem. Soc., Dalton Trans.*, 1992, 2451; D. Hoebel, K. Endres, T. Reinert, I. Pitsch, *J. Non-Cryst. Solids*, 1994, **176**, 179.

70. C. Marcolli and G. Calzaferi, *Appl. Organomet. Chem.*, 1999, **13**,213

71.W. M. Meier and D. H. Olson, *Atlas of Zeolites Structure Types*, 2nd. edn., Butterworth, London, 1987.

72. F. J. Feher, D. N. Newman and J. F. Walzer, *J. Am. Chem. Soc.*, 1989, **111**, 1741.

73. F. J. Feher and T. A. Budzichowski, *J. Organomet. Chem.*, 1989, **379**, 33.

74. C. G. Swain, S. H. Unger, N. R. Rosenquist and M. S. Swain, *J. Am. Chem. Soc.*, 1983, **105**, 472.

75. A. F. Wright and A. J. Leadbetter, *Phil. Mag.*, 1975, **31**, 1391.

76. K. Kihara, *Kristallogr.*, 1978, **148**, 237.

77. R. K. Iler, *The Chemistry of Silica*, Wiley-Interscience, New York, 1979.

78. F. J. Feher, and T. A. Budzichowski, *J. Organomet. Chem.*, 1989, **373**, 153.

79. J. F. Brown and L. H. Vogt, *J. Am. Chem. Soc.*, 1965, **102**, 199.

80 F. J. Feher and J. F. Walzer, *Inorg. Chem,.*1991, **29**, 1689.

81. F. J. Feher, *J. Am. Chem. Soc.*, 1986, **108**, 3805.

82. F. J. Feher, S. L. Gonzales and J. W. Ziller, *Inorg. Chem.*, 1988, **27**, 3440.

83. F. J. Feher and T. A. Budzichowski, *Organomet.*, 1991, **10**, 812.

84. F. A. Cotton and G. Wilkinson, *Advanced Inorganic Chemistry*, 5th edn., Wiley, New York, 1988.

85. G. I. Golodets in *Heterogeneous Catalytic Reaction Involving Molecular Oxygens*, Elsevier, New York, 1983.

86. F. J. Feher and J. F. Walzer, *Inorg. Chem.*, 1990, **29**, 1604.

87. *Reviews in Computational Chemistry*, Ed. by K. B. Lipkowitz and D.B. Boyd, vol.1, VCH Publishers Inc., New York, 1990.

88. F. H. Allen, S. A. Bellard, M. D. Brice, B. A. Cartwright, A. Doubleday, H. Higgs, T. Hummelink, B. G. Hummelink-Peters, O. Kennard, W. D. S. Motherwell, J. R. Rodgers and D. G. Watson, *Acta Cryst.*, 1979, **B35**, 2331.

89. F. H. Allen, J. E. Davies, J. J. Galloy, O. Johnson, O. Kennard, C. F. Macrae, E. M. Mitchell, G. F. Mitchell, J. M. Smith and D. G. Watson, *J. Chem. Inf. Comput. Sci.*, 1991, **31**, 187.

90. O. Kennard and F. H. Allen, *Chem. Des. Autom, News*, 1993, **8**,31.

91. F. C. Bernstein, T. F. Koetzle, G. J. B. Williams, E. Meyer, M. D. Bryce, J. R. Rogers, O. Kennard, T. Shikanouchi, M. Tasumi, *J. Mol. Biol*, 1977, **112**, 535.

92. G. Bergerhoff, R. Hundt, R. Sievers and I. S. Brown, *J. Chem. Inf. and Comp. Sci.*, 1983, **23**, 66.

93. H. M. Bermanm, W. K. Olson, D. L. Beveridge, J. Westbrook, A. Gelbin, T. Demeny, S. H. Hsieh, A. R. Srinavasan, and B. Schneider, *Biophys. J.*, 1992, **63**, 751.

94. F. H. Allen, *Acta Cryst.*, 1998, **A54**, 758.

95. Allen F. H., O. Kennard, D. G. Watson, L. Brammer, A. G. Orpen and R. Taylor, *J. Chem. Soc. Perkins Trans.*, 1987, **II**, S1.

96. J. P. Glusker, *Acta. Cryst.*, 1995, **D51**, 418.

97. P. M. Murray-Rust and J. P. Glusker, *J.Am.Chem.Soc.*, 1984, **106**, 1018.

98. The United Kingdom Chemical Database Service, D. A. Fletcher, R. F. McMeeking, D. Parkin, *J. Chem. Inf. Comput. Sci.*, 1996, **36**, 746.

99. See CCDC homepage at http://ccdc.cam.ac.uk

100. O. Kennard, D. G. Watson and W. G. Town, *J.Chem.Doc.*,1973, **12**, 14.

101. F. H. Allen, O. Lennard, W. D. S. Motherwell, W. G. Town, and D. G. Watson, *J.Chem.Doc.*,1973, **13**, 119.

102. P. Murray-Rust and S. Motherwell, *Acta Cryst.*, 1978, **B34**, 2518; P. Murray-Rust and S. Motherwell, *Acta Cryst.*, 1978, **B34**, 2534.

103. P. Murray-Rust and R. Bland, *Acta Cryst.*, 1978, **B34**, 2527

Chapter 2

Theoretical Chemistry: Theory and Method

Chapter Two : Theory and Method

2.0 Introduction

The key to theoretical chemistry is quantum mechanics, which is the science of relating molecular properties to the motion and interactions of electrons and nuclei.[1] According to quantum mechanics, the energy and many properties of a molecule can be obtained, in principle, by solving Schrödinger's wave equation.

The Schrodinger equation:

$$\hat{H}\Psi = E\Psi$$

Where

$\hat{H}$ = an operator known as the Hamiltonian, it represents the total energy of the system

Ψ = a function known as an eigenfunction or wavefunction, which described spatial motion of electrons

E = a scalar energy value known as an eigenvalue

Ψ is not directly related to any physical observable but:

$$\Psi^2 (x,y,z) \alpha P_e$$

where P_e is the probability of finding electron density in a particular region of space.

The total Hamiltonian can be written as a sum of the kinetic (T) and potential energies (V) of all particles (nuclei and electrons), in which

$$T = -\frac{h^2}{8\pi^2}\sum_i \frac{1}{m_i}\left(\frac{\partial^2}{\partial x_i^2}+\frac{\partial^2}{\partial y_i^2}+\frac{\partial^2}{\partial z_i^2}\right) \qquad \textbf{(2. 1)}$$

where h is the Plank's constant and m is the mass of the particle i. The potential energy is the coulomb interaction,

$$V = \sum_{i<j}\sum\left(\frac{e_i e_j}{r_{ij}}\right) \qquad \textbf{(2. 2)}$$

where the sum is over the distinct pairs of particles (i,j) with electric charges e_i, e_j separated by a distance r_{ij}.

Exact solutions to the Schrödinger equation are possible only for the simplest one electron-one nucleus system. These solutions, however, yield the basis for all of quantum

mechanics. For example, by finding the minimum of the potential energy surface of a stable molecule, it is possible to characterize the equilibrium structure of the species in terms of its bond length and bond angles.[1] For molecules, the Schrödinger equation cannot be solved unless approximations are made.

2.1 Molecular Orbital Theory

In a way, molecular orbital theory is a method of reducing the complexity of the Schrödinger wave equation by making specific approximations.

a). Time independent

The wavefunction is in a stationary state and therefore depends only on the spatial coordinates of the particles present in the system under investigation.

b). Nonrelativistic

That is electrons are described as having a constant mass i.e. relativity is neglected.

c). Born-Oppenheimmer Approximation

Due to the large mass difference between an electron and a nucleus, a nucleus moves so much more slowly than that of an electron, so it can be regarded as motionless relative to the electron. In effect, this approximation considers electrons to be moving with respect to a fixed nucleus allowing separate treatment of the electronic and nuclear energies.

In other words, the Bond Oppenheimer approximation removes the nuclear mass from the Schrödinger equation, and accounts only for the movement of electrons. This simplifies the Hamiltonian operator to a more workable format:

$$H_{el} = T_{el} + V$$

where T_{el} is the electronic kinetic energy

$$T_{el} = -\left(\frac{h^2}{8\pi^2 m}\right)\sum_{i}^{electrons}\left(\frac{\partial^2}{\partial x_i^2}+\frac{\partial^2}{\partial y_i^2}+\frac{\partial^2}{\partial z_i^2}\right)$$

while V is the coulomb potential energy

$$V = -\sum_{i}^{electrons}\sum_{s}^{nuclei}\frac{Z_s e^2}{r_{is}} + \sum_{i<j}^{electrons}\sum_{i<j}^{electrons}\frac{e^2}{r_{ij}} + \sum_{s<t}^{nuclei}\sum_{s<t}^{nuclei}\frac{Z_s Z_t e^2}{R_{st}}$$

Solving the Schrödinger wave function can be further simplified by employing a molecular orbital approach.[1]

2.2 Molecular Orbital Approach

The total wavefunction is represented as a combination of one-electron functions called spin orbitals which are a product of spatial functions called molecular orbitals, $\psi(x,y,z)$ and an α and β spin components. When spin orbitals are combined to form the total wavefunction certain rules must be obeyed. These are:

a). Electron must be indistinguishable. This is a direct result of the Heisenberg uncertainty principle, which states that the wave-particle duality of electrons means that it is impossible to determine both the momentum and position of an electron simultaneously. Since the electrons are identical in mass and charge the only way to distinguish them is by their paths. However, the Heisenberg uncertainty principle shows that it is not possible to specify these paths. Therefore, one electron must be seen as identical to another electron.

b). The overall wavefunction of the system of electrons must be antisymmetric with respect to the interchange of any two electrons. A spatial function or spin function can be symmetric or antisymmetric but when combined together they must be antisymmetric. This is known as the Pauli exchange principle. This antisymmetry constraint is not due to any theoretical reasoning but because it is found to be the case experimentally.[2]

c). Pauli exclusion principle which states that is not possible for a molecular orbital to be occupied by two electrons of the same spin.

Overall wavefunctions that satisfy the Pauli principle are often written as Slater determinants[3]:

$$\Psi = \frac{1}{\sqrt{n!}} \begin{vmatrix} \psi_1(1)\alpha(1) & \psi_1(1)\beta(1) & \psi_2(1)\alpha(1) & \cdots & \psi\beta \\ \psi_1(2)\alpha(2) & \psi_2(2)\beta(2) & \psi_2(2)\alpha(2) & \cdots & \psi\beta \\ \vdots & & & \vdots & \\ \psi_1(n)\alpha(n) & \psi\ (n)\beta(n) & \psi_2(n)\alpha(n) & \cdots & \psi\beta \end{vmatrix} \quad (2.3)$$

Since it is certain that a particle is found somewhere within the system, we have a condition

$$\int \psi_i^* \psi_j dx\, dy\, dz = 1$$

When this condition is satisfied, the molecular orbitals are said to be normalized. If i≠j, then $\int \psi_i^* \psi_j\, dx\, dy\, dz = 0$, the molecular orbitals are said to be orthogonal. This type of determinant [2.3] can be seen to satisfy the antisymmetry requirements. If labels 1 and 2 are interchanges, the rows of the determinants are exchanged and hence the overall signs of the determinant also changes. In addition to that, the Slater determinant also neatly accommodates the Pauli exclusion principle.

2.2.1 Hartree Fock Approximations

Almost all procedures in quantum mechanics calculations rely on Hartree Fock (HF) or self consistent field (SCF) approximations. The HF approximations assume that the n-particle wavefunction, Ψ(r), can be written as an antisymmetrized product (in the form of a determinant) of one electron functions, which are products of space functions, ψ_i, and spin functions, α or β.

2.2.2 Linear Combination of Atomic Orbitals (LCAO)

Direct solutions to HF equation are not practical to solve for molecules, so another alternative approach was to write each spin orbital as linear combination of single electron orbitals of N functions ϕ_v .

$$\psi_i = \sum_{v=1}^{N} c_{vi}\,\phi_v \qquad (2.4)$$

Where ψ_i is the molecular orbital, ϕ_v corresponds to the atomic orbitals or more generally known as the basis functions and c_{vi} is the molecular orbital expansion coefficients.

2.2.3 Variational Principle

Variational Principle can be summed up in one equation.:

$$\int \Phi^* \hat{H} \Phi \, d\tau \geq E_o \qquad (2.5)$$

where Φ is any function , $\hat{H}$ is the exact Hamiltonian and E_0 is the unknown exact ground state energy.

This approximation means that whatever the initial function we take, the energy calculated using it will always be greater than that of the ground state of the true systems. This allows the Schrödinger equation to be solved with an interactive procedure. By initially selecting appropriate basis function, a set of coefficients is obtained. These coefficients can be altered until a minimum expectation value of energy is achieved.

2.2.4 Hartree Fock- Closed Shell system

The variational condition above leads to the Roothaan-Hall equation;[4,5]

$$\sum_{\nu}^{N}(F_{\mu\nu} - \varepsilon_i S_{\mu\nu})c_{vi} = 0 \qquad \mu = 1,2,....,N \qquad (2.6)$$

Where;

$S_{\mu\nu} = \int \phi_U^*(1)\phi_v(1)dx_1 dy_1 dz_1$ = overlap matrix

$F_{\mu\nu} = H_{\mu\nu}^{co} + \sum_{\mu=1}^{N}\sum_{\nu=1}^{N} P_{\lambda\sigma}[\langle\mu\nu|\lambda\sigma\rangle - \frac{1}{2}\langle\mu\lambda|\nu\sigma\rangle]$ = which is the Fock matrix

In this expression

$$H_{\mu\nu}^{core} = \int \phi_u^*(1)\hat{H}^{core}(1)\phi_v(1)dx_1 dy_1 dz_1 \equiv \text{core Hamiltonian}$$

$$\hat{H}^{core}(1) = -\frac{1}{2}\nabla_1^2 - \sum_{A=1}^{nuclei}\frac{Z_A}{r_{1A}}$$

Here, Z_A is the atomic number of atom A, and the summation is carried out over all atoms. The quantities $(\mu\nu|\lambda\sigma)$ are *two electron repulsion integrals* and $P_{\lambda\sigma}$ is the density matrix.

Note also the similarity of the Roothaan-Hall equation.

$$Fc = \varepsilon Sc$$

to the Schrödinger equation.

$$\hat{H}\Psi = E\Psi$$

Here ε_i is the energy, F corresponds to $\hat{H}$ and *c* corresponds to Ψ.

The solution to the Roothaan-Hall equation depends on the Fock matrix which itself depends on the molecular coefficients, $c_{\mu i}$. The solution for this equation involves an iterative procedure, a technique frequently called *self consistent field* (SCF) theory, Figure 2.2.

2.2.5 Open Shell system

Open shell systems are usually modelled by a spin unrestricted model. Restricted, closed shell calculations force each electron pair into a single spatial orbital, while open shell calculations use separate spatial orbitals for the spin up and spin down electrons, α and β separately, Figure 2.1.

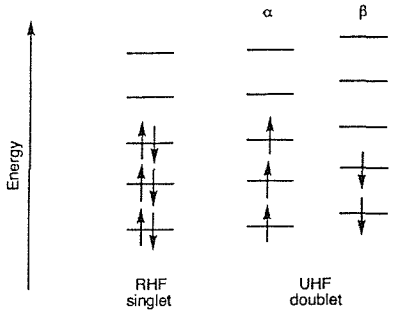

Figure 2.1: Illustrating an RHF and UHF state

Figure 2.2: Sequences of program steps required for solving the Roothaan-Hall equation.

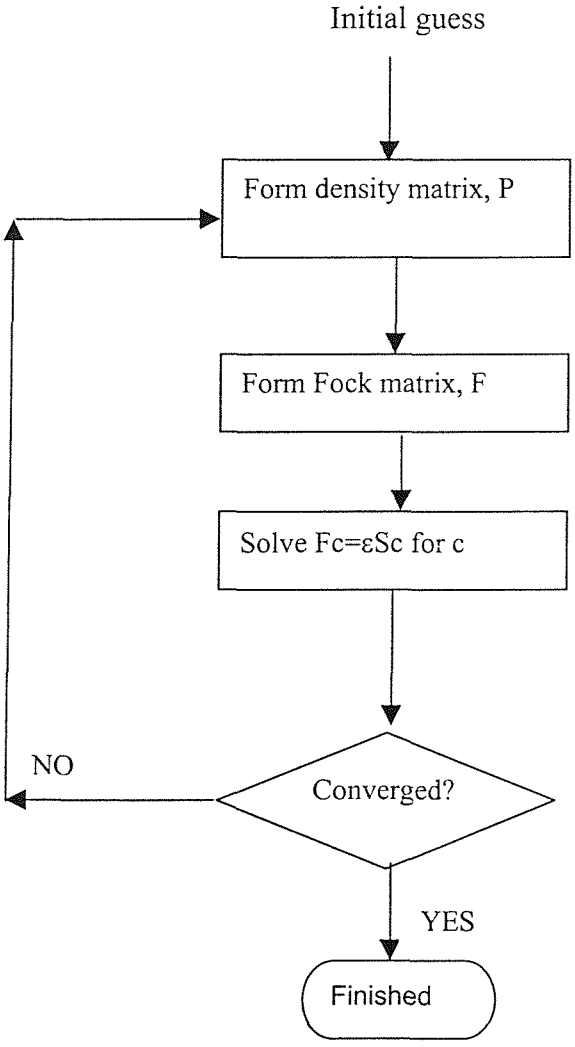

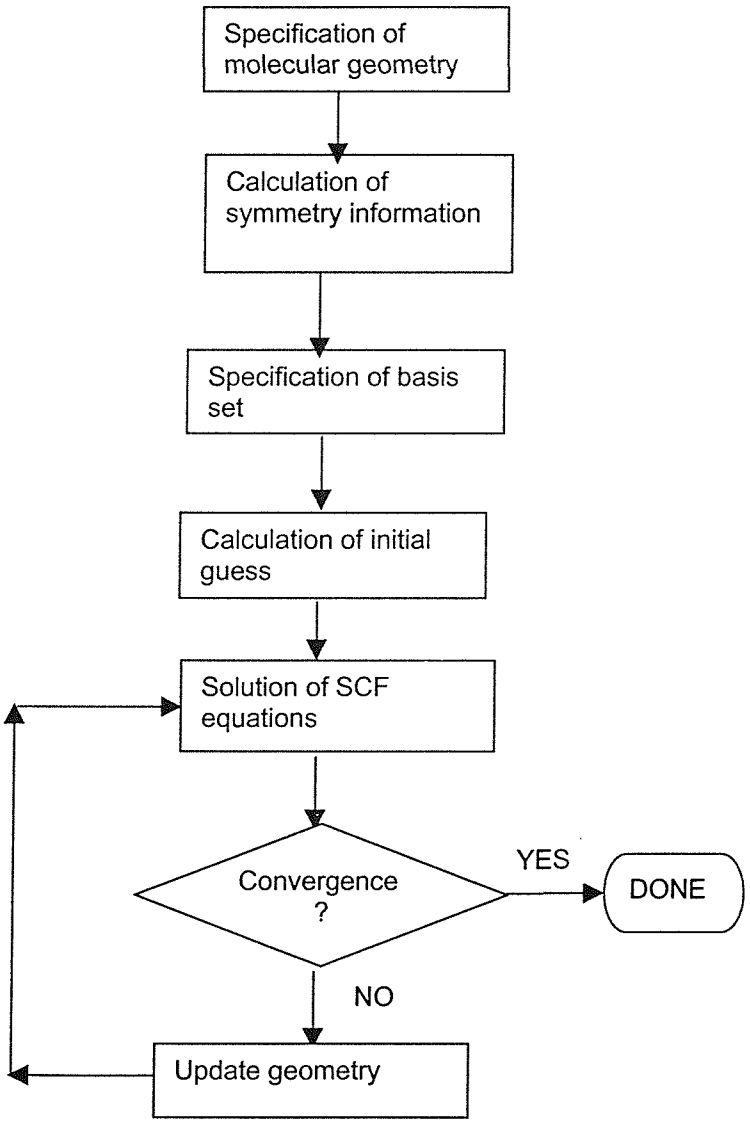

Figure 2.3: Flowchart of a typical molecular orbital approach

2.2.6 Molecular Orbital Calculation

Figure 2.3 is a flowchart, which illustrates the procedure in MO calculation. First an initial basis set is chosen and an initial set of coefficients is predicted. The energy of system is then calculated, the coefficients are varied and the energy of the system and a new set of coefficients are obtained. This iterative cycle continues until the coefficients are no longer changing and the energy of the system has reached a minimum. At this

point, the average electric field by the other electrons in the system on one given electron is said to be "self consistent", a self-consistent field (SCF) has achieved.

2.3 Basis set

A basis set is a mathematical representation to describe the orbitals within a system used to perform the theoretical calculation. The basis set assigns a group of basis functions to each atom within a molecule to approximate its orbitals. It can be interpreted as restricting each electron to a particular region of space.

An individual molecular orbital is defined as;

$$\phi_i = \sum_{\mu=1}^{N} c_{\mu i} \chi_\mu \qquad (2.7)$$

where the coefficients $c_{\mu i}$ are known as the *molecular orbital expansion coefficients* and χ_μ are the basis function.

2.3.1 Slater and Gaussian basis set

There are two main types of atomic basis functions: i). Slater-type orbitals(STO's) ii). Gaussian-type orbitals (GTO's)

i). Slater-type orbitals (STO's) can be defined as

$$X_{kmn} = N x^k y^m z^n \exp(-\xi r) \qquad (2.8)$$

The main claims to the superiority of these orbitals are their short range and long range behaviour.

ii). Gaussian-type orbitals (GTO's)

$$X_{kmn} = N x^k y^m z^n \exp(-\xi r^2) \qquad (2.9)$$

The comparison between STO and GTO was described by Figure 2.4. Since GTO has wrong behaviour both at near and far from nucleus, it was clear that more Gaussian functions were needed to describe an atomic orbital than if STO basis functions were

used. Nevertheless, the STO's are unfortunately mathematically difficult, expensive and produce unfriendly integrals.

Boys[6] first advocated the use of Gaussian-type basis functions on the ground that all the integrals required for a molecular calculation could be easily and efficiently evaluated.

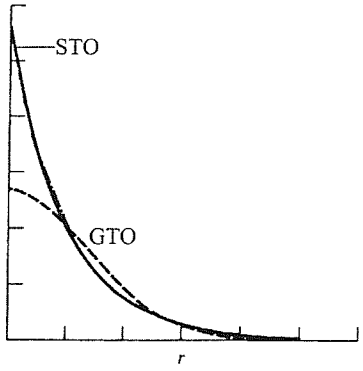

Figure 2.4: Comparison of Slater type and Gaussian type orbital.

An appropriate basis set is an important factor in ab initio calculations. Choice of basis set must be guided by considerations of the desired accuracy in the result and the computational cost. Most often, a smaller basis set yet capable of producing result equivalent to the larger one is chosen.

2.3.2 Classification of basis set

The simplest basis set, known also as a *minimal basis* set is defined, as having the minimum number of basis functions needed for each atom. For example, a minimum basis set for H and He atoms consists of a single 1s function, while a minimum basis set for C,N and O consists of five functions: 1s, 2s, $2p_x$, $2p_y$, $2p_z$. A minimal basis set is known to have several inadequacies as the Gaussian exponent is unable to expand and contract in response to differing molecular environment.

Multiple-zeta basis sets contain two or more contracted Gaussian functions. For example, a *double-zeta* basis set, such as the DZ basis set, [7]contains twice as many basis functions as the minimal one, and a *triple-zeta* basis set, such as TZ,[8] contains three times as many basis functions. Double zeta basis set provides greater flexibility in the orbital

expansion and avoids the need to reoptimise the orbital exponents when the basis set is used in a molecular calculation.[9]

A *split valence* basis set, where the core region is described by a minimal basis and the valence region is split into outer and inner parts. An example of common basis set is the 3-21G basis set, where the numbers refer to the number of Gaussian functions which make up core orbitals (3) and valence orbitals (2 inner and 1 outer).[1]

Split valence basis sets allow orbitals to change size. However, they do not change the shape of the orbital. The *polarization function,* denoted by * mark, removes this limitation by adding angular momentum beyond what is required for the ground state to the description of each atom. In other words, a polarized basis set adds *f* functions to the transition metal, *d* functions to carbon atom and *p* functions to hydrogen atom. So in the case of CH_4 for example, the used of 6-31G* basis set means a *d* functions was added to the C atom. An additional *, i.e. 6-31G**, means a polarization function, a *p* function was added to the H atoms.

A *diffuse function*, denoted by (+) symbol, is a larger version of *s* and *p* type functions which allow orbitals to occupy a larger space. A basis set with diffuse functions is important to systems where electrons are relatively far away from the nucleus such as molecules with lone pairs, anion, systems in their excited state and so on.

2.3.3 Pseudo potential basis set

Larger basis sets impose less constraint on electrons and more accurately approximate the exact molecular orbital. Understandably, larger basis sets require correspondingly larger computer resources.

Basis sets for atoms beyond the third row of the periodic table are usually handled in a different way than that of the light elements. For these atoms, electrons near the nucleus are treated in an approximate way, via *effective core potentials* (ECPs), sometimes called *pseudo potentials*. The core electrons and the core orbitals are normally assumed to have minor effects on most chemical phenomena. The ECP treatment also includes some relativistic effects which are vital in these atoms.

The ECPs have the functional form shown in equation 2.10.

$$r^2 V_l(r) = \sum A_{l,k} r_{l,k}^{n} \exp(-B_{l,k} r^2) \qquad (2.10)$$

Coefficient ($A_{l,k}$), radial exponent ($n_{l,k}$) and gaussian exponent ($B_{l,k}$) describe the radial extent and shape of the model potential. Basis sets for describing the valence electrons are of the same familiar Gaussian variety.

The ECPs basis set is only applied to the heavy atoms and it replaces the innermost core orbitals for transition metals and all core orbitals for main groups elements.[10] Thus for the d-blocks elements, ECPs basis set treats the ns, np, nd, (n+1)s, and (n+1)p electrons explicitly. The core electrons are modelled by the ECP function. Since only the valence electrons are treated in ECPs basis set calculations, the computational effort and times are greatly reduced.

2.4 Theoretical Method

In any theoretical methods, a number of desirable characteristics were set.[1] They are;

1. Unique and well defined. Theoretically, a model must be applicable to any molecular system given only the positions and kinds of nuclei and the number of electrons.
2. Continuous. The potential energy surface should be continuous with respect to changes in geometry
3. Size consistent. Errors in calculations should increase more or less in proportion to overall molecular size.
4. Variational. The total energy should represent an upper bound to which result from the exact solution to the many-electron Schrödinger equation., i.e., satisfy the variation principle.
5. Unbiased. No appeal to the "chemical intuition" should be made.

The quality of a theoretical calculation is difficult to quantify but can be viewed separately in two parts. First, from a strictly computational viewpoint, there is the sensitivity of the computed quantities to user defined features such as basis set size and

electron correlation treatment. According to the variational principle by increasing the basis set size the 'better' will be the result. The second aspect is how well the method reproduces the actual experimental result.

2.4.1 Ab initio

Ab initio which means *from the beginning or from scratch*, is a general term used to describe methods seeking solutions to the many electron Schrödinger equation on the basis of well-defined approximations such as the Born-Oppenheimer and the variational principle without empirical data, relationships or adjustable parameters. For molecules in the gas phase, ab initio calculation has become an alternative to experiments for determining accurately structures, vibrational frequencies, and electronic properties as well as intermolecular forces and reactivities.[1,11,12]

2.4.2 Semi empirical

Both ab initio and semi empirical methods are based on the principles that nuclei and electrons are distinguished from each other, electron-electron (usually averaged) and electron-nuclear interactions are explicit and that interactions are governed by nuclear and electron charges (i.e. potential energy) and electron motions.

Semi empirical methods however make use of simplified form of the Hamiltonian as well as adjustable parameters derived from experimental data to simplify the computation. The solution to the Schrödinger equation depends on having appropriate parameters available for the time of chemical system under investigation. Different empirical methods are largely characterized by their differing parameter sets.

2.4.3 Hartree Fock

The Hartree Fock energy may be written as a sum of one- and two- electron terms together with the nuclear repulsion, simplified as

$$E^{HF} = E_{nuclear} + E_{core} + E_{Coulomb} + E_{exchange} \qquad (2.11)$$

where

$E_{nuclear}$ = the nuclear repulsion energy

E_{core} = the one electron energy (kinetic plus potential energy)

$E_{Coulomb}$ = the classic coulomb repulsion energy of electrons

$E_{exchange}$ = the exchange energy resulting from the quantum nature of electrons.

The primary deficiency of HF theory is the inadequate treatment of the correlation between motions of electrons. In reality, electrons in a molecular system react to one another's motion and tend to keep out of one another's ways. The HF method, however, treated this only in an average sense, that is, each electron sees and reacts to an averaged electron density. The corresponding reduction energy is referred to as the "correlation energy".

The lack of electron correlation in the SCF method can have a significant effect when determining properties where electron-electron interactions are important. As the repulsive forces between non-bonded atoms have been incorrectly increased, the SCF method overestimates bond dissociation energies, underestimates bond lengths and overestimates the corresponding bond angles. Such defects are due to the electrons being predicted to be more densely populated than in the actual case, creating more compact bonds. Force constants are predicted to be too large, so HF theory always results in the overestimation of vibrational frequencies.

2.4.4 Correlated Method

The objective of correlated methods such as configuration interaction (CI) and many body pertubation theory (Moller-Plesset pertubation theory, MPn, where n is the order of correction), is to provide a more accurate description of electron motions. The complexity and cost of computing the energy terms increase rapidly with the order.

2.4.5 Density Functional Theory

Density functional theory (DFT) represents an alternative approach to the approximate solution of the Schrodinger equation. The DFT method is similar to the

Hartree Fock (HF) method in many ways and shares with ab initio methods that they avoid empirical relationship or adjustable parameters but using different approximations. The basic idea behind DFT is that the energy of an electronic system can be written in terms of electron probability density, ρ.[13,14] For a system with n electrons, ρ(**r**) denotes the total electron density at a particular point in the surface **r**.

The difference between the DFT method and the HF method is that the DFT method includes the electron correlation effect. Energy in density functional theory comprises of the same nuclear, core, Coulomb part as that of Hartree Fock theory, plus the exchange energy $E_X[\rho]$ and a correlation functional $E_C[\rho]$, both in the function of density matrix.

$$E^{DFT} = E_T + E_V + E_J + E_{XC} \qquad \textbf{(2. 12)}$$

where

E_T = Kinetic energy

E_V = Potential energy of electron-nuclear attraction and nuclear-nuclear repulsion

E_J = Electron-electron repulsion term (Coulombic)

E_{XC} = Exchange-correlation energy term

The E_{XC} term accounts for the exchange energy arising from the antisymmetry of the quantum mechanical wavefunction and the dynamic correlation in the motions of the individual electrons. All terms in equation 2.12, except the nuclear-nuclear repulsion, are functions of ρ, the electron density.

Hohenberg and Kohn demonstrated that E_{XC} was a function of electron density entirely.[15] They proved that the ground state molecular energy, wavefunction and related molecular properties can be described by the electron probability density ρ(x,y,z). Hence theoretically, if we know the ground state electron density ρ(x,y,z), we can calculate all the properties that are possible with Hartree-Fock theory.

As shown by Kohn and Sham[16], the exact ground state electronic energy E of n-electron system can be written as

$$E_{[\rho]} = -\frac{\hbar^2}{2m_e}\sum_i^n \psi_i^*(\mathrm{r})\nabla_i^2\psi_i(\mathrm{r}_1)\mathrm{d}\mathrm{r}_1 - \sum_{I=1}^{N}\int\frac{Z_I}{4\pi\varepsilon_0 \mathrm{r}_{1i}}\rho(\mathrm{r}_1)\mathrm{d}\mathrm{r}_1 + \frac{1}{2}\int\frac{\rho(\mathrm{r}_1)\rho(\mathrm{r}_2)e^2}{4\pi\varepsilon_0 r_{12}}\mathrm{d}\mathrm{r}_1\mathrm{d}\mathrm{r}_2 + E_{XC}$$

(2. 13)

where the one electron spatial orbital ψ_i *(i=1,2,3...n)* is the Kohn-Sham orbitals while the exact ground state charge density, ρ at location **r** is given by

$$\rho(\mathrm{r}) = \sum_{i=1}^{n} |\psi_i(\mathrm{r})|^2 \qquad \textbf{(2. 14)}$$

The first term in (2.13) represents the kinetic energy of the electrons, the second term represents the electron-nucleus attraction with the sum of over all N nuclei with atomic number Z_I, while the third term represents the Coulomb interaction between the total charge distribution (summed over all orbitals) at $\mathbf{r}_1$ and $\mathbf{r}_2$. The last term is the exchange correlation energy of the system which is also a function of density and takes into account all nonclassical electron-electron interactions.

In practice the E_{XC} term is usually approximated as an integral involving only the spin densities and their gradients:

$$E_{XC}(\rho) = f(\rho_\alpha(\mathrm{r}), \rho_\beta(\mathrm{r}), \nabla\rho_\alpha(\mathrm{r}), \nabla\rho_\beta(\mathrm{r}))\mathrm{d}^3\mathrm{r} \qquad \textbf{(2. 15)}$$

where ρ_α refers to the α spin density, ρ_β refers to the β spin density and ρ refers to the total electron density($\rho_\alpha + \rho_\beta$). E_{XC} is usually divided into separate parts, referred to as the exchange functional term and the correlation functional term.

$$E_{XC}(\rho) = E_X(\rho) + E_C(\rho) \qquad \textbf{(2. 16)}$$

Both terms can be of two distinct types: the *local* functional, which depends only on the electron density ρ and the *gradient corrected* functional which depends on both ρ and its gradient $\nabla\rho$. As described previously, the HF energy also comprises of an exchange term as part of its formula with $E_c = 0$. Many different density functionals are currently available, using different formulae to represent E_{XC}. Such functionals tend to be the combination of an exchange functional and a correlational functional.

Popular exchange functionals are the Slater (S) functional, which corresponds to the free electron gas,[17] Becke (B) functional, which includes corrections to the electron density gradient[18] and Becke-three parameter hybrid functional which includes the mixture of Hartree Fock and DFT exchange functional along with DFT correlation functional.[19]

Conceptually the E_{XC} in DFT method was defined as

$$E_{XC} = c_{HF} E_X^{HF} + c_{DFT} E_{XC}^{DFT} \quad (2.17)$$

where c's are constants. In the Becke-style three parameter functional (B3LYP), also known as the *hybrid functionals* and which has been proven to be superior to the other DFT functionals, the energy is defined as

$$E_{B3LYP}^{XC} = E_{LDA}^{X} + c_0(E_{HF}^{X} - E_{LDA}^{X}) + c_X \Delta E_{B88}^{X} + E_{VWN3}^{C} + c_C(E_{LYP}^{C} - E_{VWN3}^{C}) \quad (2.18)$$

where the energy terms are the Slater exchange (E_{LDA}), the Hartree Fock exchange (E_{HF}), Becke's 1988 exchange functional correction (E_{B88}), the gradient corrected correlation functional of Lee, Yang, and Parr (E_{LYP}) and the local correlation (E_{VWN}). The parameter c_0 allows the admixture of Hartree Fock and LDA local exchange to be used. The Becke's gradient correction to LDA exchange is also included, scaled by parameter c_X. Similarly, the VWN3 local correlation functional is used, and may be optionally corrected via the parameter c_C.

The value of the coefficients determined by Becke are:

c_0 =0.20

c_X=0.72

c_C=0.81

Good correlation functionals include that of Lee, Yang and Parr (LYP) and Perdew (P86).[20]

Theoretical calculations which utilise DFT methods are now perhaps amongst the most frequently performed because of their relatively low cost and greater accuracy. For example study of the excitation and ionization of the atoms of the first transition series[21] showed that the Becke exchange functional coupled with the Lee, Yang and Parr functional- BLYP method gave exceptional results for the ionization energies (mean errors of ~0.1 eV) and acceptable results for the excitation energies (mean errors of ~0.5eV) compared to the mean errors of ~1.7 eV and ~0.8 eV, respectively, in the HF method. This level of agreement was also been reported by others using different exchange and correlation functionals.[22,23] Bond energy calculation using DFT methods also shows better accuracy when compared to the HF method. Studies on the ScF_3, TiF_4, VF_5 and CrF_6 series showed the BLYP method overestimated the bond energies by ~8

kcal/mol,[24] the B3LYP method has a remarkable error of ~1-2 kcal/mol,[25,26] while the error for HF method is ~30-70 kcal/mol. Rica and Bauschlicher[27] reported similar result in a study of binding energies on series of metal carbonyls.

Calculations that involve transition metal or heavier main group elements are computationally demanding in term of CPU time and computer resources. The demand can be further reduced considerably by the use of ECP basis set. The success of using ECP basis sets is well documented and their use in conjunction with density functional theory methods is also found as reasonably adequate.[28, 29, 30,31]

2.5 Useful properties calculation

2.5.1 Single point calculation

Single point energy calculations can be used to calculate properties of the current geometry of a model. The values of these properties are dependent on where the model currently lies on the potential surface. For example, a single point energy calculation at a global minimum provides information about the model in its most stable conformation while a single point calculation at a local minimum provides information about the model in one of many stable conformations. Single point energy calculations may be performed either before or after performing an optimization.

2.5.2 Geometry optimization

Geometry optimization is a technique used for locating a stable conformation of a model. As a general rule, this should be performed before performing additional computations or analyses of a model. Theoretically, geometry optimization means the geometry will be adjusted until a stationary point on a potential surface is found. In other words, the calculations are performed to locate the molecule structure with the lowest energy.

Geometry optimizations are iterative and begin at the molecular structure specified as its input. First, a single point energy calculation is performed on the starting geometry. Then, the coordinates for some subset of atoms are changed and another

single point energy calculation is performed to determine the energy of that new conformation. The first or second derivative of the energy with respect to the atomic coordinates then determines how large and in what direction the next increment of geometry change should be. Subsequently, the change is made. Following the incremental change, the energy and energy derivatives are again determined and the process continues until convergence is achieved, at which point the minimization process terminates, Figure 2.2. [1,32, 33]

The equilibrium geometry of each isomer of a molecule corresponds to a valley or a minimum on the potential energy surface. The position of the minimum yields the bond lengths and angles of the molecules with the lowest energy locally or globally.

The first derivatives of the potential energy surface are known as the gradients while the forces on the atoms or nuclei in a molecule are equal to the negative of the gradients. Since the forces or gradients are zero at minima, transition state and saddle point, they are called the stationary points. In order to distinguish between a minimum, a saddle point or a transition state, we need the second derivatives of the energy.

The matrix of the second derivatives of the potential energy is also called the Hessian matrix or the force constant matrix. If the Hessian or the force constant matrix is transformed into mass weighted coordinates and diagonalized, then the eigenvectors are the normal modes of vibration and the eigenvalues are proportional to the squares of the vibrational frequencies.

For a potential energy surface to have a minimum with respect to a particular coordinate, the second derivative of the surface must be positive, to be a maximum, the second derivative must be negative. A minimum must have all its vibrational frequencies real that, is no imaginary frequencies.

2.5.3 Mulliken population analysis

An additional property of considerable interest is the charge distribution as derived from Mulliken population analysis.[34] However, the charge on an atom in a molecule is not subject to experimental measurement nor can it be defined. Nevertheless, Mulliken population analysis is widely empolyed as a basis for qualitative discussions of

reactivity and bonding. In addition to that, it is also useful in order to give quantitative meaning to concept such as electron donating and electron withdrawing ability.[1]

The electron density function, $\rho(r)$ is a three dimensional function that defines $\rho(r)$ as the probability of finding an electron in a small volume element, dr, at some point in space **r**. Normalization requires that

$$\int \rho(r) dr = n$$

where n is the total number of electrons. The Mulliken electron population is thereby defined as

$$\int \rho_r dr = \sum_{\mu}^{N} \sum_{\nu}^{N} P_{\mu\nu} S_{\mu\nu} = n$$

The gross charge on atom A is the sum of the nuclear and electronic contributions. Total atomic charge on A is defined as Z_A-ρ_A where Z_A the atomic number of A.

2.5.4 Vibrational frequencies

2.5.4.1 Introduction

Vibrational spectra are not only good tests of a given theoretical model but they can also aid the identification of unusual gas-phase or matrix isolated species. Calculated normal mode vibrational frequencies play several important roles in the use of theory as a means of characterizing molecular surfaces. This includes the distinction of local minimas which have all real frequencies, from saddle points which have imaginary frequency (or frequencies).

In addition to that, for stable but highly reactive or short lived molecules, they provide a means of identification as the appearance of even a single IR line may be an identification that new molecule has been formed. The second main use of vibrational frequencies is for directly comparing and aiding in assignment of infrared spectra. Vibrational frequencies are also used in determination of range of thermodynamics quantities such as zero point energy. These properties are subjected to experimental verification and can therefore be used as the yardstick by which the 'quality' of a given theoretical method can be judged.

Experimental vibrational frequencies usually refer to the observed fundamental frequencies, anharmonic rather than the harmonic frequencies. Theoretical vibrational frequencies on the other hand, are calculated on the basis of a harmonic model. The calculated frequencies are harmonic and must therefore be corrected for anharmonicity before comparing the data with the experimental values.

The comparison between experimental frequencies and the calculated value is the only direct way in which we can obtain information about the accuracy of the computational method. So accordingly we studied molecules for which experimental vibrational frequencies are available.

Ab initio vibrational frequencies (ω) are typically larger than the fundamentals ($\tilde{\nu}$) observed experimentally.[1] A major source of this disagreement is the neglect of the anharmonicity effect in the theoretical treatment, in addition to the incomplete incorporation of electron correlation. However, this overestimation tends to be relatively uniform, therefore a frequency scaling factor is usually applied, allowing good overall agreement between the scaled theoretical harmonic frequencies and the scaled anharmonic experimental frequencies.[1]

Vibrational frequency computation using semiempirical methods such as AM1 and PM3 are attractive due to their lower computational cost. However, in contrast to the HF methods where considerable attention was given on the scaling factor, the semiempirical methods receive less systematic analysis on the performance in vibrational frequency computation. The electron correlation method MP2, however does not appear to offer significant improvement to the HF method while in the case of quadratic configuration method, the improvement comes at a significant computational cost. Table 2.1 summarizes the scaling factor and rms based on the work on a set of 122 molecules by Scott and Radom.[35]

Recent studies of the vibrational spectra of transition metal complexes suggest that DFT can be applied successfully to the calculation of force fields and vibrational frequencies[36, 37,38]. The inclusion of gradient corrections[39] has raised the accuracy of such calculation to a level which in the past can only be reached by high level methods at a very high computational effort.

The calculation of vibrational frequency[40] using DFT method is facilitated by the availability of the analytical second derivative technique. Several recent studies have shown that vibrational frequencies calculated by DFT methods agree well with the experiment and are much superior to the HF method.[41, 42, 43]

Table 2.1: Frequencies scaling factors and overall root means square error for semiempirical method, HF, Moller-Plesset, Quadratic Configuration Interaction and Density Functional Theory method.[35]

Method	scale factor‡	$rms_{ov}(cm^{-1})$ *
AM1	0.9532	126
PM3	0.9761	159
HF/3-21G	0.9085	87
HF/6-31G*	0.8953	50
HF/6-31+G	0.8970	49
HF/6-31G**	0.8992	53
HF/6-311G**	0.9051	54
MP2/6-31G*	0.9427	61
MP2/6-31+G	0.9434	63
MP2/6-31G**	0.9370	61
MP2/6-311G**	0.9496	60
QCISD/6-31G*	0.9537	37
B-LYP/6-31G*	0.9945	45
B-LYP/6-31G(df,p)	0.9986	42
B-P86/6-31G*	0.9914	41
B3-LYP/6-31G*	0.9614	34
B3-P86/6-31G*	0.9558	38
B3-PW91/6-31G*	0.9573	34

‡Scale factor λ is defined by $\lambda = \sum_{i}^{all} \omega_i^{theo} \nu_i^{exp} / \sum_{i}^{all} (\omega_i^{theo})^2$ where ω_i^{theo} and ν_i^{exp} are the *i*th theoretical harmonic and *i*th experimental fundamental frequencies in cm^{-1}, respectively.

* Overall root-mean-square, rms_{ov} error is defined by $rms_{ov} = (\sum_{1}^{n_{all}} \Delta_{min} / n_{all})^{\frac{1}{2}}$ where $\Delta_{min} = (\lambda\omega_i^{theo} - \nu_i^{exp})^2$ and n_{all} is modes of all molecules.

2.5.4.2 The Simple Harmonic Oscillator

Many volumes are dedicated to the subject of vibrational spectroscopy, such as that by Gans.[44] Atkins[2] and Hollas[45] also include discussions in their more general books.

To a first approximation, a vibrating diatomic molecule may be treated as a simple harmonic oscillator, Figure 2.5. Figure 2.6 illustrates the ball and spring model which is adequate for an approximate treatment of vibrations of a diatomic molecule. For small displacements, the stretching and compression of the bond, represented by the spring, obeys Hooke's Law.

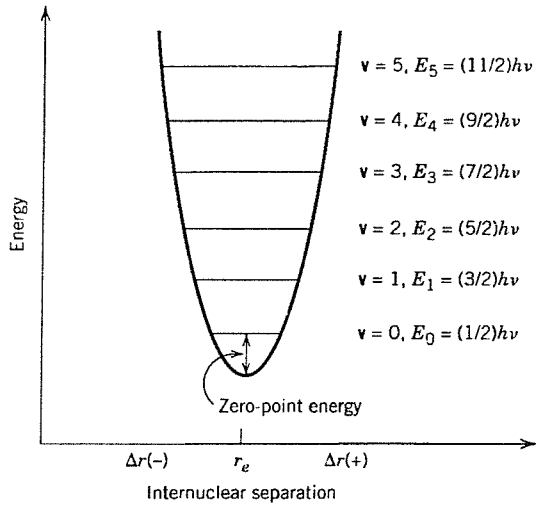

Figure 2.5: Energy level of a Harmonic Oscillator

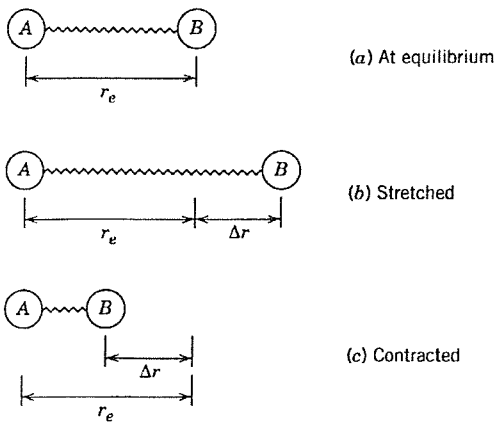

Figure 2.6: Model of a diatomic molecule, with the bond represented as a spring.

For such as a system

$$\text{Restoring force, } F = -\frac{dV(x)}{dx} = -kx \qquad \textbf{(2. 19)}$$

where V is the potential energy, k is the force constant and x is the displacement from equilibrium distance, (r- r_e). If

$$V(x) = -\int F\,dx \qquad \textbf{(2. 20)}$$

where V(x) is the potential energy, then

$$V(x) = \int kx\,dx \qquad \textbf{(2. 21)}$$

so

$$V(x) = \tfrac{1}{2}\,kx^2 \qquad \textbf{(2. 22)}$$

The Hamiltonian, H, for simple harmonic oscillator, given by the sum of the kinetic and potential energies is thus

$$H = \frac{-\hbar^2}{2\mu}\frac{d^2}{dx^2} + \frac{1}{2}kx^2 \qquad \textbf{(2. 23)}$$

where μ is the reduced mass of the molecule,

$$\mu = \frac{m_1 m_2}{(m_1 + m_2)} \qquad \textbf{(2. 24)}$$

When substituted into the generalised time independent Schrödinger Equation

$H\Psi_n = E_n\Psi_n$ will lead to

$$\frac{d^2\Psi}{dx^2} + \left(\frac{2\mu E_n}{\hbar^2} - \frac{\mu k x^2}{\hbar^2}\right)\Psi_n = 0 \qquad \textbf{(2. 25)}$$

from which it can be shown that

$$E_n = h\nu(v + \frac{1}{2}) \qquad \textbf{(2. 26)}$$

where ν is the classical vibration frequency given by

$$\nu = \frac{1}{2\pi}\left(\frac{k}{\mu}\right)^{\frac{1}{2}} \qquad \textbf{(2. 27)}$$

As expected, the frequency increases with k (the stiffness of the bond) and decreases with μ. More commonly, though, we use vibration wavenumber, ω, rather than frequency, so

$$E_n = hc\omega(v+1/2) \qquad \textbf{(2. 28)}$$

The vibrational quantum number v can take the values 0,1,2,...
This equation shows the vibrational level to be equally spaced, by hcω and that the $v = 0$ level has an energy ½ hcω, known as the zero point energy.

2.5.4.3 Calculation of Harmonic Vibrational Frequencies

The total energy of a molecule comprising N atoms near its equilibrium structure may be written as

$$\mathbf{E} = \mathbf{T} + \mathbf{V} = \frac{1}{2}\sum_{i=1}^{3N} q_i^2 + V_{eq} + \frac{1}{2}\sum_{i=1}^{3N}\sum_{j=1}^{3N}\left(\frac{\partial^2 V}{\partial q_i \partial q_j}\right)_{eq} q_i q_j \qquad \textbf{(2. 29)}$$

Here, the mass-weighted cartesian displacements, q_i, are defined in terms of the locations x_i of the nuclei relative to their equilibrium positions $x_{i,eq}$ and their masses M_i.

$$q_i = M_i^{1/2}(x_i - x_{i,,eq}) \qquad \textbf{(2. 30)}$$

V_{eq} is the potential energy at the equilibrium nuclear configuration and the expansion of the vibrational energy [2.29] in terms of a power series is truncated at the second order. For such a system, the classical-mechanical equation of motion takes the form of

$$\ddot{q}_j = -\sum_{i=1}^{3N} f_{ij} q_i \qquad j = 1,2,....3N \qquad \textbf{(2. 31)}$$

The f_{ij}, termed *quadratic force constants*, is the second derivatives of the potential energy with respect to mass-weighted cartesian displacements, evaluated at the equilibrium nuclear configuration, that is

$$f_{ij} = \left(\frac{\partial^2 V}{\partial q_i \partial q_j}\right)_{eq} \qquad \textbf{(2. 32)}$$

The f_{ij} may be evaluated by numerical second differentiation,

$$\frac{\partial^2 V}{\partial q_i \partial q_j} \cong \frac{\Delta(\Delta V)}{\Delta q_i \Delta q_j} \tag{2.33}$$

by numerical first differentiation of analytical first derivatives,

$$\frac{\partial^2 V}{\partial q_i \partial q_j} \cong \frac{\Delta(\partial V / \partial q_j)}{\Delta q_i} \tag{2.34}$$

or by direct analytical second differentiation, [2.32]. The choice of procedure depends on the quantum mechanical model employed, that is, single-determinant or post Hartree-Fock, and practical matters such as the size of the system.

Equation [2.31] may be solved by standard method to yield a set of 3N normal mode vibrational frequencies. Six of these (five for linear) will be zero as they correspond to translational and rotational rather than vibrational degree of freedom.

2.5.4.4 Harmonic and Anharmonicity

The harmonic oscillator model is in fact in poor agreement with reality, as real molecules are not perfect harmonic oscillators. The variation of the potential energy of the system with internuclear separation usually is not a systematic parabola but rather tends to have the skewed appearance of a Morse curve, as shown in Figure 2.7.

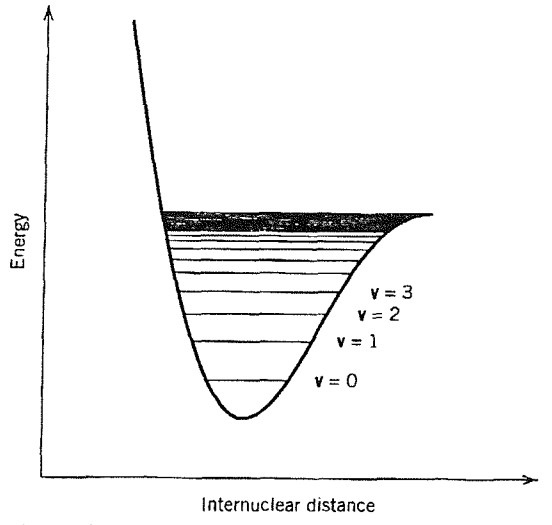

Figure 2.7: Energy level of Morse potential. Note the successively smaller separations between the energy states as v increases (bottom to top).

By solving the Schrödinger Equation for the Morse potential, energy states for the anharmonic oscillator are given by;

$$E(v) = h\nu(v + \frac{1}{2}) - h\nu x_e(v + \frac{1}{2})^2 + ... \quad (2.35)$$

where χ_e is called the anharmonicity constant.

Anharmonicity affects molecular vibrations in two important ways.[39] First, the selection rule derived for the harmonic oscillator, $\Delta v = \pm 1$, ceases to be a rigorous selection rule, and transition with $\Delta v = \pm 2$ become "allowed". Secondly, the vibrational energy is not spaces apart equally by the quantity *hv*. Overtones and combination bands are usually associated with anharmonicity.

2.5.5. Zero point Energy calculation

Experimental reactions and measurements are performed at a temperature higher than 0K on vibrating molecules. Zero point energy is the minimum energy the molecule may have even at the absolute zero temperature and is a consequence of uncertainty principle. Theoretical energies correspond to a stationary molecules in the gas phase at 0 K. It is necessary to account for these facts when comparing some calculated properties such as interaction energies with the equivalent experimental data.

2.6 References

1. W. J. Hehre, L. Radom, P. V. R. Schleyer and J. A. Pople, *Ab Initio Molecular Orbital Theory*, Wiley, New York, 1986.

2. See for example: P. W. Atkins and R. S. Friedman in *Molecular Quantum Mechanics*, 3rd ed., Oxford University Press, Oxford, 1997.

3. J. C. Slater, *Phys. Rev.*, 1929, **34**, 1293; 1930, **35**, 509.

4 . C. C. J. Roothaan, *Rev. Mod. Phys.*, 1951, **23**, 69.

5. G. G. Hall, *Proc. Roy. Soc. London A*, 1951, **205**, 541.

6. S. F. Boys, *Proc. R. Soc. London A*, 1950, **200**, 542.

7. T. H. Dunning, Jr., *J. Chem. Phys.* 1970, **53**, 2823; T. H. Dunning, Jr. and P. J. Hay in *Methods of Electronic Structure Theory*, H. F. Schaefer III, Ed., vol. 2, Plenum Press, 1977.

8. T. H. Dunning, Jr., *J. Chem. Phys.*, 1971, **55**, 716.

9. F. Jensen in *Introduction to Computational Chemistry*, John Wiley & Sons, Chichester, 1999.

10. P. J. Hay and W. R. Wadt, *J. Chem. Phys.*,1985, **82**, 270, 284, 299.

11. H. F. Schaefer, Applications of Electronic Structure Theory; *Modern Theoretical Chemistry*, Plenum, New York, 1977, vol.4.

12. P. Cársky, M. Urban, Ab Initio Calculations. Method and Applications in Chemistry, *Lect. Notes Chem.*, 1980, 16.

13. T. Ziegler, *Chem. Rev.*, 1991, **91**, 651.

14. R. G. Parr and W. Yang, *Density Functional Theory of Atoms and Molecules*, Oxford University Press, Oxford, 1989.

15. P. Hohenberg and W. Kohn, *Phys. Rev. B,* 1964, **136**, 864.

16. W. Kohn and L. J. Sham, *Phys. Rev. A*, 1965, **140**, 1133.

17. S. J. Vosko, L. Wilk and M. Nusair, *Can. J. Phys.*, 1980, **58**, 1200.

18. A. D. Becke, *Phys. Rev. B*, 1988, **38**, 3098.

19. A. D. Becke, *J. Chem. Phys.*, 1997, **107**, 8554.

20. C. Lee, W. Yang, and R. G. Parr, *Phys. Rev. B*, 1988, **37**, 785.

21. T. V. Russo, R. L. Martin and P. J. Hay, *J. Chem. Phys.*, 1994, **101**, 7729.

22. F. Kutzler and G. Painter, *Phys. Rev. B*, 1991, **43**, 6865.

23. J. P. Perdew, J. Chevary, S. Vosko, K. Jackson, M. Pederson, D. Singhand and C. Fiolhas, *Phys. Rev. B*, 1992, **46**, 6671.

24. T. V. Russo, R. L. Martin and P. J. Hay, *J. Chem. Phys.*, 1995, **102**, 8023.

25. A. D. Becke, *J. Chem. Phys.*, 1993, **98**, 5648.

26. P. Stevens, F. Devlin, C. Chabarowski and M. J. Frisch, *J. Phys. Chem.*, 1994, **98**, 11623.

27. A. Ricca and C. W. Bauschlicher, *J. Phys. Chem.*, 1994, **98**, 12899.

28. C. Sosa and C. Lee, *J. Chem. Phys,* 1993, **98**, 8004.

29. T. Ziegler, *Can. J. Chem.,* 1995, **73**, 743.

30. J. Andzelm and E. Wimmer, *J. Chem. Phys.,* 1992, **96**, 1280.

31. T. V. Russo, R. L. Martin and P. J. Hay, *J. Phys. Chem.*, 1995, **99**, 17085.

32. H. B. Schlegel, *Modern Electronic Structure Theory*, D. R. Yarkony (ed.) World Science Publisher, Singapore, 1994, pg. 459-499.

33. H. B. Schlegel, *New Theoretical Concepts for Understanding Organic Reaction*, J. Bertran and I. G. Csizmadia (eds.) Kluwer Academic Publisher, The Netherland, 1989.

34. R. S. Mulliken, *J. Chem. Phys.* , 1955, **23**, 1833, 1841, 2338, 2343.

35. A. P. Scott and L. Radom, *J. Phys. Chem.*, 1996, **100**, 16502.

36. L .Fan and T. Ziegler, *J. Phys. Chem*, 1992, **96**, 6937; A. Berces, T. Ziegler and L. Fan, *J. Phys. Chem.,* 1994, **98**, 1584; A. Berces and T. Ziegler, *J. Phys. Chem.,* 1994, **98**, 13233; A. Berces and T. Ziegler, *Top. Curr. Chem.*, 1996, **182**, 41.

37. C. Sosa, J. Andzelm, B. C. Elkin, E. Wimmer, K. D. Dobbs and D. A. Dixon, *J. Phys. Chem.,* 1992, **96**, 6630.

38. V. Jonas and W. Thiel, *J. Phys. Chem. A*, 1999, **103**, 1381;V.Jonas and W. Thiel, *Organometal.*, 1998, **17**, 353;V.Jonas and W. Thiel, *J. Phys. Chem.* , 1996, **105**, 3636.

39. P. Hohenberg, W. Kohn, *Phys Rev. B.*,1964, **136**, 864; W. Kohn, L. J. Sham, *Phys Rev. A.*, 1965, **140**, 1133.

40. B. G. Johnson and M. J. Frisch, *J. Chem. Phys.*, 1994, **100**, 7429.

41. J. A. Pople, *Israel J. Chem.*, 1993, **33**, 345.

42. B. G. Johnson, P. M. W. Gill and J. A. Pople, *J. Phys. Chem.*, 1993, **98**, 5612

43. M. W. Wong, *Chem. Phys. Lett.*, 1996, **256**, 391.

44. P. Gans in *Vibrating Molecules*, Chapman and Hall, London, 1971.

45. J. M. Hollas in *Modern Spectroscopy*, John Wiley and Sons, Chichester, 1987.

Chapter 3

Studies of rhodium gem dicarbonyl, a surface species

Chapter Three : DFT calculation on rhodium *gem* dicarbonyl

3.0 Introduction

The manner in which transition metal-based catalysts are bonded to support materials is of a fundamental interest in the field of heterogeneous catalysis. For many systems, the metal-support interactions are known to play important roles in their reactivity. Unfortunately, the interactions between functional groups on the surface of a support and single metal atoms aggregate remain ambiguous.

CO molecules have been widely used to probe the structural and electronic properties of the supported metal particles owing to their high sensitivity of the C-O stretching frequency of ν(CO) to the oxidation states of metal particles,[1] their size[2,3,4]and the strength of metal support interactions.

Various attempts are made to describe the bonds in terms of a "surface molecule", i.e. by coupling the adsorbate to only limited number of neighbouring surface atoms or by modelling it with small clusters which then, for example, be treated by computational method such as the HF and the DFT methods.

The actual valuable advantage of computational investigations is that they allow the separation of different effects. For example, computational investigations help to elucidate how such species are arranged as the ligand(s) change or when they are adsorbed on different sites of supports.

This work is devoted to the analysis of geometrical parameters, electronic structure and vibrational frequencies of rhodium *gem* dicarbonyl; of a particular interest is how these properties depend on different surface ligands, i.e. OH, O and Cl.

3.1 Theoretical approach

While there have been many calculations for adsorbates on transition metal clusters that include correlation effects, the amount of work applied to transition metal support systems is still relatively small. Rhodium also had received considerable attention from the theoretical chemists.[5,6,7] Like all transition metal containing systems, the inclusion of electron correlation effects has been found to be necessary to obtain reliable geometries, total energies and vibrational frequencies.[8,9] Thus, calculations at a

higher level than the Hartree Fock method are required. The agreement between the DFT method and the experimental results indicates that the DFT method can be a powerful tool for the investigation.[10,11,12]

The calculated frequencies essentially reproduced fundamentals observed in experimental infrared and Raman spectra. It is shown that the DFT frequency calculations can be a very important and a valuable tool to assist in analysing and assigning measured infrared and Raman spectra and to predict vibrational frequencies for large transition-metal compounds.

In the future, with the development and the availability of computer power and resources, it is anticipated that the theoretical methods will help to define the reaction intermediates on supported metal catalysts. This is due to the fact that the intermediates molecules could be highly reactive and unstable species and may be beyond the reach of experimental methods.

A review on the theoretical investigation on metal-support interactions[13] shows that although this area of research has received some considerable attention, the theoretical calculations have not "been performed on a level of sophistication that allows for reliable determination of total energies in order to predict geometries at interfaces or of metal particles on a supported surface."

There have been several theoretical studies on the free rhodium *gem* dicarbonyl species with the first possibly by McKee et al, [14] who used the Hartree Fock method. However, this method inaccurately calculates the structure of this species. With the advance of the DFT method, as far as we are aware, only Blyholder ever reported the theoretical studies on $Rh(CO)_2$.[15] This author, however, had used the modest Lanl1DZ basis set. There have been no reported computations considering the presence of chlorine.

3.2 Model systems

Metal cluster models are widely used to mimic surface phenomena. Usually, in transition metal cluster, the cluster size is limited in accordance to the method used and

the computational resources available. Obviously, the number of metal atoms used are much smaller than those are in the real experimental or industrial use.

The silica surface is modelled by a truncated silica cluster which is saturated simply by hydrogen atoms.[16,17,18] The use of three hydrogen atoms to truncate the silica cluster is regarded as a minimal first approximation to silica structure. Two types of $Rh(CO)_2$ were studied in this work 1). $Rh(CO)_2(XSiH_3)$ and 2). $Rh(CO)_2(Cl)(XSiH_3)$ where X=O, OH and Cl, Figure 3.1.

Structures were done based on the argument as to whether chlorine remained terminally bonded to the rhodium or not. Another possibility is that the chlorine atom may be absorbed to the surface. In addition to that, the surface ligands O^{-2} and ^{-}OH are indistinguishable by the EXAFS spectroscopy,[19] if they presented similar Rh-O distances, so both structures are considered here.

Throughout, the rhodium is assumed to have the +1 oxidation state, so both electroneutral, which are believed to exist in real metal support frameworks, and charged models were considered here. A full geometry optimization was done and where possible a symmetry constraint was imposed. No constraint was applied on the silica model.

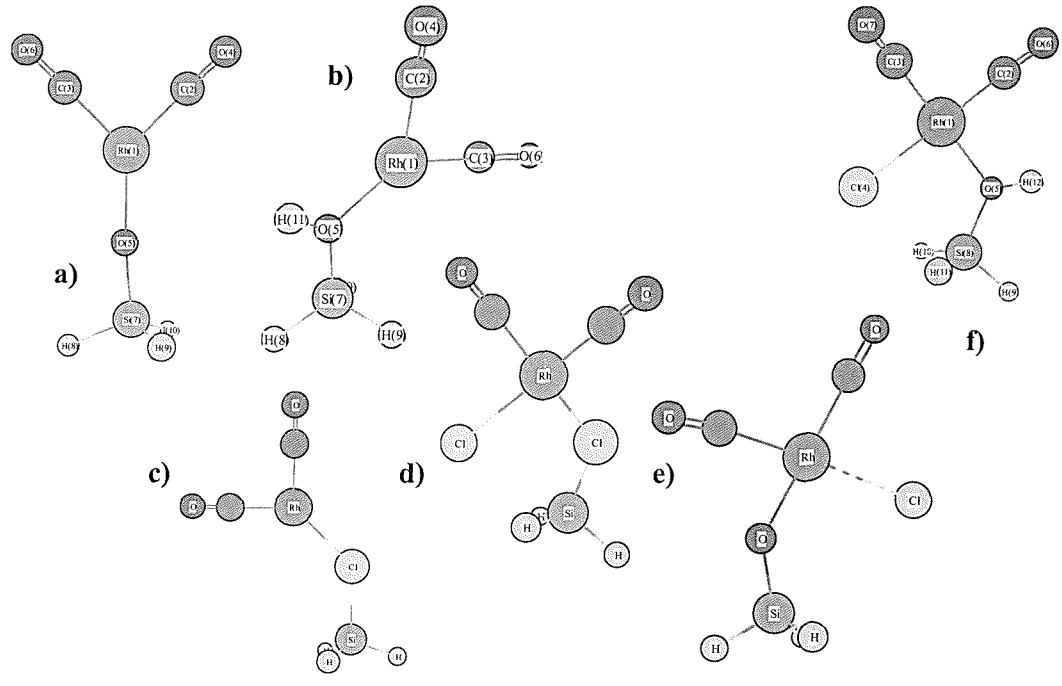

Figure 3.1 : Models of supported rhodium *gem* cabonyl **a**). $[Rh(CO)_2(OSiH_3)]$ **b** $[Rh(CO)_2(OHSiH_3)]^{+1}$ **c**). $[Rh(CO)_2(ClSiH_3)]^{+1}$ **d**). $[Rh(CO)_2(Cl)(ClSiH_3)]$ **e**). $[Rh(CO)_2(Cl)(OSiH_3)]^{-1}$ **f**). $[Rh(CO)_2(Cl)(OHSiH_3)]$

3.3 Aim

This work is devoted to the analysis of the adsorption properties such as geometrical parameters, electronic structures and vibrational frequencies of the CO of the rhodium *gem* dicarbonyl species. In addition to that, one of the ultimate goals in the application of surface science to fundamental catalytic research is the identification of intermediates during an ongoing reaction on a catalyst particle while characterising the atomic structure of surface species at the same time.

For these purposes, we have studied this system using the density functional theory method (DFT), which includes electron correlation effects. The results presented here are for the study of single rhodium *gem* dicarbonyl species on silica. The use of SiH_3 as the model of bulky silica surfaces will also be discussed.

The purpose of this calculation is to provide information about the nature of the chemical bonding on the surface, the direction of charge flows at the metal- "model" support interface, effect of different ligand(s) to ν(CO) shift and how the support affects the bonding within the adsorbed molecules.

Furthermore, this work is also intended to provide information about the nature of bonding at the surface with the help of C-O vibrational frequency as the probe molecule. In addition to that, this work explores the use of small cluster systems to model the larger one in reality.

3.4 Computational details

3.4.1 Calibration

Since the dimer is usually taken as the reference compound in Rh/support studies, thus facilitating EXAFS measurements, we have also included the study of this structure as a standard reference. Besides, the properties of the parent compound of $[Rh(CO)_2Cl]_2$, has been characterised by X-ray diffraction, infra red (IR) and EXAFS spectroscopy.

Other systems studied in this work are rhodium carbonyl compounds as well as some well studied metal carbonyls, such as Group 8 metal tetracarbonyl and rhodium

carbonyls and their analogues. In addition to that, a test was also performed to study the effect of basis sets on ν(CO) of $[Rh(CO)_2Cl_2]^{-1}$.

a). Rhodium dimer

The aim of this calibration is to estimate the accuracy of each method and basis set applied. Geometry optimization and frequencies calculation were performed using the DFT-Becke88[20] Lee-Yang and Parr and the Becke3LYP methods. The basis sets used for comparison were:

a). the standard 6-31G* basis set for C, O and Cl and LanL2DZ[21] basis set for Rh
b). DZP basis[22] set for Cl and TZ basis set[23] for C and O atoms, and LanL2DZ basis set for Rh atoms
c). Lanl2DZ basis set for all atoms

b). Metal carbonyls

Frequency analysis was performed on the optimized structures, using the appropriate point group. We adopt the standard 6-31G* basis set for C and O atoms while the ECP basis set, Lan2DZ by Hay and Wadt, was applied for the metal atoms.

c). $[Rh(CO)_2Cl_2]^{-1}$

The aim of this calibration part is to test the accuracy of the method by varying the basis set and employing the Becke's 1988 gradient corrected exchange functional and correlation functional of Lee Yang and Parr.

3.4.2 Supported rhodium *gem* dicarbonyl

The calculations were carried out at the Density Functional level of theory employing Becke hybrid three-parameter exchange functional and using the Lee, Yang

and Parr correlation functional, B3LYP[24,25] as implemented on the Gaussian94 program[26] using Gibbs Power Challenge machines.

The same method, but using the LanL2DZ pseudopotential basis set[21,26] on all atoms except H, was used to generate various stable structures by a scanning process that represents internal rotation at Rh-O-Si-H and Si-O-Rh-Y (Y=Cl or C) dihedral angles. Geometries for the lower energy conformers were next used as the trial geometry to initiate optimisation processes. The final lowest energy was then taken to be the lowest energy conformation for the method and the basis set used. The verification of the final structures a minimum on the PES was made by a vibrational frequency calculation which should yield an all positive frequencies.

The vibrational frequencies were calculated using the second derivative method available on the Gaussian94 package. The calculation of vibrational frequency using the DFT method is facilitated by the availability of analytical second derivative techniques.

The 6-31G basis sets were used for silica, carbon, chlorine and oxygen atoms. Throughout this work, the ECP basis set that of Hay and Wadt[21] was employed on the rhodium atom.

3.5 Results and Discussion

3.5.1 Calibration results

Table 3.1 gives the results of geometrical parameters and ν(CO) of $[Rh(CO)_2Cl]_2$ using various basis sets at two DFT levels; a) B3LYP b). BLYP methods. Pertinent geometry and calculated ν(CO) for the free rhodium *gem* dicarbonyl, rhodium dimer and the surface species $Rh(CO)_2Cl_2^{-1}$ are given in Table 3.1. The crystalline structures of the dimer[27] is presented in Figure 3.2

Table 3.1: Comparing B3LYP and BLYP/6-31G* geometric parameters and ν(CO) frequencies of Rh dimer and its related structures

Method	Basis set	Rh-C (Å)	C-O (Å)	Rh-Cl (Å)	CRhC (°)	$\nu(CO)_{calc}$ cm^{-1}	Scaled, cm^{-1}
$[Rh(CO)_2Cl]_2$							
B3LYP	6-31G*	1.8725	1.1466	2.4517	91.0	2124, 2170, 2183	2048, 2092, 2104
	TZ(C,O),Cl(DZP)	1.8731	1.159	2.4493	92.0	1973, 2024, 2038	
BLYP	6-31G*	1.8724	1.1626	2.4771	92.0	2014, 2062, 2074	
	6-311+G*	1.8748	1.1633	2.476	91.9	1996, 2047, 2061	
$Rh(CO)_2Cl_2^{-1}$							
B3LYP	6-31G*	1.8598	1.1565	2.4283	96.0	2055, 2117	1981, 2040
BLYP/	6-31G*	1.8695	1.1732	2.451	95.8	1949, 2010	
$Rh^I(CO)_2$							
B3LYP	6-31G*	1.8692	1.1358	-	88.0	21967, 2243	2118, 2162
BLYP	6-31G*	1.8602	1.1523	-	88.0	2290, 2348	

* IR and Raman active

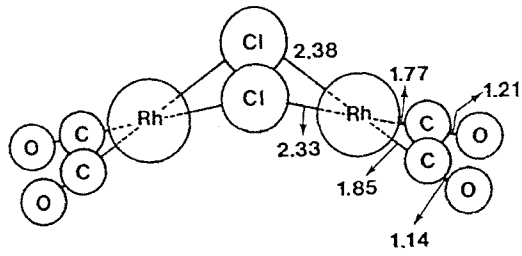

Figure 3.2: Crystal structure of $[Rh(CO)_2Cl]_2$

In agreement with other studies using the hybrid B3LYP method, our result shows that this approach overestimates the metal-ligand bond length by 0.02 Å and 0.07 Å (for Rh-C and Rh-Cl respectively) compared to the experimental value. Even though this may appear to be a rather disappointing result, it should be pointed out that these DFT approaches are superior to the HF ones. The errors in the optimized C-O distances are rather small.

In general, the geometry calculated by the hybrid method shows better agreement with the experimental value than the gradient corrected method. However, the gradient corrected method predicted better ν(CO) frequencies.

An all electron basis set calculation is not performed due to the computational resources consideration although it is known[28] to give better results than the ECP basis set, LanL2DZ. The DFT and LanL2DZ procedures on the other hand, have been reported to yield acceptable vibrational frequencies and geometries for inorganic molecules, although this approach produced results which are slightly inferior to the all electron, 6-311G* basis set, the ECP approach is less demanding.[28]

The B3LYP functional is well known for predicting higher frequencies and usually a scale factor of 0.95-1.0 is found necessary. For the dimer, we found ν_{exp}/ν_{calc} average of 0.964 for the B3LYP/6-31G** approach.

The results of the BLYP-DFT frequency calculations for several rhodium carbonyls, their analogues, rhodium carbonyl chloride in addition to some well studied metal tetracarbonyl are listed in Table 3.2. The experimental spectrum of $Ni(CO)_4$ is well known in various media. $Pd(CO)_4$ and $Pt(CO)_4$ on the other hand are very unstable and have only been observed in a matrix isolation experiment.[29] Theoretically the system has

also been studied by numerous groups. Rhodium carbonyls and their analogues have also been studied in the matrix isolation experiments.[29] Therefore, the study of these systems allows us to estimate the accuracy of the DFT method.

While the B3LYP/6-31G* approach tends to overestimate the experimental ν(CO) values, the BLYP/6-31G* approach gives quite a small $\Delta\nu$. The ν(CO) for $Pd(CO)_4$ and $Pt(CO)_4$ observed in matrix experiment was 2067 cm^{-1} and 2053 cm^{-1} respectively giving the $\Delta\nu$ for both cases as 35 cm^{-1}. Smaller $\Delta\nu$'s can be seen in Group 9 metal carbonyls while largest deviation was observed for $[Rh(CO)_2Cl_2]^{-1}$, 60 cm^{-1}. Further calculations, comparing the result with larger basis sets and addition of diffuse functions did not seem to improve the result, Table 3.3.

In spite of the fact that these DFT methods slightly underestimate/overestimate the experimental ν(CO) values and overestimate the geometrical properties, the excellent agreement between experimental results and frequencies from DFT calculations shows that these methods can be used as support in vibrational assignments, identification and interpretation of metal carbonyl complexes.

Table 3.2: Frequencies calculation for metal carbonyl, $M(CO)_4$ with M=Ni, Pd, Pt , Co, Rh,Ir at BLYP/6-31G** level

System	Point Group	$\nu(CO)_{calc}$	$\nu(CO)_{exp}$ [29]	$\Delta\nu(CO)_{exp-calc}$
$Co^{-1}(CO)_4$	T_d	1899	1890	-9
$Rh^{-1}(CO)_4$	T_d	1894	1900	-6
$Ir^{-1}(CO)_4$	T_d	1889	1898	-9
$Fe^{-2}(CO)_4$	T_d	1761	1790	-29
$Ni^0(CO)_4$	T_d	2033	2052	+19
$Pd^0(CO)_4$	T_d	2032	2070	+38
$Pt^0(CO)_4$	T_d	2018	2053	+35
$Co^0(CO)_4$	T_d*	2011	2129	+18
		1999	2011	+12
$Rh^0(CO)_4$	T_d*	2005	2019	+14
		1998	2012	+14
$Ir^0(CO)_4$	T_d*	1996	2008	+12
		1984	2001	+17
RhCO	$D_{\infty h}$	2003	2013	+10
$[Rh(CO)_2Cl]_2$	C_{2v}	2014	2043	+29
		2062	2095	+33
		2074	2105	+31
$Rh(CO)_2Cl_2^-$	C_{2v}	1950	1944	-6
		2010	2070	+60
Average $\Delta\nu(CO)$				-19.5
$\nu(CO)_{exp}/\nu(CO)_{calc}$				1.01

* starting geometry

Table 3.3: Effect of different basis set on $Rh(CO)_2Cl_2^{-1}$

Method	Basis set	$\nu(CO)_{calc}$	$\Delta\nu(CO)$
Expt		1944, 2070	-
B3LYP	6-31G*	2055, 2117	111, 47
	6-311G*	2056, 2117	112, 47
	6-311+G*	2057, 2119	113, 49
	6-31++G*	2057, 2119	113, 49
	TZ(C,O) DZP(Cl)	1897, 1967	47, 103
BLYP	6-31G*	1950, 2010	6, 60
	6-31G*(C,O) 6-31+G*(Cl)	1953, 2014	9, 56
	TZ(C,O) DZP(Cl)	1789, 1857	155, 213
	6-31+G*(Cl) TZ(C,O)	1797, 1865	147, 205

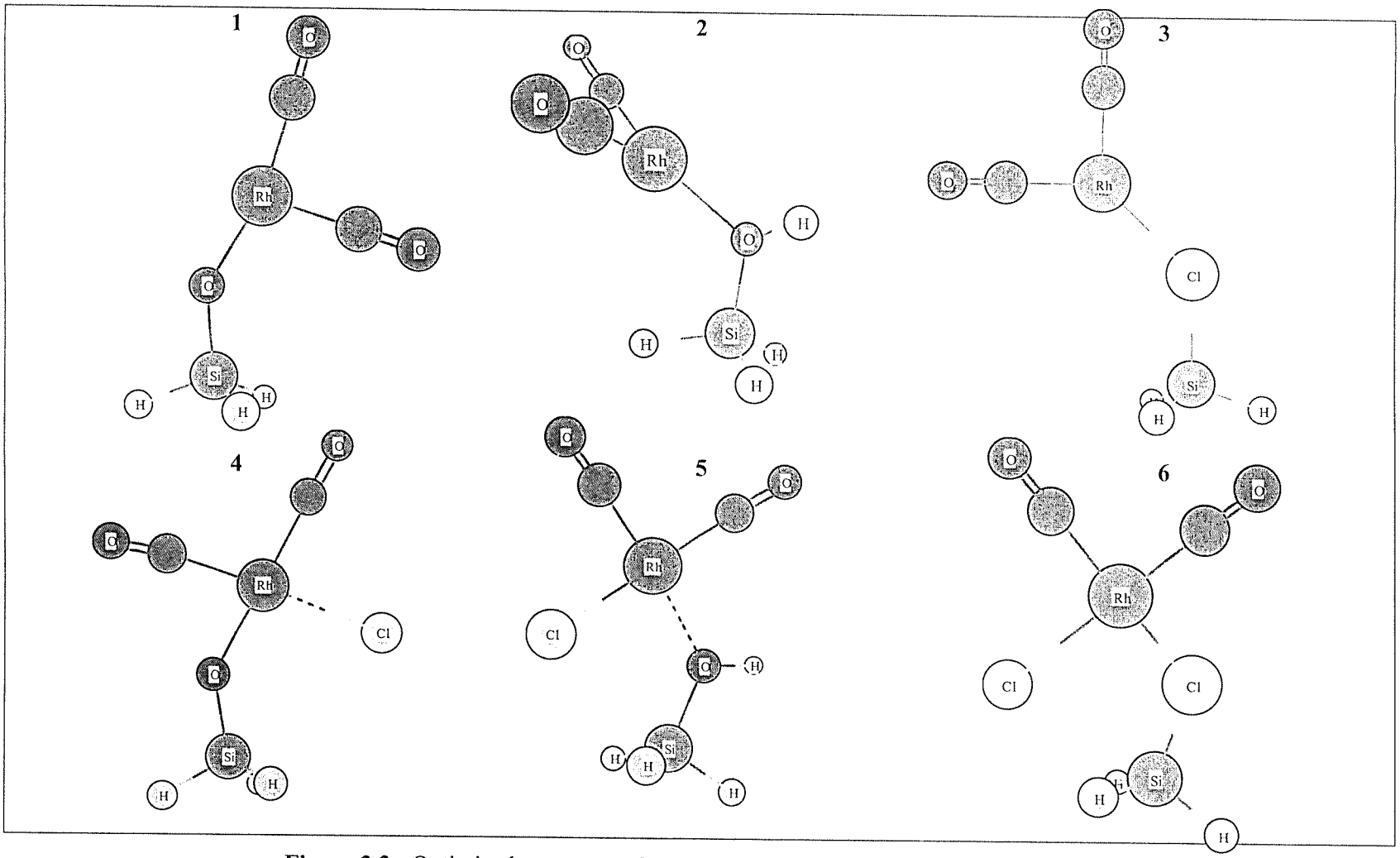

Figure 3.3 : Optimized structures of **1-6**.

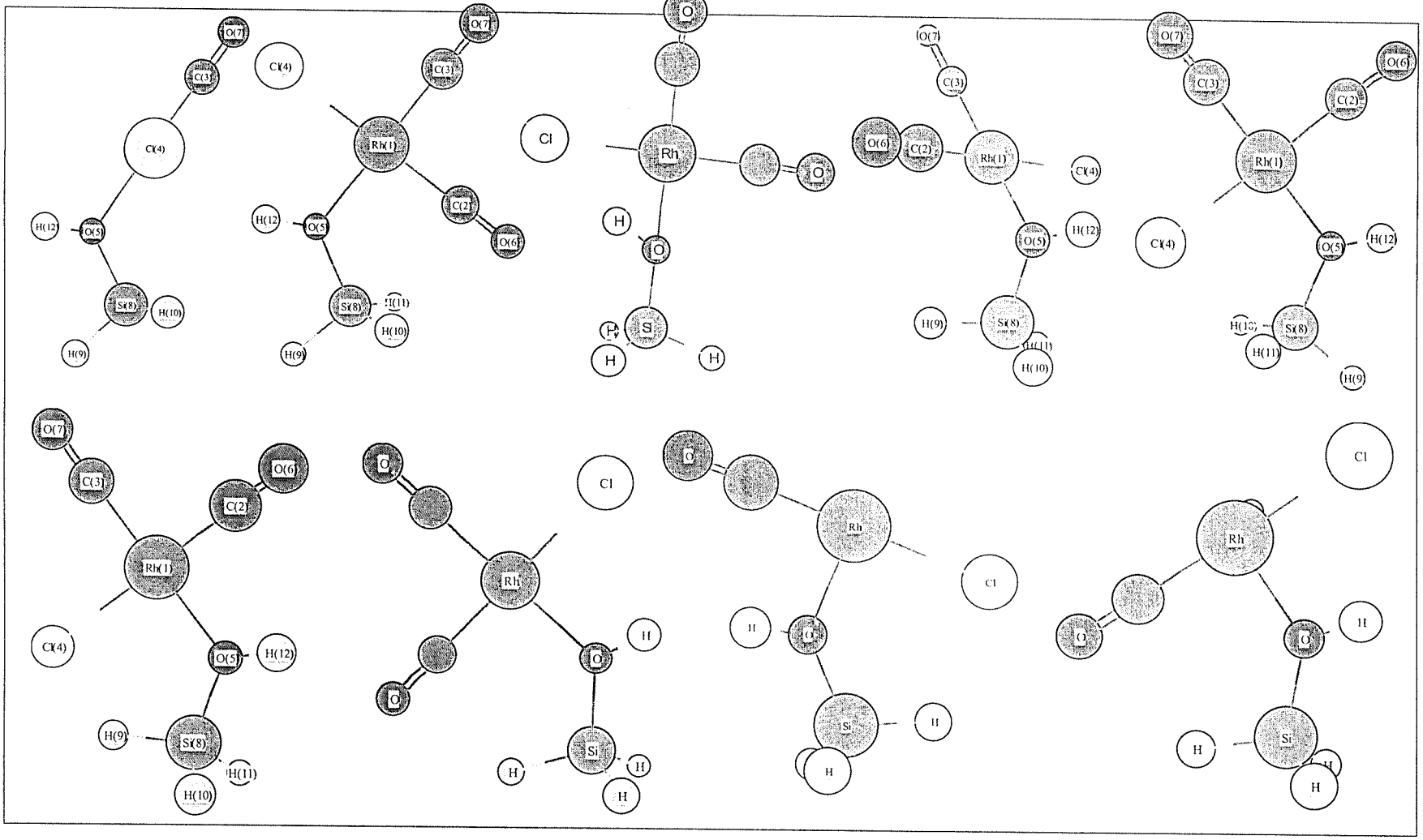

Figure 3.4: Some of conformations tested for $Rh(CO)_2Cl(HOSiH_3)$

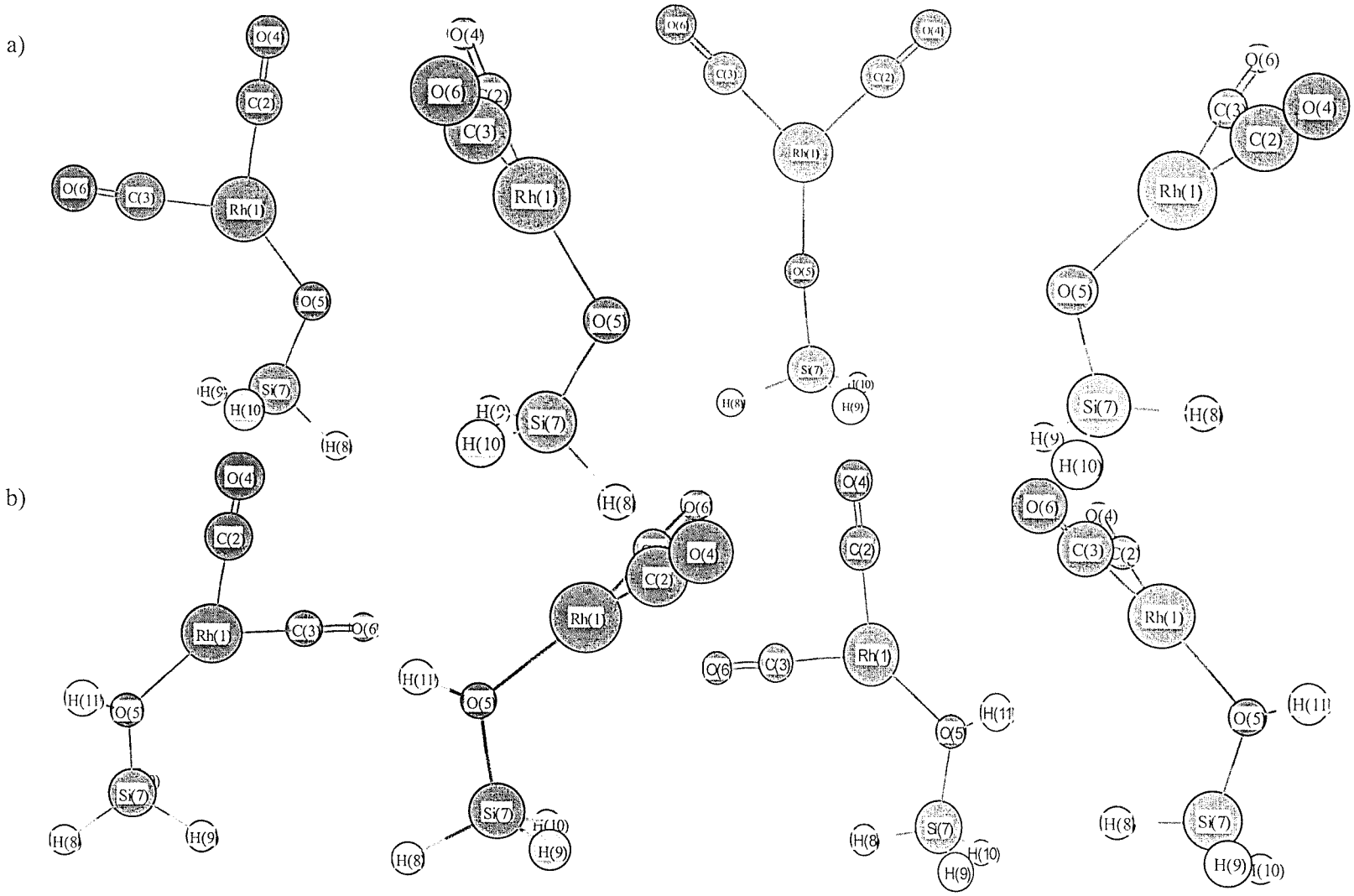

Figure3.5: Some possible conformations of a). $Rh(CO)_2(OSiH_3)$ and b). $Rh(CO)_2(HOSiH_3)$

3.5.2 Models of supported rhodium *gem* dicarbonyl

3.5.2.1 Geometrical parameters

Figure 3.3 shows optimized structures of $[Rh(CO)_2(OSiH_3)]$ (**1**), $[Rh(CO)_2(OHSiH_3)]$ (**2**), $[Rh(CO)_2(ClSiH_3)]^+$ (**3**), $[Rh(CO)_2(Cl)(OSiH_3)]$ (**4**), $Rh(CO)_2$-$(Cl)(OHSiH_3)$ (**5**) and $[Rh(CO)_2(Cl)(ClSiH_3)]$ (**6**). Table 3.4 and 3.5 give the calculated properties of optimized structure **1-6**. Lowest energy conformations are obtained based on the results of potential energy surface scans and frequency calculations, which yield no imaginary frequency. Some of the possible conformations for **1**, **2** and **4** analysed are given in Figure 3.4 and Figure 3.5.

Typical calculated Si-O distances for silicon-oxygen containing compounds are usually around 1.645-1.650 Å, although these values would vary with the choice of basis set. Theoretical calculation using the HF/3-21G* method gave Si-O 1.653 Å and 1.645 Å for SiH_3OH and SiH_3OSiH_3, respectively.[30] The Si-O distance for model structure $[Rh(CO)_2(OSiH_3)]$ **(1)** was found to be 1.653 Å, which is also in agreement with the predicted Si-O distance in ranges of silica based clusters as by Pereira et al.[31] Model structures with OH ligand, $[Rh(CO)_2(OHSiH_3)]$ (**2**) and $Rh(CO)_2$-$(Cl)(OHSiH_3)$ (**5**), show a longer Si-O bond distance. The model structure $[Rh(CO)_2(Cl)(OSiH_3)]$ **(4),** however, shows a strikingly short Si-O distance, 1.6212 Å. If we took into account the fact that the B3LYP method usually overestimates the bond length approximately +0.02 Å, this means this model structure has a considerably short Si-O distance, as compared to the average experimental Si-O distance, 1.63 Å.

Table 3.4: The calculated geometric, spectroscopic and electronics properties of the model of supported $Rh^{I}(CO)_2(XSiH_3)$ where X=O, OH and Cl . Distances in Å, angles in ° .

Structure	**1**	**2**	**3**
Point group	C_s	C_1	C_s
r(Rh-C1)	1.835	1.852	1.849
r(Rh-C2)	1.898	1.898	1.904
r(Rh-X)	1.925	2.109	2.459
r(C1-O)	1.150	1.140	1.137
r(C2-O)	1.149	1.138	1.140
C-Rh-C	89.9	88.8	89.2
RhXSi	143.9	128.1	99.8
r(Si-X)	1.653	1.760	2.195
r(O-H)	-	0.970	-
ν(CO), cm^{-1}	2020(833)	2090(525)	2096(480)
	2073(431)	2138(290)	2142(316)
$\Delta\nu$(CO) , cm^{-1}‡	+18	-54	-60
	+23	-42	-42
ν(OH), cm^{-1}	-	3657(176)	-
q(Rh), a.u	0.3178	0.3940	0.2919
q(C), a.u	0.2334	0.2758	0.2967
	0.2675	0.3056	0.2835
q(O), a.u	-0.2080	-0.1284	-0.1232
	-0.2177	-0.1257	-0.1172

Scaled frequencies. Value in parenthesis is intensity in Km/mole
‡ with respect to the rhodium *gem* dicarbonyl, $Rh^{I}(CO)_2$/oxide values, $\nu(CO)_{exp\text{-}calc}$

Table 3.5: The calculated geometric, spectroscopic and electronics properties of the model of supported $Rh^{I}(CO)_2(Cl)(XSiH_3)$ where X=O, OH and Cl . Distances in Å, angles in °,

Structure	**4**	**5**	**6**
Point group	C_s	C_s	C_s
r(Rh-C1)	1.861	1.885	1.890
r(Rh-C2)	1.864	1.852	1.854
r(Rh-X)	2.041	2.179	2.563
r(Rh-Cl)	2.427	2.366	2.368
r(C1-O)	1.158	1.151	1.148
r(C2-O)	1.1565	1.149	1.146
C-Rh-C	86.7	92.3	92.6
Rh-X-Si	131.2	128.6	110.0
r(Si-X)	1.621	1.729	2.149
r(O-H)	-	0.964	
ν(CO), cm^{-1}	1969(899)	2023(754)	2035(704)
	2030(641)	2084(520)	2090(532)
$\Delta\nu$(CO) , cm^{-1}‡	+69	+15	+3
	+66	+12	+6
ν(OH), cm^{-1}	-	3729(85.8)	-
q(Rh), a.u	0.0716	0.1316	0.0514
q(C), a.u	0.2524	0.1953	0.2228
	0.2160	0.2761	0.2705
q(O), a.u	-0.2834	-0.2198	-0.2109
	-0.2895	-0.2115	-0.2029

Scaled frequencies. Value in parenthesis is intensity in Km/mole
‡ with respect to the rhodium *gem* dicarbonyl, $Rh^{I}(CO)_2$/silica values

This calculation yields an average Si-H distance of 1.475 Å, in agreement with experimental Si-H distance in $H_8Si_8O_{12}$ compound but slightly longer than its value calculated at the Becke3LYP/6-31G** level, 1.4645 Å.

Of all the Rh-O containing structures analysed, **1** shows a very short Rh-O distance, 1.9252 Å, an indication of strong metal-"support" interaction. Crystallographically, a short Rh-O distance has also been reported, 1.906 Å for trans(μ-oxo)-tris(bis(μ-acetato)-aqua-rhodium(III)) perchlorate dihydrate, CSD refcodes OXARCH[32], Figure 3.5.

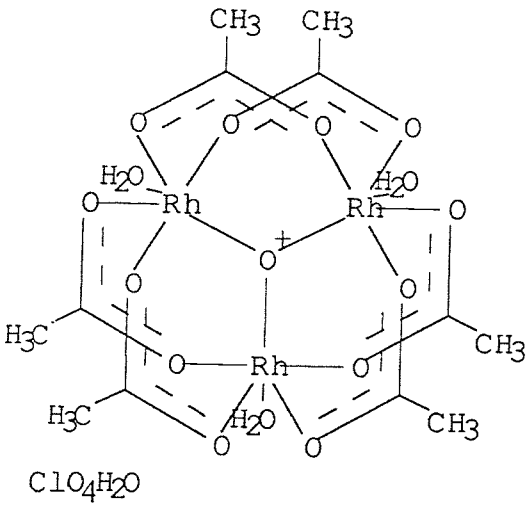

Figure 3.5: Crystal structure of OXARCH

$[Rh(CO)_2(Cl)(OSiH_3)]$, **3**, gives Rh-O distances similar to that reported for $Rh_4(CO_{12})/Al_2O_3$ by Evans et al, [33] while slightly longer Rh-O distances, at around 2.1 Å match that of 2.12 Å by Koningsberger and co-workers[34] for $RhCl_3/Al_2O_3$. The Rh-O_{surf} distances are found to be similar to other Rh-O coordination compound reported in the literature. In fact, some authors believed these M-O_{surf} bonds are as strong as other common coordination compound, thus justifying the concept of surface sites as polydentate ligands being able to anchor organometallic fragments to the supports.[35] Figure 3.6 and 3.7 illustrate the normal Rh-O distances distribution extracted from CSD.

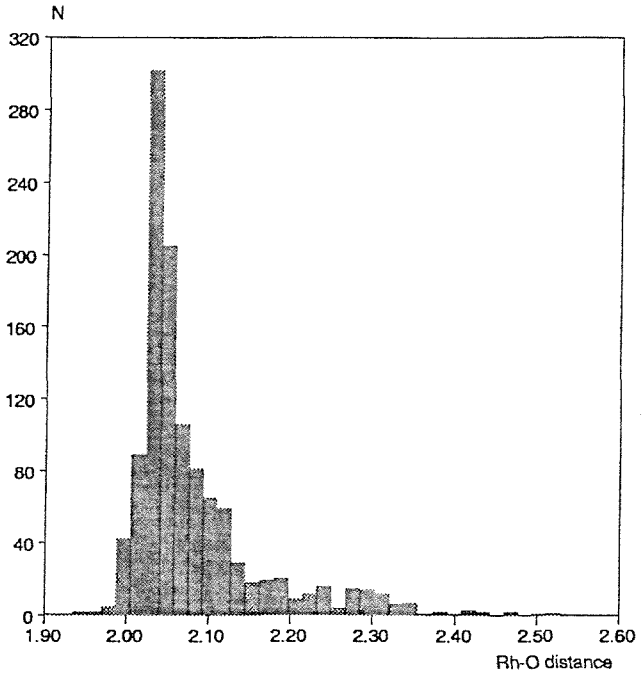

Figure 3.6: Rh-O distances distributions based on CSD data collection, all oxidation state

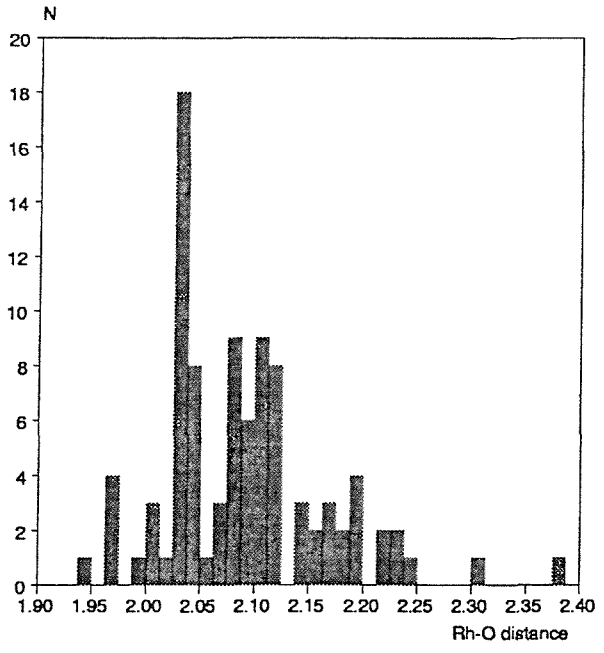

Figure 3.7: Rh-O distances distributions based on CSD data collection, oxidation state +1

Koningsberger and Gates[36] had previously reported that the average distance between the metal ion and the oxygen of the support is typically in the range of 2.1-2.2 Å, see Table 3.6 for details. These authors also reported the presence of longer metal-oxide distances at around 2.5-2.7 Å for supported metal particles.

One explanation suggested for these distances is as follows. The longer metal-oxygen distance is normally observed by EXAFS spectroscopy when the metal is reduced in a H_2 atmosphere at a low temperature whereas, after reduction at higher temperatures, (>600°C), only a distance at 2.2 Å are observed. This result has been interpreted as the longer metal-support oxygen distance at 2.5-2.7 Å is observed when hydrogen is chemisorbed on the metal cluster and/or when the metal oxide surface is sufficiently hydroxylated.

Table 3.6: Metal-support oxygen distances determined by EXAFS spectroscopy. The {} refers to groups terminating the metal oxide support.

Metal source	Support	Proposed Surface structure	Average distance (Å)	Ref
$Ru_3(CO)_{12}$	γ-Al_2O_3	$Ru(CO)_2\{OAl\}_2$	2.17	37
$Ru_3(CO)_{12}$	SiO_2	$Ru(CO)_2\{OSi\}_n$	2.08	33
$RhCl_3$	γ-Al_2O_3	$Rh(CO)_2\{OAl\}_3$	2.12	34
$Rh_4(CO)_{12}$	γ-Al_2O_3	$Rh(CO)_2\{OAl\}_3$	2.04	33
$H_3Re_3(CO)_{12}$	MgO	$Re(CO)_3\{OMg\}\{HOMg\}_2$	2.15	38
$HRe(CO)_5$	MgO	$Re(CO)_3\{OMg\}\{HOMg\}$	2.13	39
$Os_3(CO)_{12}$	γ-Al_2O_3	$Os(CO)_{2\text{-}3}\{OAl\}_3$	2.17	40

Upon hydroxylation, a significant Rh-O bond elongation was observed, 2.1094 and 2.1972 Å for structure $[Rh(CO)_2(OHSiH_3)]$ (**2**) and $Rh(CO)_2(Cl)(OHSiH_3)$ (**5**), respectively. This too is within the range suggested in experimental data of Rh-O containing compounds. For an instance, the X-ray structure for the compound [Rh(μ-

$OH)(\eta^3\text{-}C_3H_5)_2]_2$ gives Rh-O distances of 2.15-2.20 Å.[41] Furthermore, this Rh-O distance is also consistent with the bond distance predicted by Koningsberger et al.[34]

Calculation using a longer Rh-O distance of 2.5 -2.7 Å as suggested by Gates and Koningsberger,[36] as an initial estimate on $[Rh(CO)_2(Cl)(OHSiH_3)]$, (**5**), resulted in the same geometric data as reported in Table 3.6. So an alternative interpretation is that the longer metal-oxygen distances arise from weak interactions between the rhodium metal and the support. The calculated results seem to be in accord with this suggestion, although, in view of the simplified nature of our structural models, they are not sufficient to confirm it.

The hypothesis that some of the Rh-Cl bonds are retained upon adsorption to the surface comes from a preliminary report of an EXAFS study of $[Rh(CO)_2Cl]_2$ supported on alumina,[42] and titania.[44] Keyes and Watters[43] observed a considerable difference in $[Rh(CO)_2Cl]_2$ adsorption behaviour between silica and alumina. These authors believed that the $[Rh(CO)_2Cl]_2$ was only weakly physisorbed on silica. EXAFS studies of the species supported on high surface area titania have also shown isolated rhodium dicarbonyl units, with the chlorine also bound to the rhodium at 2.28 Å while the surface oxygen was observed at 2.14 Å.[44]

This level of calculation predicted three different Rh-Cl distances for the structures analysed in this study; ~2.45 Å, 2.36 Å and 2.56 Å. Understandably, the longer distances are the nonbonding $Rh..Cl_{surf}$ distances, as observed in **3** and **6**, while a shorter Rh-Cl bond at about 2.36 Å can be observed in $[Rh(CO)_2(Cl)(OHSiH_3)]$, (**5**) and $[Rh(CO)_2(Cl)(ClSiH_3)]$, (**6**). The model structure of $[Rh(CO)_2(Cl)(OSiH_3)]^{-1}$, (**4**) yields an Rh-Cl distance of 2.4269 Å rather similar to that of the calculated Rh-Cl distance in the dimer and $[Rh(CO)_2Cl_2]^-$, 2.4517 Å and 2.476 Å respectively.

The similarity of the Rh-Cl bond distance observed for rhodium *gem* dicarbonyl with Rh-Cl bond distance in the parent dimer compound, has been reported by various authors based on EXAFS data both on titania and alumina. For example Johnston et al[45] in the studies involving Rh/Al_2O_3 had also reported the existence of Rh-Cl bond at Rh-Cl distance similar to the dimer compound. These workers also considered the chlorine atom as directly bounded to the $Rh(CO)_2$.[45]

XPS measurements have shown that the chlorine remains upon the surface with a binding energy [($Cl2_{p3/2}$) =198.5 eV], a shift from that of the physisorbed parent dimer $Rh_2(CO)_4Cl_2$ [($Cl2_{p3/2}$) =199.1 eV]. This has led the authors to propose that the dimer dissociates, with chlorine either being adsorbed on to the titania surface[46] or remained attached to the rhodium.[47]

The calculated geometries for $[Rh(CO)_2(Cl)(OSiH_3)]^{-1}$ is perhaps the most interesting. Optimization of this structure result in two almost similar Rh-C distances, 1.86 Å. This result seems to be consistent with the X-ray data reported by Johnstons et al.[45] The authors reported only a single Rh-C distance was observed, in contrast to two different Rh-C distances observed in crystal environment for $[Rh(CO)_2Cl]_2$. Williams in the study of this species (on titania) also reported a single Rh-C distance.[44] Other structures yielded clearly two different Rh-C distances.

However, this feature (i.e single Rh-C distance) may be due to the method of refinement itself. In many instances, many workers would look for one kind of Rh-C group only and unable to resolve any difference between them.[48] So the average predicted Rh-C distance, 1.87 Å is actually in close agreement with the EXAFS data, if we took into account the fact that B3LYP usually overestimates the Rh-C bond by about 0.02 Å.

The C-O bond distances were all predicted to be slightly longer than the experimental C-O distance 1.132 Å found in the CSD database collection. Clear inverse relationship between Rh-C and C-O distance is not observed but the trend of short C-O bond with long Rh-C bond is quite apparent, Figure 3.8.

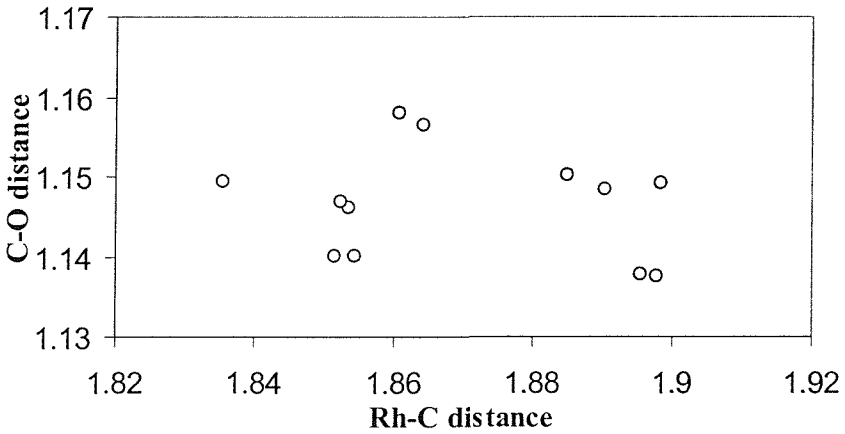

Figure 3.8: General relationship between the calculated of Rh-C and C-O distances, in Å for structures **1-6.**

From the estimated relative intensities of symmetric and assymmetric stretching frequencies of rhodium *gem* dicarbonyl species, the C-Rh-C angle was estimated to be around 91° which is very similar to the value for the parent dimer, $[Rh(CO)_2Cl]_2$. This calculation gave an average value of about 90°. The previous calculations on $Rh(CO)_2$, using the HF method, favoured a linear species in contrast to the surface species which is known to have the angle around 90°. The recent work by Blyholder gives the C-Rh-C angles of 85°.[15]

3.5.2.2 Vibrational frequencies

The results for frequency calculations on structures **1-6** calculated at B3LYP/6-31G** level are given in Table 3.4. Generally, the ν(CO) frequencies calculated at the two DFT levels, B3LYP and BLYP, have the same general trend for structures **1-6**, Figure 3.9. The unscaled ν(CO) frequencies calculated at BLYP level consistently underestimate the ν(CO) bands. Nevertheless, it is believed that the theoretical data generated in this work can provide a qualitative description, in term of the trends of the properties observed.

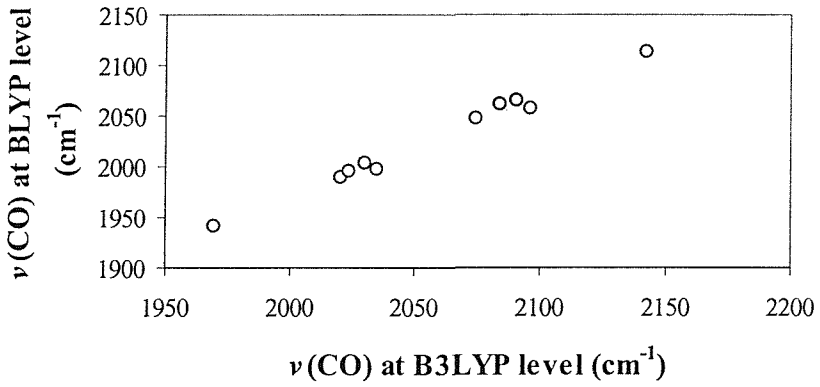

Figure 3.9: Predicted ν(CO) frequencies at B3LYP/6-31G** vs. ν(CO) frequencies at BLYP/6-31G**

Unless mentioned, the B3LYP level is employed and discussed in this part of work. All structures of the extended 'model of rhodium *gem* dicarbonyl' have a reduction in

symmetry from C_{2v} of $Rh(CO)_2$ to C_s. This reduction in symmetry, however, would still give rise to two IR active CO vibrational modes.

On silica, two conclusions were made based on the IR spectra of rhodium *gem* dicarbonyl group by various authors regarding this species. The first one is by Graydon and co-workers[49] and is summarised below;

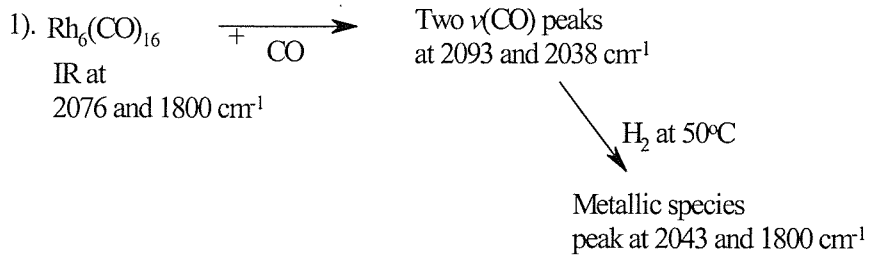

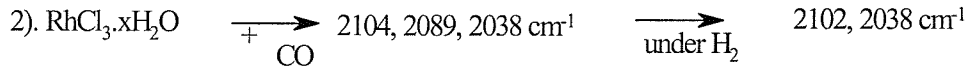

The second observation is made by Keyes and Watters[43] who reported sublimation of $[Rh(CO)_2Cl]_2$ onto silica gave a three infrared band which is very similar, except for small upward shifts, 5-10 cm^{-1}, to that of the molecular $[Rh(CO)_2Cl]_2$. This complex could easily be removed by solvent extraction. These authors believed $[Rh(CO)_2Cl]_2$ adsorbs without decomposition and binding to the surface only slightly perturbed the bonding and structure of the complex.

Calculations for **1-6** gave frequencies at around 1969-2038 cm^{-1} and 2030-2158 cm^{-1}. Structure **1**, **5** and **6** yield ν(CO) values which are comparable to experimental frequencies for the *gem* dicarbonyl rhodium structure on silica, 2038 $cm^{-1}$and 2096 cm^{-1} reported by Graydon group[48] while other structures have higher or lower ν(CO).

3.5.2.3 Properties of adsorbed CO

Properties of adsorbed CO as a probe molecule is an indirect but an efficient way to monitor the changes in the electronic structure of a supported metal species.

The ν(CO) stretching frequencies in carbonyl complexes are strongly dependent on electron density of the metal atoms. The electron density is, on the other hand, influenced by the nature of the metal, its oxidation state, the structure of the complex and the electron donating/accepting properties of the remaining ligands. A shorter metal-CO distance should imply a change in the CO vibrational frequencies. It is thus not surprising that a considerable change occurs for the CO vibration in these sets of calculations, as the C-O distances varies from 1.137 Å to 1.158 Å, Figure 3.10. Although the inverse relationship is apparent, the scatters observed in the histogram may be attributed to the presence of Cl ligand(s), such as in structures **3 - 6**.

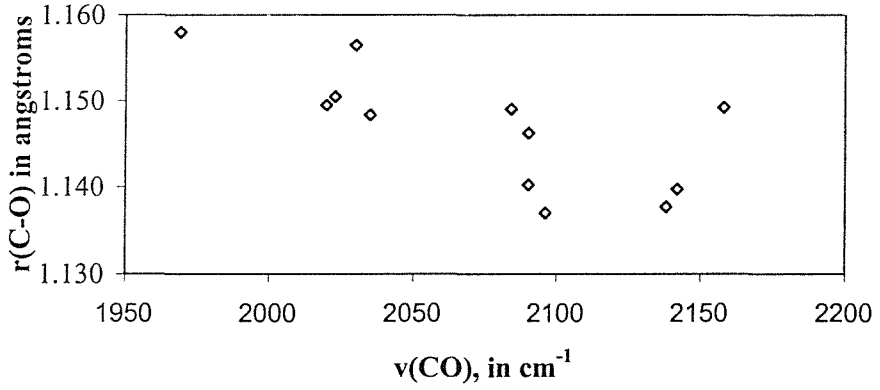

Figure 3.10: Relationship between the calculated ν(CO) frequencies and C-O distance

The bonding of CO to a transition metal is commonly described by the donor-acceptor mechanism with electron donation from the adsorbate to the unoccupied metal orbitals through the CO 5σ molecular orbital (MO) and back donation from the d_π metal orbitals to the unoccupied 2π* level of CO. The 4σ and 1π MOs of CO, to a small extent, also participate in the donation. The link between π back donation and CO vibrational properties has been theoretically tested in a wide number of different systems including metal carbonyl complexes and CO on metal surfaces.

A linear relationship between the charge of metal and the CO stretching frequency has been reported based on the studies of the interaction of CO probe molecule with neutral and charges species[50]. It has been shown in the literature that the change in

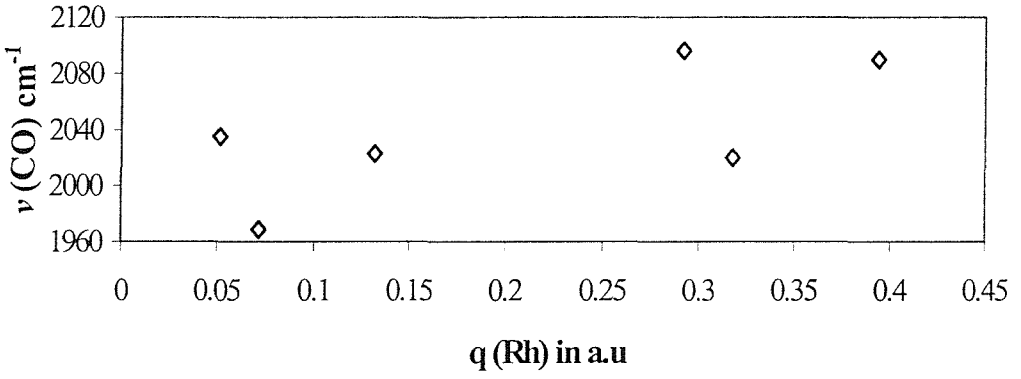

Figure 3.11: Relationship between the calculated Rh charges and ν(CO) frequency.

frequency increases with the charge. This correlation, though not very clear, can still be observed in this work, Figure 3.11. It is known that, as the metal becomes more positive the CO π population decreases, consequently the CO frequency increases due to there being fewer electrons in the π antibonding orbitals.

3.5.2.4 HOMO-LUMO energy analysis

According to frontier orbital theory,[51] the electron transfer between HOMO and LUMO is a key intermolecular interaction for chemisorption between an adsorbate and the corresponding adsorbant. HOMO and LUMO interactions are greatest when HOMO–LUMO energy level is lying close together and their overlap is large. Furthermore, the theory of polarisability shows that the ability of a substrate molecule to undergo a redox reaction varies inversely with the energy difference between the ground state and various excited states. This implies that the reactivity of a substrate molecule is controlled by the energy gap between the HOMO and LUMO energies. The trends of the HOMO, LUMO and E_{gap} for " supported" $Rh(CO)_2$ species is given in Table 3.8.

Table 3.8: HOMO LUMO energy (in eV), see also Figure 3.3

Structure	No.	E_{LUMO}	E_{HOMO}	E_{gap}
$[Rh(CO)_2(OSiH_3)]$	**1**	-3.3171	-7.0552	3.7381
$[Rh(CO)_2(OHSiH_3)]^+$	**2**	-8.1711	-11.8003	3.6289
$[Rh(CO)_2(ClSiH_3)]^+$	**3**	-8.4299	-11.9312	3.5930
$[Rh(CO)_2(Cl)(OSiH_3)]^-$	**4**	+2.2597	-2.5103	4.7700
$[Rh(CO)_2(Cl)(OHSiH_3)]$	**5**	-2.2594	-6.8268	4.5728
$[Rh(CO)_2(Cl)(ClSiH_3)]$	**6**	-2.6705	-7.0823	4.4118

1 Hartree=27.2116 eV= 627.5095 kcal/mol

The results show that the surface species **1 - 6** have low lying LUMO energies between ~+2.25 and ~-8.4 eV, with the lowest LUMO energy is associated with the postively charge structure and vice versa. None of these species show a very small E_{gap}, a usual indication of a second order Jahn Teller distortion. It is known that, if the LUMO energy is low, then the species will readily accept electrons either by a reduction procces or an electron pair donor, in which species **2** and **3** fit this description. On the other hand, a very high HOMO energy, as observed for species **4,** would probably mean that this species is more likely to lose electrons as compared to the other species.

In both the $Rh(CO)_2(XSiH_3)$, **(1 - 3)** and $Rh(CO)_2(Cl)(XSiH_3)$, **(4 - 6)** systems, the presence of chlorine or an additional chloride ligand, result in the lowering of LUMO energy relative to the non-chlorinated analogue. Of a particular note is the pronounced reduction observed in $[Rh(CO)_2(ClSiH_3)]^+$. This decrease in LUMO energy due to chlorine addition, is similar to the results in the study of chlorine into alumina cluster.[52]

It is thought that the role of halogen promoter at the surface is to enhance the Lewis or Brønsted acid environments.[53] The addition of chlorine to alumina for an example, enhances the activity of the catalyst for skeletal transformations of hydrocarbons.[54,55]

It is thought that the role of halogen promoter at the surface is to enhance the Lewis or Brønsted acid environments.[53] The addition of chlorine to alumina for an example, enhances the activity of the catalyst for skeletal transformations of hydrocarbons.[54,55]

$[Rh(CO)_2(Cl)(OHSiH_3)]$, **5**, and $[Rh(CO)_2(Cl)(ClSiH_3)]$, **6**, have an almost similar LUMO energy but the latter has bigger E_{gap}. Structure **6**, is more stable than **5** by E_{gap} difference of about 0.161 eV, which is equivalent to 3.7127 kcal/mol. The results also show that in both the system containing Cl or without Cl, dehydroxylation significantly increases the LUMO energies, as observed in **1** and **4**.

It is paramount to mention that while the importance of chlorine can be quantitatively described here, experimentally $Rh^1(CO)_2$ can also be generated using non-chlorine based material such as $Rh(NO)_3$.[56]

3.5.2.5 Reliable Predictions on Limited Model?

Theoretical results on molecular models of these kinds of calculations are affected by two types of errors; i). errors due to the approximations connected by the methods and ii). errors due to replacing the solid by finite model. Solid supports are in reality made of large molecule systems frequently containing defects, impurities and also unusual bonding types.

Being a 16-electron system plus having results which are in agreement with the data from the EXAFS and the IR spectroscopy, structures **5** and **6** appear to be the most reasonable structure of $Rh^1(CO)_2$ supported on silica or other support system. However, the result for structure **4**, deserves some comments. Apparently, the high LUMO energy is associated with the structure being negatively charged. In reality, the chloride ion is more likely to be bonded to the nearby surface, giving an overall neutral charge, which may result in a different HOMO and LUMO energy.

3.6 Further work

Other possible structures not investigated in this work are $Rh^1(CO)_2$ bound by two or three surface oxides giving the metal center a coordination number 4 and 5 respectively. The latter, although surprising, given the usual four-coordinate, square planar structure observed for Rh^1 molecular complexes is supported by EXAFS data[57,40]

In addition to these structures, further calculations on this system should also be tested against similar or larger SiO_2 surface model. A surface model containing three active OH sites, would probably be a better model for this purpose, providing a migration pathway for the surface species, better support effects and at the same time neighboring OH group(s) effect.

3.7 Conclusion

We have theoretically investigated the interaction between rhodium *gem* dicarbonyl species and a model silica surface. Rhodium oxidation state of +1 is used throughout, so both the charged and neutral systems were considered. These calculations lead to the following conclusion.

1. Density functional calculations using the BLYP and B3LYP hybrid correlation, the ECP and the moderate basis sets gave results which are in good agreement with the EXAFS and the IR values and within the usual range of accuracy of density functional calculations.
2. The presence of chlorine in the system obviously lowered the LUMO energy
3. Dehydroxylation increased the LUMO energy.
4. Based on the agreement with EXAFS, IR data and low E_{gap}, this work predicted the most favorable rhodium *gem* dicarbonyl model are $Rh(CO)_2(Cl)(ClSiH_3)$ or $Rh(CO)_2(Cl)(HOSiH_3)$.

Although this result is only a preliminary and should be expanded to a larger silica model which resembles SiO_2 surface better, the present result demonstrates how the theory, used in parallel with the experimental data, can be a powerful tool for progresses in the research involving supported metal catalysts.

3.8 References

1. Y. Barshad, X. Zhou, and E. Gulari, *J. Catal.*, 1985, **94**, 128.

2. M. Primet, *J. Catal.*, 1984, **88**, 273.

3. W. J. Han, A. B. Kooh, and R. F. Hicks, *Catal. Lett.*, 1993, **18**, 193.

4. M. J. Kappers and J. H. Van der Maas, *Catal. Lett.*, 1991, **10**, 365.

5. Y. Musashi and S. Sakaki, *J. Chem. Soc. Dalton Trans.*, 1998, 577.

6. F. Hutschka, A. Dedieu, M. Eichberger, R. Fornika, W. Leitner , *J. Am. Chem. Soc.*, 1997, **119**, 4432.

7. Z. Y. Lin, M. B. Hall, M. F. Guest, P. Sherwood, *J. Organometal. Chem.*, 1994, **478**, 197.

8. R. J. Deeth, *J. Chem. Soc. Dalton Trans.,* 1993, 3711.

9. E. A. Salter and A. Wierzbicki, *Theochem-J. Mol. Struct.*, 1998, **425**, 101.

10. M. D. Su and S. Y. Chu, *Chemistry-A European Journal*, 1999, **5**, 198.

11. F. A. Cotton and X. J. Feng, *J. Am. Chem. Soc.,* 1998, **120**, 3387.

12. W. Biemolt and A. P. J. Jansen, *J. Comp.Chem.*, 1994, **15**, 1053.

13. H. Haberlandt in J. B. Moffat (ed), *Theoretical Aspects in Heterogeneous Catalysis*, Van Nostrand Reinhold, New York, 1990 and references therein.

14. M. L. Mckee and S. D. Worley, *J. Phys. Chem.*, 1988, **92**, 3699.

15. G. Blyholder, *J. Mol. Catal.*, 1997, **A119**, 11.

16. J. Sauer, *Chem. Rev.*, 1989, **89**, 199.

17. H. Haberlandt and F. Ritschl, *J. Phys. Chem.*, 1983, **87**, 3244.

18. J. Sauer, P. Ugliengo, E. Garrone and V. R. Saunders, *Chem. Rev.*, 1994, **94**, 2095.

19. J. R. Chang, L. U. Gron, A. Honji, K. M. Sandez and B. C. Gates, *J. Phys. Chem.*, 1991, **95**, 9944.

20. A. D. Becke, *Phys. Rev. A*, 1988, **38**, 3098.

21. P. J. Hay and W. R. Wadt, *J. Chem. Phys.*, 1985, **82**, 270, 284, 299.

22. T. H. Dunning , Jr., *J. Chem, Phys.*, 1970,. **53**, 2823; T.H. Dunning, Jr. and P. J. Hay, in *Methods of Electronics Structure Theory*, vol. 2, H. F. Schaefer III, Ed., Plenum Press, 1977.

23. T.H. Dunning, Jr., *J. Chem. Phys.*, 1971, **55**, 716.

24. A. D. Becke, *J. Chem. Phys*, 1993, **48**, 5648; A. D. Becke, *J. Phys. Chem,* 1993, **98,** 1372.

25. C. Lee, W. Yang, R. G. Parr, *Phys. Rev. B*, 1988, **37**, 785.

26. Gaussian Inc. 17. Gaussian 94, Revision D.4, M. J. Frisch, G. W. Trucks, H. B. Schlegel, P. M. W. Gill, B. G. Johnson, M. A. Robb, J. R. Cheeseman, T. Keith, G. A. Petersson, J. A. Montgomery, K. Raghavachari, M. A. Al-Laham, V. G. Zakrzewski, J. V. Ortiz, J. B. Foresman, J. Cioslowski, B. B. Stefanov, A. Nanayakkara, M. Challacombe, C. Y. Peng, P. Y. Ayala, W. Chen, M. W. Wong, J. L. Andres, E. S. Replogle, R. Gomperts, R. L. Martin, D. J. Fox, J. S. Binkley, D. J. Defrees, J. Baker, J. P. Stewart, M. Head-Gordon, C. Gonzalez, and J. A. Pople, Gaussian, Inc., Pittsburgh PA, 1995

27. L. F. Dahl, C. Martell and D. L. Wampler, *J. Am. Chem. Soc.* , 1961, **83**, 1761.

28. I. Bytheway and M. W. Wong, *Chem. Phys. Lett.*, 1998, **282**, 219.

29. G.A. Ozin and A.J. Lee Hanlan, *Inorg. Chem.*, 1979, **18**, 2091. $(M(CO)_4^{-1}$ M=Co, Rh, Ir); R. L. De Kork, *Inorg. Chem.*, 1971, **10**, 1205, $(Ni(CO)_4)$; E.P. Kündig, M. Moskovits and G. A. Ozin, *Can. J. Chem.*, 1972, **50**, 358. $((Pd(CO)_4)$; J. S. Ogden and J. H. Darling, *Inorg. Chem.*, 1972, **11**, 666. $(Pt(CO)_4)$; L. Hanlan, H. Huber, E. P. Kündig, B. R. McGarvey and G. A. Ozin, *J. Am. Chem. Soc.*, 1975, **97**, 7054. $M(CO)_4$ M=Rh, Co, Ir

30. W. J. Hehre, L. Radom, P. V. R. Schleyer and J. A. Pople, *Ab Initio Molecular Orbital Theory*, Wiley, New York, 1986.

31. J. C. G. Pereira, C. R. A. Catlow, and G. D. Price, *J. Phys. Chem. A.,* 1999, **103**, 3252.

32. T. Glowiak, M. Kubiak and T. Szymanska-Buzar, *Acta Crystallogr.*,1977, **33B**, 1732. (RFAC=0.0490, CSD RefCode OXARCH)

33. N. Binstead, J. Evans, G. N. Greaves and R. J. Price, *Organometal.*, 1989, **8**, 613.

34. H. F. J.van't Blik, J. B. A. D. van Zon, T. Huizinga, J. C. Vid, D. C. Koningsberger and R. Prins, *J. Am. Chem. Soc.*, 1985, **107**, 3139.

35. J.Y. Carriat, M. Che, M. Kermarec, M. Verdaguer, A. Michalowicz, *J. Am. Chem. Soc.*, 1998, **120**, 2059; J. C. Papile and B. C. Gates, *Langmuir*, 1992, **8**, 74.

36. D. C. Koningsberger and B. C. Gates, *Catal. Lett.*, 1992, **14**, 271.

37. Y. Asakura, Y. Yamada, and Y. Iwasawa, *Chem. Lett.*, 1985, 511.

38. P. S. Kirlin, F. B. M. van Zon, D. C. Koningsberger, and B. C. Gates, *J. Phys. Chem.*, 1990, **94**, 8439.

39. J. R. Chang, L. U. Gron, A. Honji, K. M. Sanchez and B. C. Gates, *J. Phys. Chem.*, 1991, **95**, 9944.

40. F. B. M. Duivenvoordeen, D. C. Koningsberger, Y. S. Uh and B. C. Gates, *J. Am. Chem. Soc.*, 1986, **108**, 6254.

41. I. Tanaka, N. Jin-No, T. Kushida, T. Ashida, H. Suzuki, H. Sakurai, Y. Moro-Oka, T. Ikawa, *Bull. Chem. Soc. Jpn.*, 1983, **56**, 657.

42. S. A. Vierkotter, C. E. Barnes, T. L. Hatmaker, J. E. Penner-Hahn, C. M. Stinson, B.A. Huggins, A. Benesi and P. D. Ellis, *Organometal.*, 1991, **10**, 3803.

43. M. P. Keyes and K. L. Watters, *J. Catal.*, 1986, **100**, 477; M. P. Keyes and K. L. Watters, *J. Catal.*, 1986, **110**, 96.

44. N. A. Williams, *PhD Thesis*, University of Southampton, 1992.

45. P. Johnston, R. W. Joyner, P. D. A. Pudney, E. S. Shpiro, and B. P. Williams, *Faraday Discuss. Chem. Soc.*, 1990, **89**, 91.

46. J. Evans, B. Hayden, F. Mosselmans and A. Murray, *J. Am. Chem. Soc.*, 1992, **114**, 6912.

47. J. Evans, B. Hayden, F. Mosselmans and A. Murray, *Surf. Sci.*, 1994, **301**, 61.

48. J. Evans, private communication.

49 . J. L. Bilhou, V. Bilhou-Bougnol, W. F. Graydon, A. K. Smith, G. M. Zanderighi, J. M. Basset and R. Ugo, *J. Organomet. Chem.,* 1978, **153**, 73.

50. A. M. Ferrari, K. M. Newman, T. Belling, M. Mayer and N. Rösch, *J. Phys. Chem. B*, 1999, **103**, 216.

51. R. Hoffman, *Solids and Surfaces, a Chemist View of Bonding in Extended Structures*, VCM, New York, 1988.

52. J. Thomson, G. Webb, B. C. Webster and J. M. Winfield, *J. Am. Chem. Soc.*, 1995, **91**, 155.

53. C.Dossi, R. Psaro and R. Ugo, *J. Organometal. Chem.*, 1989, **359**, 105.

54. B. C. Gates and J. V. Boegel and G. A. Fuentes, *J. Catal.*, 1982, **78**, 436.

55. F. G. Ciapetta and D. N. Wallace, *Catal. Rev.*, 1971, **5**, 67.

56. S. S.C. Chuang, G.Srinivas and A. Mukherjee, *J. Catal.*, 1993, **139**, 490 and references therein.

57. F.G.A van den Berg, J. H. E. Glezer, and W. M. H. Sachtler, *J. Catal.*, 1985, **93**, 340.

Chapter 4

Systematic structural analysis of silsesquioxane cages

Chapter Four : Systematic Analysis of Silica cage system

4.0 Introduction

Crystallography is the most powerful method available for studying crystal structures and this technique has become increasingly important in recent years with the introduction of new instrumentation and computational procedures. Detailed analysis of individual crystal structures is commonplace, but systematic analysis of large numbers of related structures is less common. This is usually done by studying a number of molecules with features in common, to postulate a model which suggests relationship between two parameters or more, the most common one and simplest one is the angle and bond length relationship. Other examples include bond angle and NMR shift, bond length or bond angle and electronegativity, and bond length and vibrational frequencies.[1]

The use of Cambridge Crystallographic Data File[2] (CCDC) for systematic analysis on the conformations, reaction pathways, hydrogen bonding, and intermolecular interactions and for visual display of crystals and molecular structures is now fairly established. Works by Murray-Rust[3,4] and Allen et al.,[5,6] for example, illustrated that the systematic analysis of crystallographic data can be a versatile research technique in chemistry.

In recent years, a number of silsesquioxane base structures has been synthesised. Elegant work by Feher et. al.[7] has demonstrated that partly condensed silsesquioxanes are suitable structural models for a variety of surface sites ranging from silanols and silanol nests as found in silica and zeolite systems. Apart from its striking similarity with the SiO_2, the flexibility of this system in adopting different size of atoms into its cage structures also is very interesting. This flexibility which also leads to different conformation with significant differences in the structures, was believed to be, though perhaps not solely, due to the Si-O framework. Being suggested as the potential model of silica surfaces, possessing striking similarity with SiO_2 polymorphs, resembling the zeolite frameworks together with increasing importance and potential of this compound; this work is done with the aim of understanding the nature of these structures.

During the past years, high resolution ^{29}Si NMR has greatly contributed to the deeper understanding of various aspects of the structure of silica. The basic assumptions

behind this approach are that the chemical shielding of a nucleus reflects the local magnetic environment and that the above parameters may be the major contributor in determining this local environment. In general, contributions diminish with the distance between the nuclei.

In an effort to obtain more quantitative information regarding the local environment, there have been numerous attempts to correlate solution NMR chemical shifts with structural parameters such as bond length, bond angles etc.[8] The magnitude of the ^{29}Si NMR reflects sensitively the structural surrounding of the Si atoms in SiO_2.

In this chapter, we shall discuss systematic structural analysis of these sets of silsesquioxane based molecules. The purpose of this investigation was to explore this relationship in detail for a carefully chosen series of silsesquioxanes based molecules whose range of structural data are known from single crystal diffraction studies and to compare this with data with those of silica polymorphs and silicates. This accumulated data may help "to recognise and classify new patterns by noting their points of similarities and dissimilarity to existing entries in the library" to quote the exact explanation by Allen and Fortier.[9]

Moreover, we shall also discuss a correlation study between the ^{29}Si NMR chemical shifts and geometric parameters of silsesquioxane based molecules. More importantly, the aim is to study the relationship between the openness of the incompletely condensed POSS structures and the up field shift of ^{29}Si NMR chemical shift reported for many of the incompletely condensed POSSs.

4.1 Detail of Analysis

4.1.1 Crystals data analysis

The Cambridge Structural Database (CSD) version 5,[10,2] has been used in this study. The quick search on search program QUEST3D using the substructure

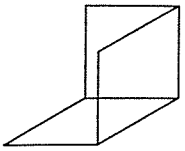

where ——— = Si-O-Si

resulted in 66 hits from which 10 are in the form of ionic silsesquioxane. Based on the search, the silsesquioxanes molecules could be divided into three subgroups: Si_8, Si_7 and Dimer. Si_7 however, can be further subdivided into two classes, Si_7 and Si_7X. Dimers, on the other hand, are actually made up of either two Si_7 or Si_7X or both, as simplified below.

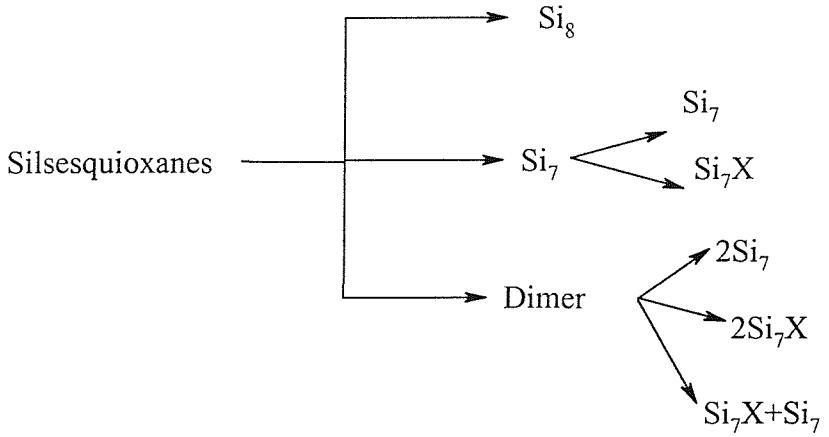

Figure 4.1 to 4.4 divide all refcodes into their subgroups.

Data analysis was performed using VISTA. As some of the initial data involved in the study were based on the work of J.Grimshaw,[11] the result from the search on the CSD was exported to Microsoft Excel spreadsheet and analysed using this software.

The following strategy has been adopted with the aim of having reliable data.

(i). R factor of less or equals 10% is chosen

(ii). No disorder reported

(iii). No error

Search with PERMUTE key ON, is in many cases avoided, as this keyword is very sensitive to the environment of the chosen atom(s) and may result in incomplete accumulation of data (leave out some relevant data).

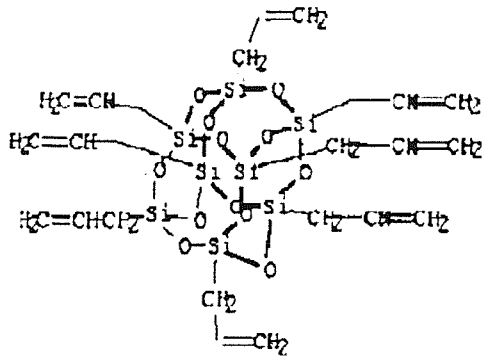

BEGGEZ

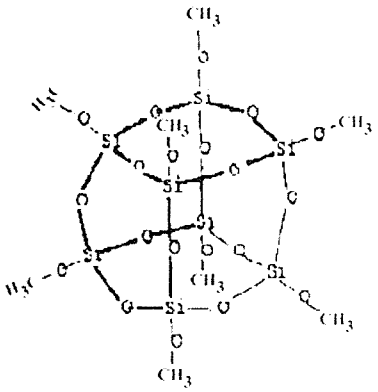

DIRXAD

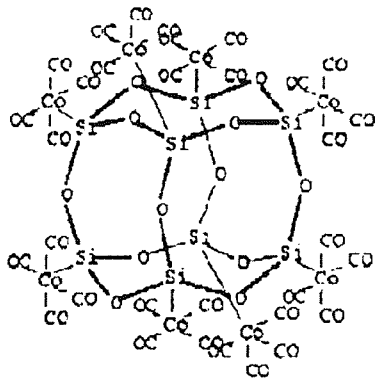

GEYPAB

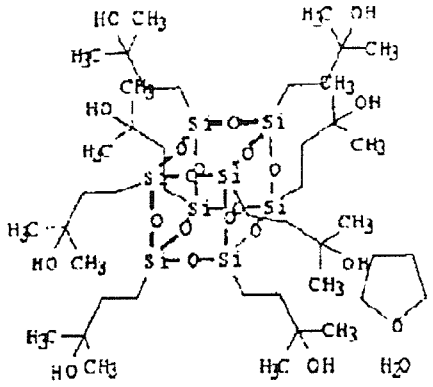

FAQWID

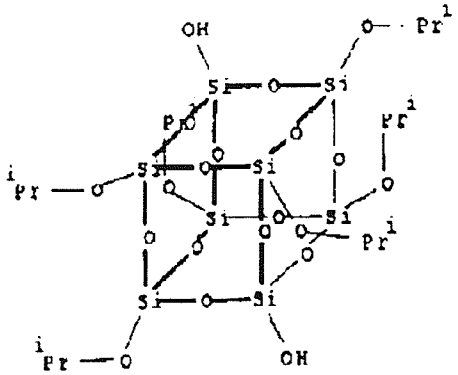

FAQWOJ

Figure 4.1a: Silsesquioxanes of group Si_8

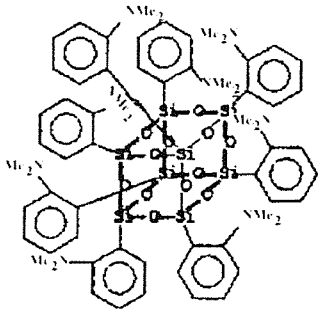

JUWPAS

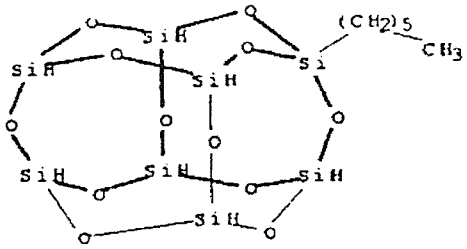

LIGJUG

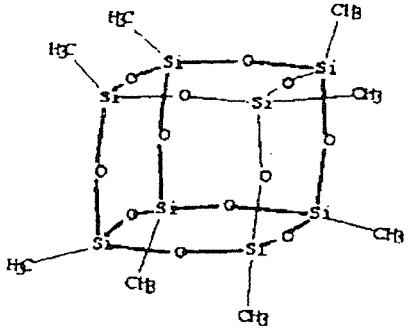

OCMSIO

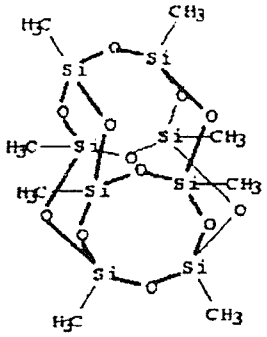

OCMSIO01

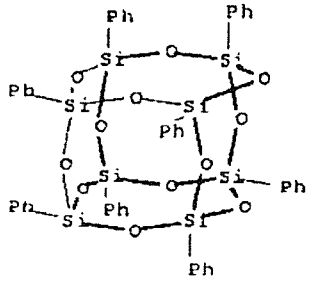

OCPSIX

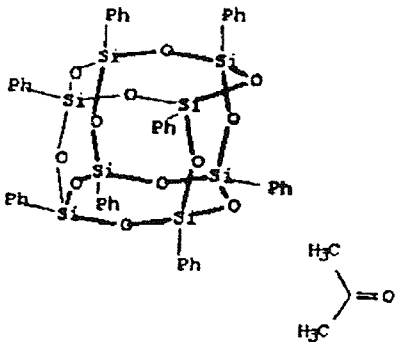

OPSIOY

Figure 4.1b: Silsesquioxanes of group Si_8 (cont.)

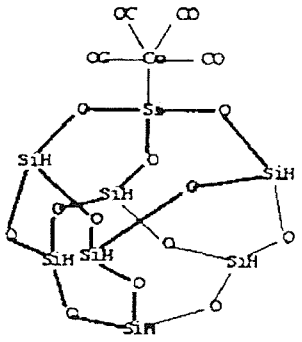

PIFFEP

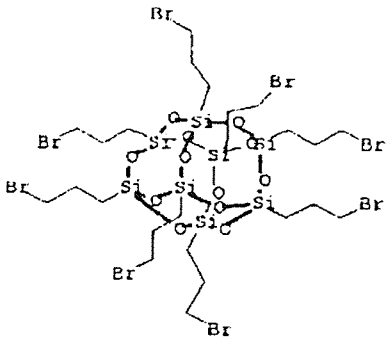

RESXAO

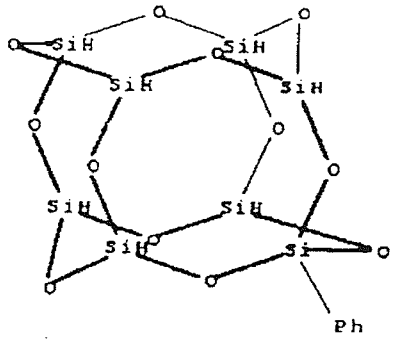

TOGTIS

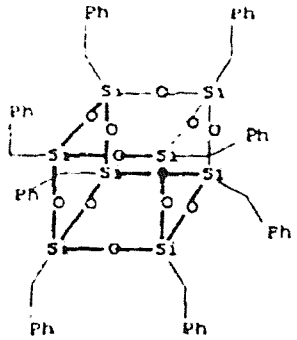

VAWXUM

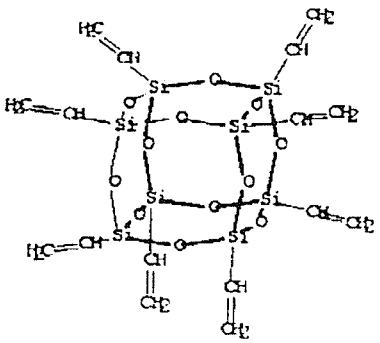

VINSIO01

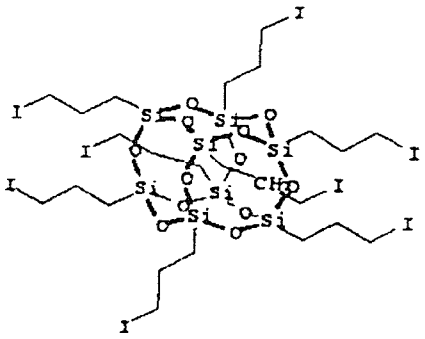

YUMYOU

Figure 4.1c: Silsesquioxanes of group Si_8 (cont.)

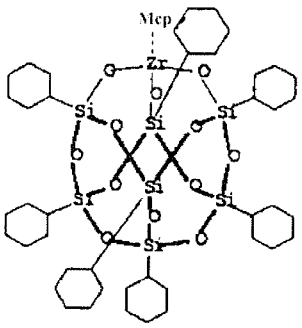

DURPAH

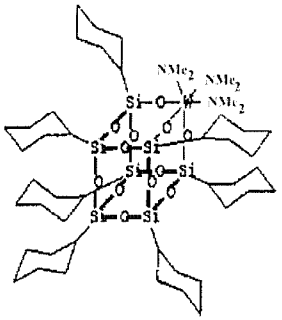

JOZHAH

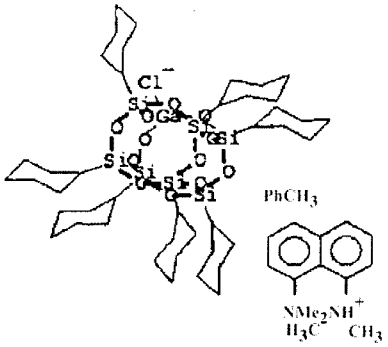

NITKEG

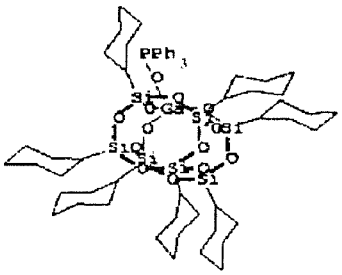

NITKIK

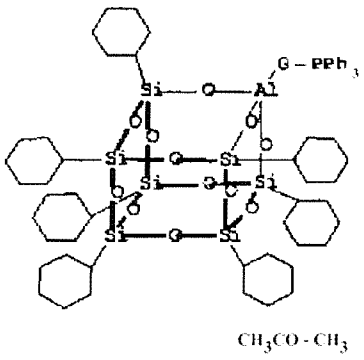

SEDCAF

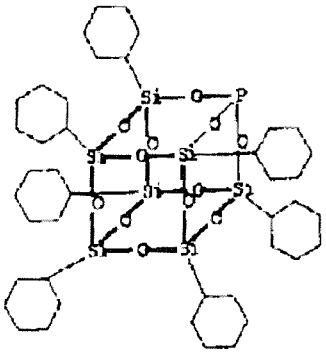

TAKBUC

Figure 4.2 : Silsesquioxanes of group Si_7X

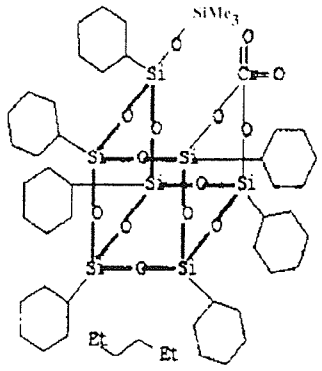

JEWXAK

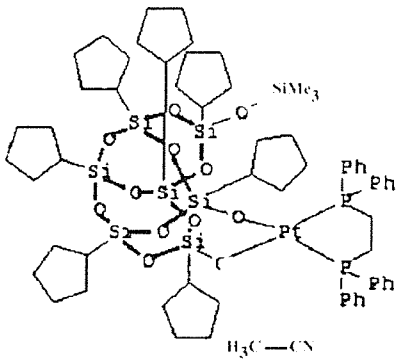

JOFWOQ

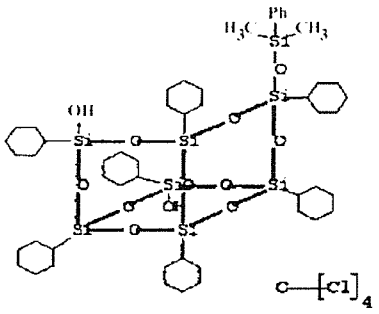

KELJIU

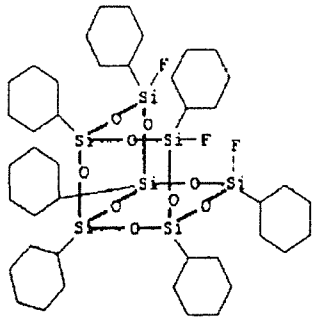

RITCAY

Figure 4.3a: Silsesquioxanes of group Si_7

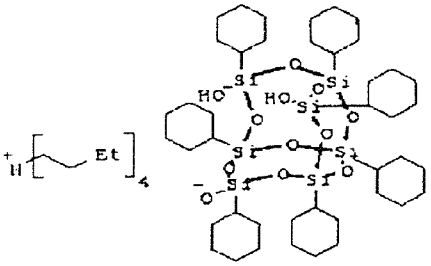

RONSES

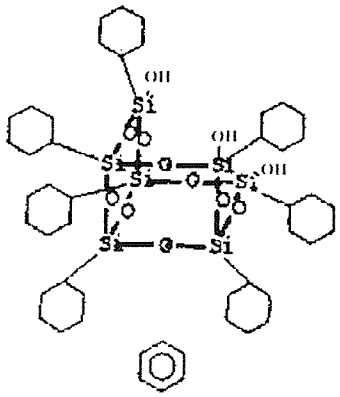

VAMVIO

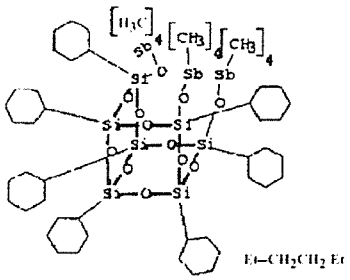

VUFNOZ

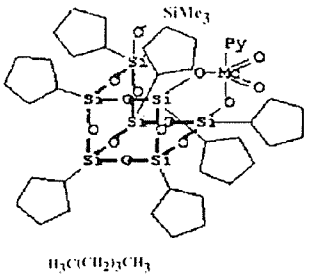

ZEGVUC

Figure 4.3b: Silsesquioxanes of group Si_7 (cont.)

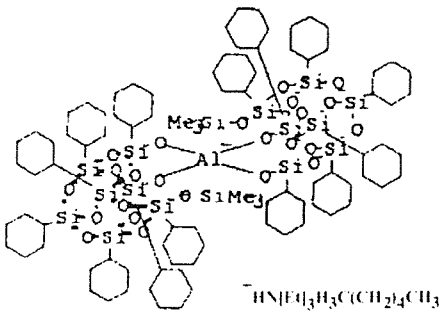

FEQCIN

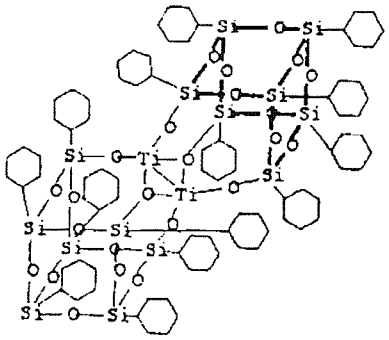

GEZGIB

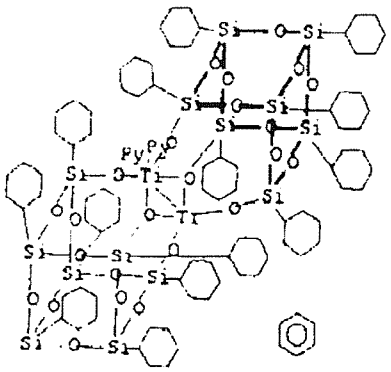

GEZGOH

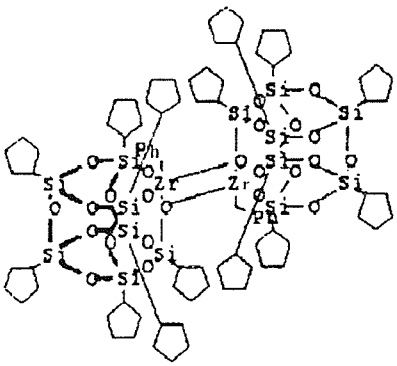

HITZUF

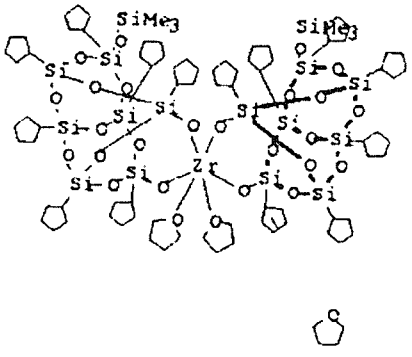

HIVBAP

Figure 4.4a: Silsesquioxanes dimer

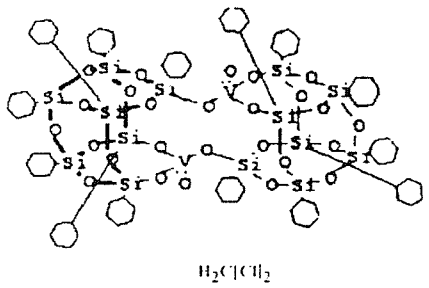

KIVYET

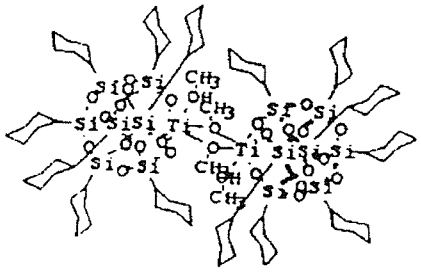

NIWQIT

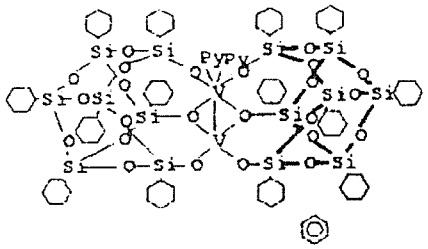

SIBXEG

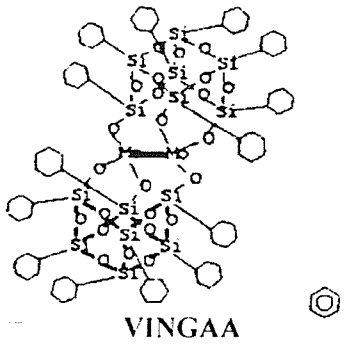

VINGAA

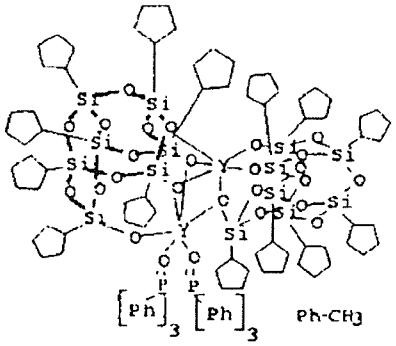

LEXCOG

Figure 4.4b: Silsesquioxanes dimer (cont.)

A search which involved data having disorder in the R group with the R factor less or equal to10% was also performed just as a comparison. Conformational disorder of the cyclopentyl and of the cyclohexyl rings on silsesquioxanes based molecules can be observed in many cases [Table 4.1]. This not that unusual behaviour was first understood by Ries et. al in their study of $Cr(CO)_5$ piperidine.[12] The puckered organic unit was disordered over two alternating positions. Since each of the six atoms of the ring in the two alternative positions are separated by 0.5 Å or less, the refinement spontaneously converged into a roughly planar geometry, Figure 4.5.

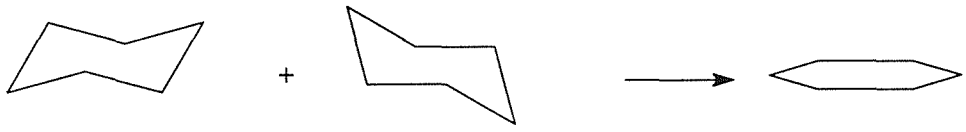

Figure 4.5: How the structure with a planar ring resulted from inadequate refinement of a disordered $Cr(CO)_5$ piperidine molecule containing a puckered ring.

Another set of work which selected only entries with no disorder, error free, not polymers, perfect match between chemical and crystallographic connectivity and had R factor ≤ 5% was also presented as a comparison in the Si-O bond distance and Si-O-Si angle search.

Table 4.1 shows the refcodes of R factor less or equals 10% through a quick search using QUEST.

Table 4.1: Refcodes included in analysis

Si_8		Si_7		Si_{7X}	
BEGGEZ	13	FEQCIN[D]	30	DURPAH	45
DIRXAD	14	GEXGIB[D]	31	JOZHAH*	46
GEYPAB[e]	15	GEZGOH[D]	31	LEXCOG	47
FAQWID*	16	HITZUF*[D]	32	NITKEG*	48
FAQWOJ	16	HIVBAP*[D]	32	NITKIK	48
JUWPAS	17	JEWXAK*	33	SEDCAF	49
LIGJUG	18	JOFWOQ*	34	TAKBUC	50
OCMSIO	19	KELJIU	35		
OCMSIO01	20	KIVYET*[D]	36		
OCPSIX[E]	21	NIWQIT[D]	37		
OPSIOY*	22	RITCAY	38		
PIFFEP	23	RONSES	39		
RESXAO	24	SIBXEG[D]	40		
TOGTIS	25	VAMVIO	41		
VAWXUM	26	VINGAA	42		
VINSIO*	27	VUFNOZ	43		
VINSIO01*	28	ZEGVUC	44		
YUMYOU	29				

[D] Dimer [e] Error * Disorder of R group

4.1.2 ^{29}Si NMR Correlation studies

The influence of molecular geometries on ^{29}Si chemical shift has long been recognised. Although in most of the study the NMR data was based on solution data, many have reported that there is no substantial changes in the NMR data of solid phase and solution phase.

$R_8Si_8O_{12}$ cages with equivalent R display a single signal in a very large range reported to be from 5.7 ppm (in $H_8Si_8O_{12}$) to -101.4 ppm (DIRXAD). FAQWOJ, the trans $R'_2R_6Si_8O_{12}$ type cages, exhibit two signals at -103.3 and -103.0 ppm. It is also interesting to point out that the chemical shift reported for DIRXAD and FAQWOJ is in the same range reported for silica polymorphs i.e. cristobalite (-109.9 ppm), tridymite (-109.3 to –114.0 ppm) and zeolites, NaX (- 103.4 ppm).[51]

The selection of crystal data used in the correlation studies in Si_8 cages and the ^{29}Si NMR chemical shifts are given in Table 4.2.

The following strategy has been adopted with the aim of having reliable data.

(i). Values of the δ were from the literature data of the crystal data.

(ii). R factor of less or equals 10% is chosen, except for FAQWOJ which has R factor of 0.1014

(iii). No disorder reported

(iv). No error

Table 4.2: Geometric parameters of selected Si_8 cages and its ^{29}Si NMR chemical shift

RefCode	^{29}Si NMR chemical shift	SiO_{mean}	$SiOSi_{mean}$	$Si..Si_{mean}$
DIRXAD	-101.4	1.603	148.2	3.083
FAQWOJ	-64.9	1.603	148.6	3.087
FAQWID	-103.3,-103.0	1.623	148.5	3.121
JUWPAS	-79.5	1.618	147.7	3.105
RESXAO	-66.8	1.619	148.8	3.116
VAWXUM	-71.28	1.616	148.9	3.112
YUMYOU	-67.93	1.615	149.0	3.114

With the Si_7 group, it would be very nice if the above mentioned requirements can be met, but due to the limited data, we have also included JOZHAH and NITKEG which are reported as having R group disorder. However, all the refcodes selected have $R=C_6H_{11}$, so that the effect of the R group could be minimised. Table 4.3 lists the chemical shifts δ and the refcodes for the data studied.

The selected Si_7X and Si_7 cages, all exhibit three signals which indicate, three chemically different Si nuclei within the molecule. Feher *et al* reported peaks with relative intensity of 3:3:1 of DURPAH,[45] in which he assigned it to silicon atoms 2 atoms, 4 atoms and 6 atoms away from the zirconium atom.

Examination of the corresponding δ, intensity ratio and the SiO data based on the data on $Cy_7Si_7O_9(OH)_3$, VAMVIO, and the rest of Si_7 cage molecules analysed, [Table 4.3], shows that in general, of the three signals, two of those signals vary very little at

around –66.0 ppm and -69.9 ppm (relative intensity 1:3 respectively). Using this knowledge, we could therefore assigned the peak with relative intensity of 3 as Si_b and the peak with relative intensity 1 as Si_c. Leaving the peak which varies most as Si_a.

This is summarised below.

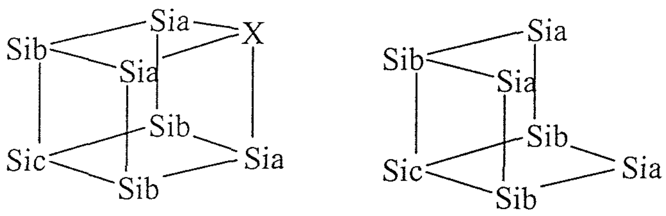

Si (a,b,c) =Signal (3:1:3)

As the relative intensity of the peaks gives a quantitative information of the number of Si atoms, we could assign the peak with relative intensity 1 to Si_c, leaving the other 2 peaks to be assigned.

The Si..Si distance differentiates one from another as illustrated by Figure 4.6.

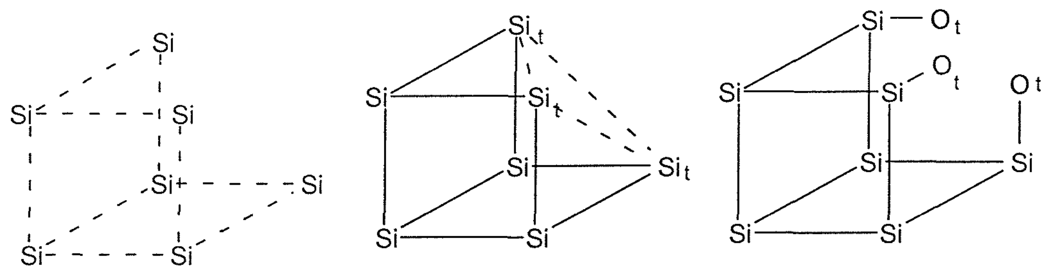

Figure 4.6: Fragment used the Quest3D substructure search; from left to right, a c-three fold symmetry Si..Si distance, Si_t...Si_t distance and the O_t...O_t distance

Table 4.3: Solution $^{29}Si\{H\}$ NMR for Si_7X and Si_7 cages.

RefCodes	R group	δ ^{29}Si NMR	Signal Ratio	SiO_{mean}	$SiOSi_{mean}$	$Si..Si_{mean}$
VAMVIO‡	C_6H_{11}	-60.159, -67.993, -69.544	3:1:3	1.613	152.6	3.126
VUFNOZ‡	C_6H_{11}	-67.94, -70.58, -71.87	1:3:3	1.619	148.8	3.123
DURPAH	C_6H_{11}	-66.058, -68.486, -70.286	3:1:3	1.623	150.8	3.135
JOZHAH	C_6H_{11}	-66.54, -68.68 -69.03	3:1:3	1.612	148.0	3.104
NITKIK	C_6H_{11}	-64.26, -68.65, -70.20	3:1:3	1.621	148.6	3.116
NITKEG	C_6H_{11}	-65.64, -68.66, -70.24	3:1:3	1.614	149.7	3.12
SEDCAF	C_6H_{11}	-65.85, -68.85, -69.98	3:1:3	1.615	149.2	3.116
TAKBUC	C_6H_{11}	-66.95, -67.99, -71.44	3:1:3	1.622	146.9	3.102

‡Si_7 cages

4.2 Results and Discussion

4.2.1 Si-O bond

The overall distribution of Si-O bond distance is given in Figure 4.7. The histogram in Figure 4.7 has maxima at around 1.60-1.62 Å in both cases, Si_8 and Si_7 cages. The Si-O distances in Si_8 cages are in wider ranges, 1.51-1.72 Å. However, it is also important to note that the shorter and longer distances at the tail and the head of the histograms, are due to BEGGEZ, which surprisingly has a reported R factor of 0.0. If we remove BEGGEZ from the list, the range in both Si_7 and Si_8 are about the same.

Another important point observed is the maxima was right shifted in Si_7 cages (i.e. longer) as compared to the Si_8 cages.

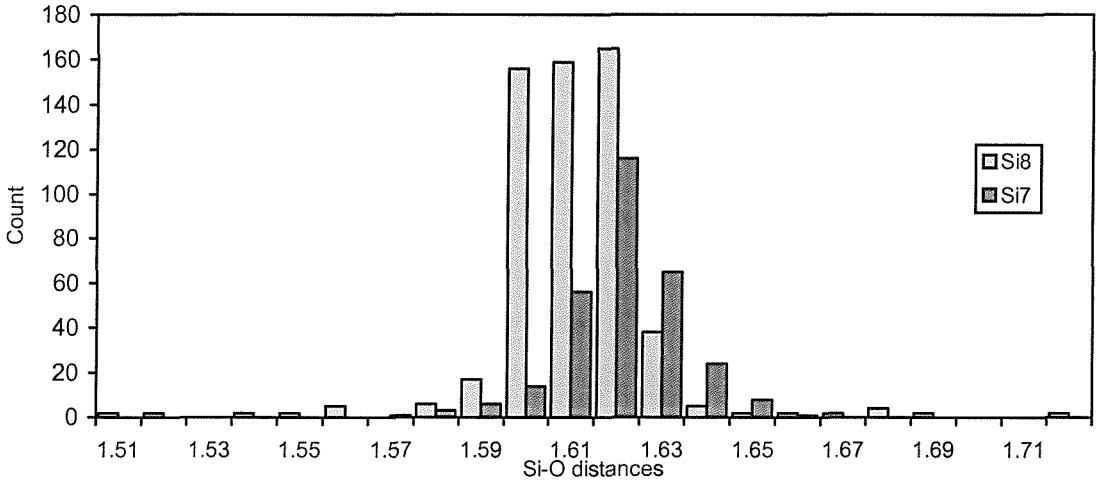

Figure 4.7: d(Si-O) distances in Si_8 and Si_7 cages

The slight deviation in Si_7X and Si_7 could be attributed to steric effect such as strain due to the accommodation of metal cation, eg. Zr atoms, into the framework. Clearly the average Si-O distances in silsesquioxanes (Si_8 and Si_7 cages), are very similar to the average Si-O distances found in the various SiO_2 modifications; 1.615Å in low quartz,[52] 1.61 Å in high quartz, 1.59 Å in low cristobalite and 1.60 Å in SiO_2 glass.[53]

The Si-O distances of the adjacent bonds sharing a Si-O-Si angle in Si_8 cages can differ by about 0.036 Å, this is in the similar range of the reported variation of Si-O bond length observed on SiO_2 polymorphs. However, in both Si_7 and Si_{7x} cages, the variations

are significantly greater, up to 0.07 Å. Apparently, the greater differences are for terminal Si-O than for the inner part of the Si_7 cages.

In the Si_7X cages, the differences are about the same as that of Si_7 cages, despite the more obvious opening up of the system of the latter cages. Clearly, the stretching of one Si-O bond leads to shortening of the other but differences as large as 0.07 Å again indicate the flexibility of this cage and Si-O framework which allows the Si-O framework to adapt to varied sizes of metal and various conformations.

In a study of silica frameworks, Gibbs et al reported 50% of the variation in T-O distances (T=Al or Si) can be explained in terms of a linear dependence on T-O-T.[54] Differences in the type of bond should also cause perceptible differences in the internuclear distances, so that the Si-O(→M) distances with strong electron donor atoms should be smaller than the Si-O(→Si) distances, similar to the phenomena observed in silicates. Other factors that have been reported to influence the Si-O distances in silica and silicates are structural disorder and thermal motion of the atoms in the crystal data.

Atomic distances determined from diffraction methods differ from the actual bond length to an extent which depend on the amplitudes of the thermal motion and the strength of the coupling of the individual motions of the atoms involved in the bond.

The influence of even a relatively inaccurate correction of $Si\text{-}O_{br}$ distance for thermal motion on correlation between d(Si-O) and Si-O-Si angle has been studied by Taylor using a limited data set for the silica polymorphs. The study of the correlation between the degree of static and/or dynamic disorder and atomic distances d(Si-O) and angles Si-O-Si on silica have been reported previously by Liebau[55], Gies [56]and Gerke and Gies.[57] The regression equation of

$$d_{ind}^{real}(Si-O) = d_{ind}^{r\ddot{o}}(Si-O) + 0.007B(O) \text{ in Å}$$

where

$d^{r\ddot{o}}$(Si-O) is the mean value of all Si-O distances

‹B(O)›is the value of the isotropic temperatures factors of the oxygen atoms within a particular structure, determined from X-ray diffraction data

has been deduced based on the 25 structure determinations of silica polymorphs and clathrasils performed at various temperatures which enable workers to correct the Si-O distances obtained from X-ray structure analysis of silica framework for dynamics and static disorder and to transform them into actual Si-O bond lengths with the aid of the equation. However the author cautions that the equation should be used only on similar frameworks until it is proven the equation holds for Si-O bonds in other silicates as well.

4.2.2 Bond angle

While the O-Si-O bond angles seem to fall into comparatively small ranges of (107°-111°), nearly tetrahedral as expected, Figure 4.8, a much smaller range than the range suggested in silicate studies, the Si-O-Si bond angles seem to be as flexible as the SiO_2 framework. The Si-O-Si angle stretches from 135° to 172° in Si_7 cages while the Si-O-Si angles are much in narrower range in Si_8 cages, 140° to 156°. Wide ranges of Si-O-Si angles have also been reported for polymorphs of silica for example, from 143.4° in low quartz[58] to 180.0° in tridymite.[59]

Based on a total of 162 angles, the histogram in Figure 4.8 of Si_7 cages, the Si-O-Si bond angles in the silsesquioxanes framework give no clear maximum. This point deserves further comments. The maxima at 172° of the histogram was due to $Cy_7Si_7O_{12}Ga(OPPh_3)$, CSD refcode NITKIK. Another maxima, at 168° was due to $Cy_7Si_7O_{12}(OSbMe_4)_3$, CSD refcode VUFNOZ. The same is also true for the smaller angles at around 135°. Interestingly, the former is from Si_7X cage group and the latter is Si_7 cage indicating real flexibility of the silsesquioxane system. This flexibility is also known for other types of silica-oxygen framework.

The average Si-O-Si bond angles for Si_8 was at 149° and the same value was found for Si_7 and Si_7X respectively which shows agreement with experimental data of α-cristobalite, 150° and close to theoretical calculated energetic minimum for Si-O-Si angle near 150°. [60]

In silicates Si-O-Si angle of 139°, was interpreted to be the value which is energetically most favourable for a strain-free Si-O-Si bond. Larger deviations were attributed to either steric effects such as forced accommodation of cations of

unfavourable size or to purely chemical effects such as the influence of cations of extremely low electronegativity or high valence.[68] These phenomena also explained the large deviation from 139° in both cases, Si_8 and Si_7 silsesquioxanes cages.

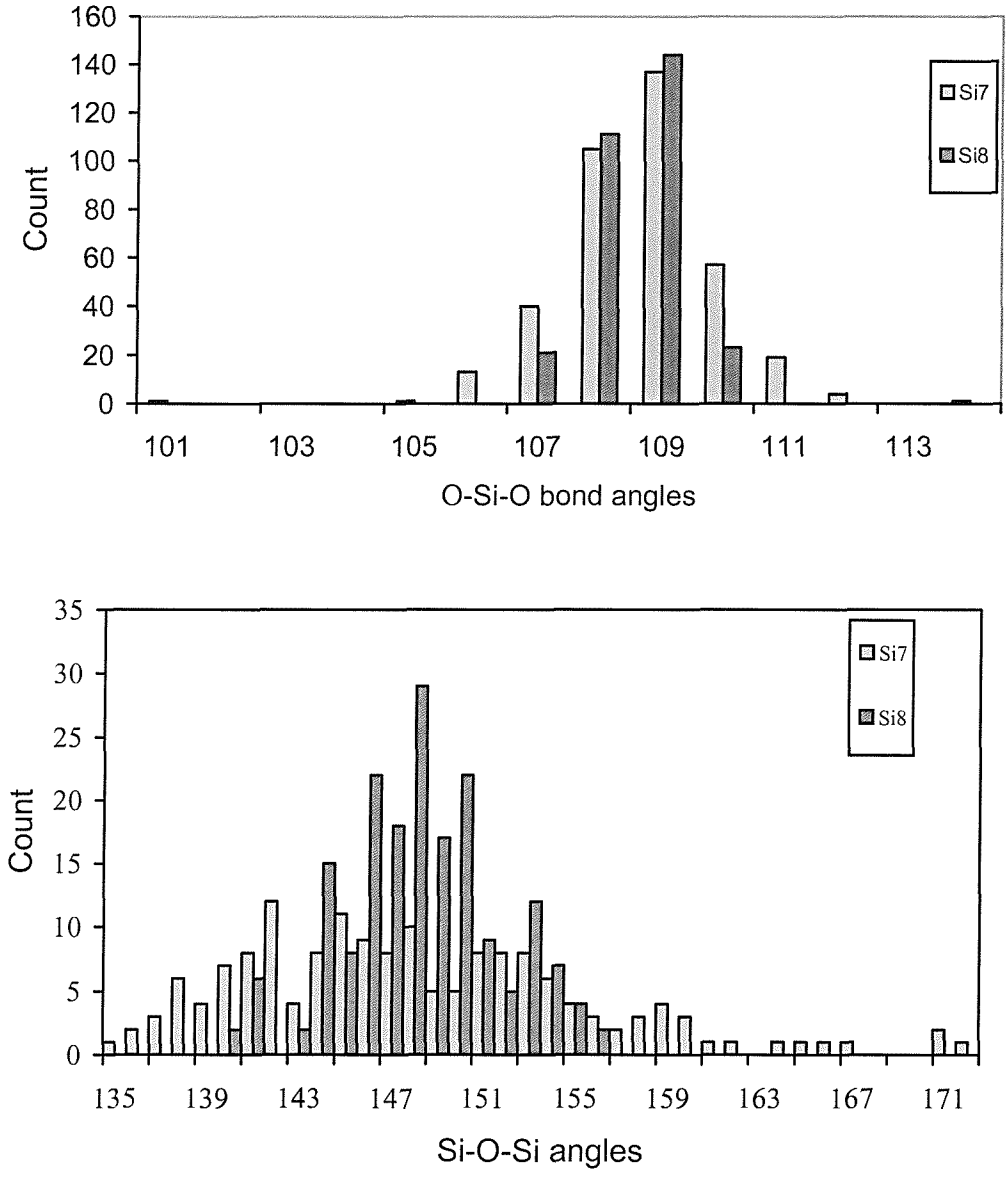

Figure 4.8: O-Si-O and Si--O-Si bond angles of Si_8 and Si_7 cages at R value of 0.10

The range within which individual atomic distances Si-O and Si..Si, and Si-O-Si and O-Si-O bond angles vary for silsesquioxane published with R values less or equal 0.10 using X-ray diffraction are given below.

a). Si_8 cages	b).**Si_7 cages**
1.51 Å < d(Si-O) < 1.72 Å*	1.57 Å < d(Si-O) < 1.66 Å
3.06 Å < d(Si..Si) < 3.16 Å	3.0 Å < d(Si..Si) < 3.24 Å
107° < O-Si-O < 110°	101° < O-Si-O < 114°
140° < Si-O-Si < 156°	135° < Si-O-Si < 172°

* include BEGGEZ, R factor 0.0

For silicate structures with R values below 0.08 using X-ray or neutron diffraction collected near or below room temperature these ranges are;[61]

1.57 Å < d(Si-O) < 1.72 Å

98° < O-Si-O < 122°

120° < Si-O-Si < 180°

According to Liebau, when inter atomic distances and bond angles determined at room temperature are reported near or outside the limits of these ranges, the deviation is probably a result of inaccuracies in the structure determination or of considerable disorder in the structure. Only in very rare cases will they be caused by unusual chemical or steric effects.[62]

If we compare and take these values to Si_8 and Si_7 cages considered in this work, all bond lengths and bond angles are within the range suggested. Despite the various R group in the $R_8Si_8O_{12}$ or $R'R_7Si_8O_{12}$ system, the changes or deviation of these parameters also appear to be insignificant. Bond distance distributions in Si_8 and Si_7 cages with disorder (on the R group) also fall within the ranges above and there are no apparent short Si-O distance usually associated with thermal motion.

The nature of the Si-O bond has been addressed in numerous literature reports so it is not the aim of this chapter to discuss it in detail. The nature of the relationship between bond length and the bond angle of the adjacent atoms is an old problem. It is

well documented that an inverse relationship exists, i.e. increase in the bond angle is connected to the decrease of the respective Si-O distance. (See for example ref. 63 and 64). Interest in this area has renewed as experimentalists begin to make highly strained molecules.

The result for the $Si\text{-}O_{ind}$ vs. Si-O-Si bond angles shows little correlation, certainly the bond length does not decrease uniformly as the angles widen. Nevertheless, the general integrity of the inverse bond length/bond distance correlation for silsesquioxane is apparent.

4.2.3 Data set with R factor 0.05

For Si_8 and Si_7 structures involving smaller number of data set, i.e. with R values below 0.05, the histogram, Figure 4.9, shows a maximum peak at 1.61 Å for Si_8 cages, and again shoulders at short distances of 1.51 Å and longer, both due to BEGGEZ.

The shift observed in the larger data set is also evident even in this smaller data set. This is also evident by the shift in the overall mean Si-O distances in each case. Si_8 cages have a mean at 1.61 Å while the Si_7 cages have a slightly longer mean Si-O distance, (1.62 Å) similar to the larger set, of R factor 0.10.

For a smaller set comprising 92 and 27 Si-O-Si angles obtained for Si_8 and Si_7 cages respectively, the histogram, Figure 4.10, has a maximum at around 147 ° to 151° for Si_8 cages while for the Si_7 cages, the same large distribution and scattering is observed. Again both sets, Si_8 and Si_7, have the same Si-O-Si mean, 149°.

In all the range are as the following;

a). **Si_8 cages**

1.51 Å < d(Si-O) < 1.72 Å*

142° < Si-O-Si < 157°

b).**Si_7 cages**

1.58 Å < d(Si-O) < 1.65 Å

138° < Si-O-Si < 172°

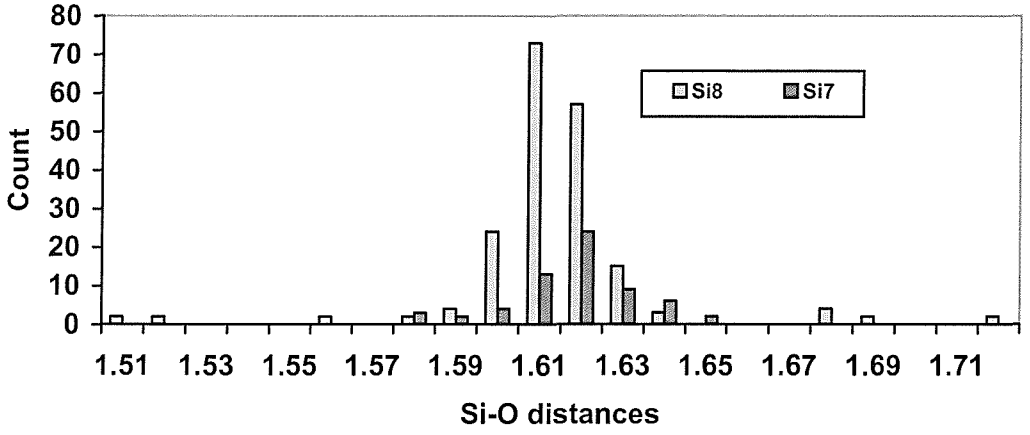

Figure 4.9: Si-O distances in Si_7 and Si_8 cages with R value of 0.05 or less

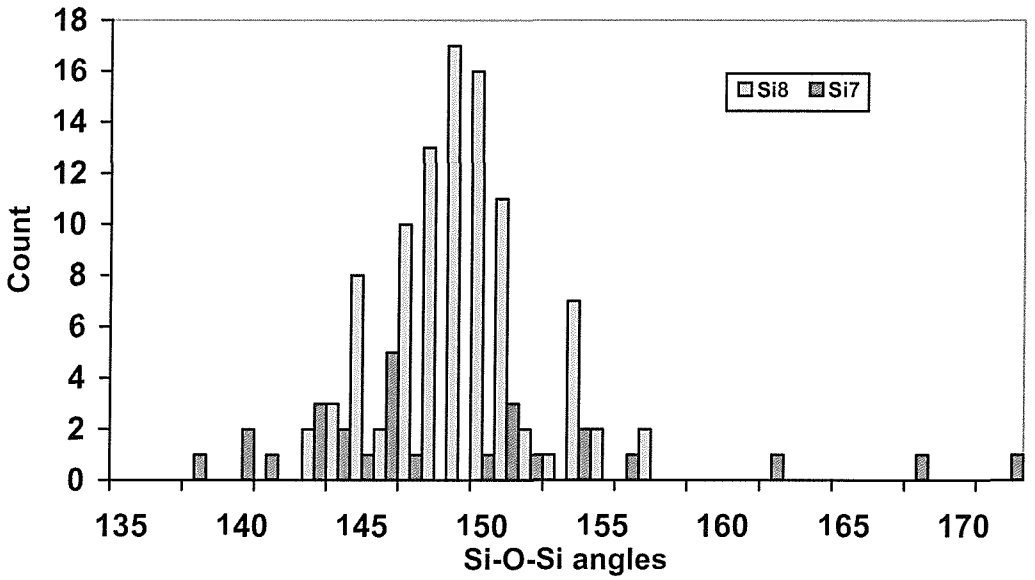

Figure 4.10: Si-O-Si bond angles at R value of 0.05

4.2.4 Si..Si nonbonding distances

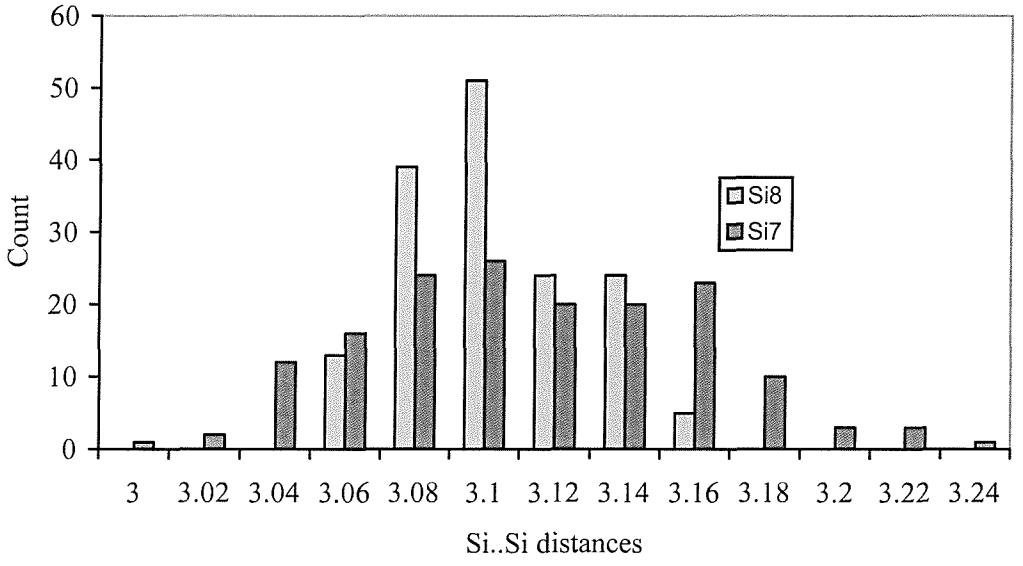

Figure 4.11: Non bonding Si..Si distances in Si_8 and Si_7 cages.

The Si..Si nonbonded distances are known to vary very little despite the wide range of Si-O-Si angles. In Si_8 cages, while the Si-O distances vary from 1.55 to 1.69 Å, the Si..Si nonbonding distances vary very little in Si_8, despite the various R group considered. However in Si_7 cages, this range is wider and more obvious, from 3.02 to 3.24 Å, Figure 4.11.

A Si..Si distance of 3.20 Å has been reported for the linear Si-O-Si bridges in coesite. The range of Si..Si distances in SiO_2 was also reported as remarkably small, all were very close to the ideal 3.1 Å expected in the hard atom approximation.[65] This led to a concept that such geometries are determined at least in part, by non bonded Si..Si repulsion [65] Cruickshank however, interpreted that the large Si-O-Si angles as due to d_π-p_π bonding of Si- and O atoms. [66]

The relationship between Si..Si distances and the Si-O-Si angles are nicely shown in Figure 4.12 which indicates a linear relationship between the two parameters, i.e the Si..Si distances vary with shorter nonbonding distances involving smaller angles.

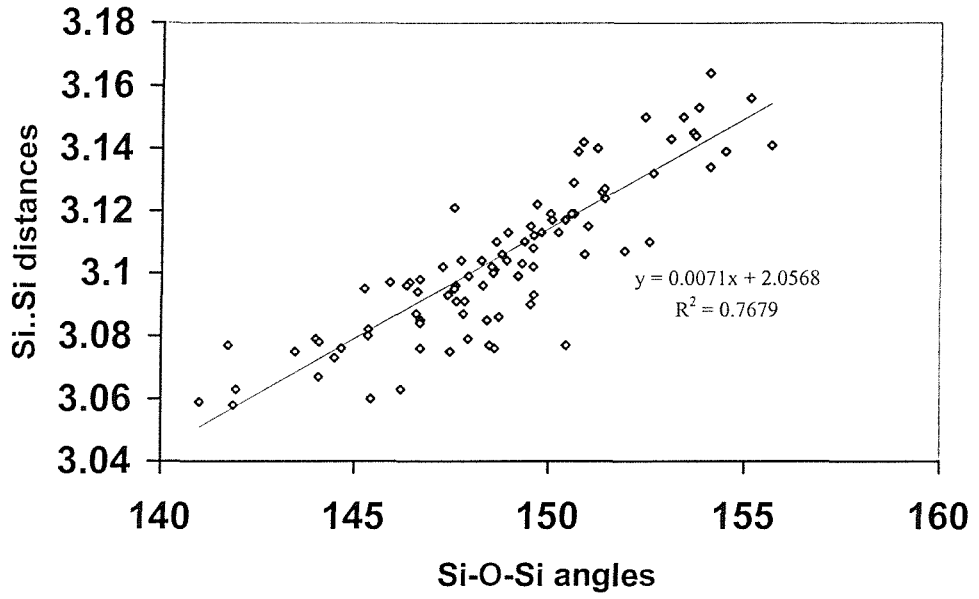

a).

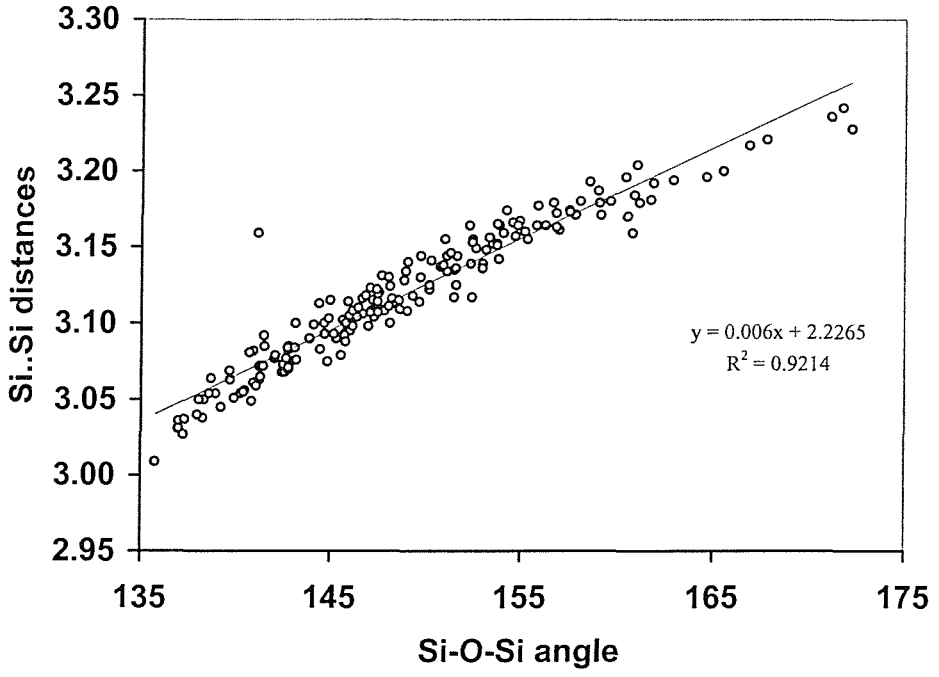

b).

Figure 4.12: The relationship between Si..Si distances and Si-O-Si angles in a). Si_8 and b). Si_7 cages

So, if we consider the fact that the inverse relationship between the angle and the Si-O distance, the Si..Si distances are actually the result of a compromise between Si-O distances and Si-O-Si bond angles.

4.2.5 Openness of silsesquioxane cages

A relationship between the $Si_t..Si_t$ and the $O_t..O_t$ distance of the open face of the cage Si_7 cages is illustrated by Fig. 4.12. Obviously the O..O distance increases as the Si..Si increases, but the increase in the Si..Si distances are smaller compared to the O..O distances. Short $O_t..O_t$ distances are attributed to the $O_t..O_t$ distance in Si_7Xcages and also that of Si_7O_{11} systems (such as ZEGVUC) while obviously the large Si..Si and O..O distances are attributed to system such as VUFNOZ which has three $OSbMe_4$ groups. Table 4.4 shows some O..O distance of the open cage of selected Si_7 silsesquioxanes.

This opening up was expected to be due to the bulky nature of the substituents in conjunction with the flexibility of the silicon-oxygen framework to accommodate range of complexes and conformations.[7] Another factor is the existence of hydrogen bonding, either inter molecular or intra molecular or both.[41] Factors such as electron repulsion from the metal towards TMS group for example are also believed to contribute to the extent of the openness of the cage. [33]

Table 4.4: Distance in Å between the oxygen atoms on open face cage in various Si7 complexes.

Molecules	O..O distances	REFCODE/ Ref
$Cy_7Si_7O_9(OGeMe_3)_3$	6.311 ,6.175, 5.33	[11]
$Cy_7Si_7O_{11}(OTMS)(SiMe_2)$	5.986, 5.334, 3.162	[11]
$Cy_7Si_7O_{11}(OTMS)(ZrCp^*_2)$	3.505, 6.522, 6.187	[11]
$Cy_7Si_7O_{11}(OTMS)(CrO_2)$	2.827, 4.815, 5.345	JEWXAK
$Cy_7Si_7O_9(GaOPPh_3)$	3.017, 3.022, 2.886	NITKIK
$Cy_7Si_7O_9(AlOPPh_3)$	2.854, 2.848, 2.861	SEDCAF
$Cy_7Si_7O_9(P)$	2.466, 4.488, 2.465	TAKBUC
$Cy_7Si_7O_9(OH)_3$	4.033, 4.095, 4.092	VAMVIO
$Cy_7Si_7O_9(OSbMe_4)_3$	6.057, 6.192, 5.728	VUFNOZ
$Cy_7Si_7O_{11}(OTMS)(MoPyO_2)$	4.632, 2.761, 5.517	ZEGVUC

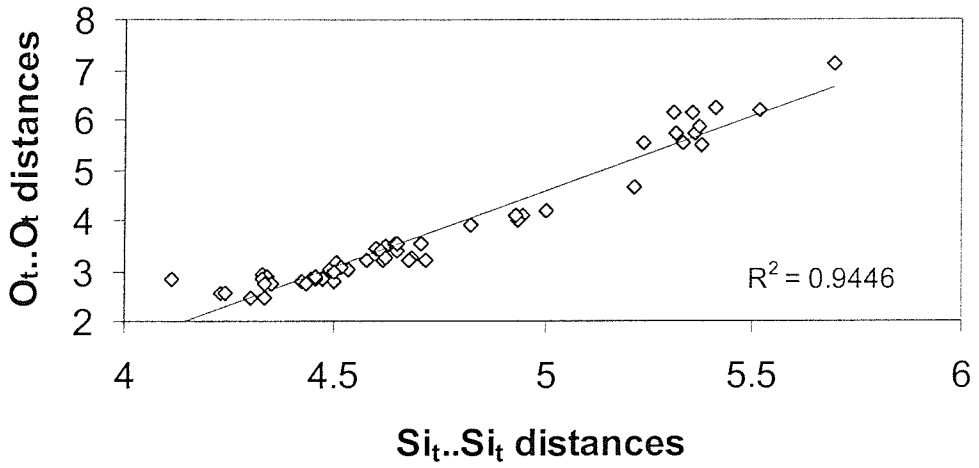

Figure 4.13: Relationship between Si..Si distances and O..O distances in Si_7 cages

Grimshaw[11] in her thesis pointed out that the increase of these O..O distances were always accompanied by an upfield shifts in ^{29}Si NMR spectra. Figure 4.13 shows quite a good correlation, r value of 0.9446, between $Si_t..Si_t$ and $O_t..O_t$ distances. In the following section, we will discuss the correlation between these parameters and the chemical shifts.

4.2.6 NMR chemical shift/geometric parameter correlations studies

In general, all attempts to correlate the chemical shift with the geometric parameters seem to result in a considerable scatter. For Si_8, correlation was sought between chemical shift and 1). Si-O bond distance 2). Si-O-Si bond angles 3). Si..Si bond distance. Figure 4.15 shows weak correlation between the Si-O-Si and δ (R=0.46), good correlation was observed with mean Si-O distance, while a better r value was observed with mean Si..Si distances of the cage The correlation with mean Si-O distances shows considerable scatter, almost no correlation with mean Si-O-Si bond angles, r=0.4601, but high correlation can be observed with mean Si..Si distances, r=0.9863, of the Si_8 cages giving the following regression

$$\delta \text{ (ppm)} = 1216.1 d_{Si..Si} - 3856.6 \qquad \textbf{(4.1)}$$

Smith and Blackwell[67] had also reported that an excellent correlation exists with Si..Si nonbonding distance of silica polymorphs. Clearly it is not fair to use this correlation on silica polymorphs or vice versa. The presence empirical equations, Equation 4.1, should be tested on other Si_8 cages when accurate crystal data and NMR data become available.

We were unable to elucidate the cage size effect to the chemical shift since only a few data were reported and in many cases when crystal data was available there was no ^{29}Si NMR data accompanied. But, the definite dependence of cage size is quite clear and this was first reported in 1970, by Frye and Collins[68] The authors reported an up field chemical shift on $(HSiO_{1.5})_n$ n=8,10,12,14 as the cage size increases, [Figure 4.14].

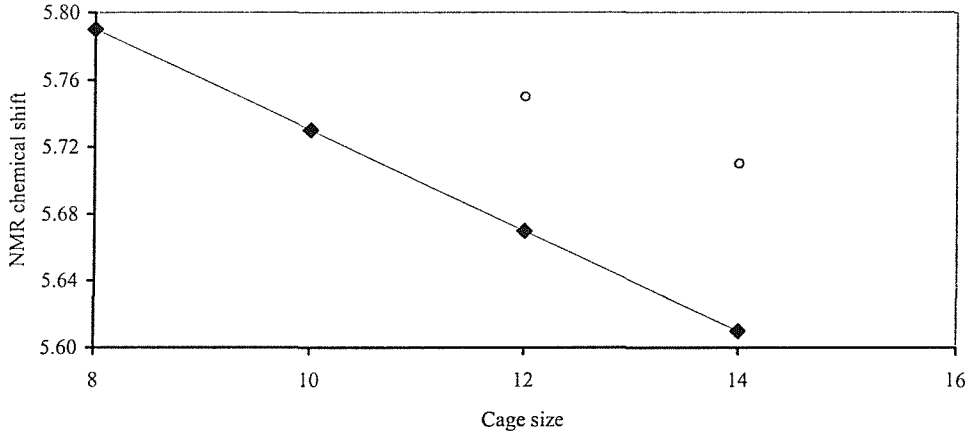

Figure 4.14: Correlation between cage size and ^{29}Si NMR chemical shift of $(HSiO_{1.5})_{n=8,10,12,14}$ Data from ref. 68. Diamonds shapes are due to the Si_4O_4 rings while circles are due to Si_5O_5 and Si_6O_6 rings.

Attempts to establish the correlation with all the possible parameters failed to establish nearly the same high correlation as Si_8 cages. Table 4.5 summarizes the correlations tested against the ^{29}Si NMR chemical shift.

While this type of correlation may be a useful approach to a physically meaningful rationalization of the up field shift observed in the ^{29}Si NMR spectra of incompletely condensed POSS, the present research shows no apparent correlation. When there are both precise structural and spectral data to make meaningful correlations, then further analysis may be possible.

The scatter of the points of the present correlation study may be due to the errors in determining δ (up to 0.5 ppm)[69] and to some points by the errors caused by averaging the

individual values of Si..Si and Si-O distances and Si-O-Si angles. Another possibility which should not be overlooked is that NMR is a very sensitive method so slight structural change would definitely affect the chemical shift. More likely the change on neighbouring cation affects the chemical shift through its bonding with the shared electrons.

Another alternative to study these chemical shift and geometrical parameter correlation, would be varying a single substituent, while others such as R group and other ligands, remain the same. This is illustrated by Weller et al on $M_8[TO_2]_{12}.X_2$ where T=Si,Al,Ga, Ge, B and Be sodalite framework and X is monovalent or divalent anion.[69] Futhermore, the computational method approach can also offer another alternative for this purpose.

Table 4.5: Summary of correlation test of Si_7 cages

	Parameter	Correlation with	Quality
1.	$r(Si\text{-}O)_{mean}$	chemical shifts $(3:1:3)_{each}$	×,S
2.	$(Si\text{-}O\text{-}Si)_{mean}$	chemical shifts $(3:1:3)_{each}$	×,S
3.	$r(Si..Si)_{mean}$	chemical shifts $(3:1:3)_{each}$	×,S
4.	$(SiO_a, SiO_b, SiO_c)_{mean}$	chemical shifts (3:1:3)	×,S
5.	Regression eqn. 1	$Si..Si_{calc}$ vs $Si..Si_{expt}$	×,S
		δ_{calc} vs. δ_{expt}	×,S
6.	$(Si..Si_a, Si..Si_b, Si..Si_t)_{mean}$	chemical shifts (3:1:3)	×,S

×=poor correlation, S= scatter

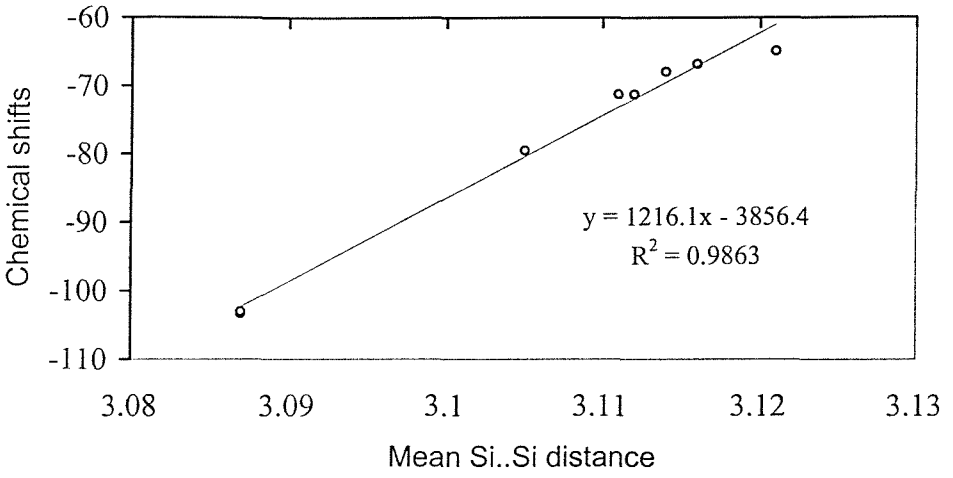

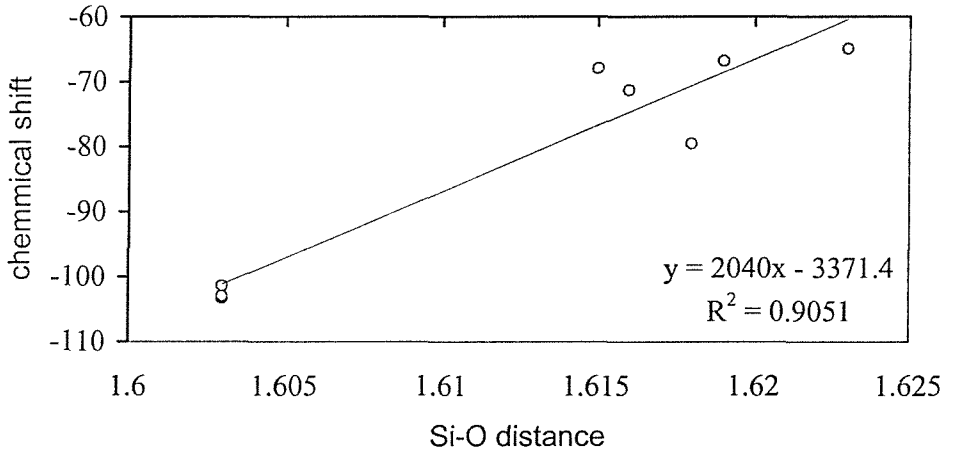

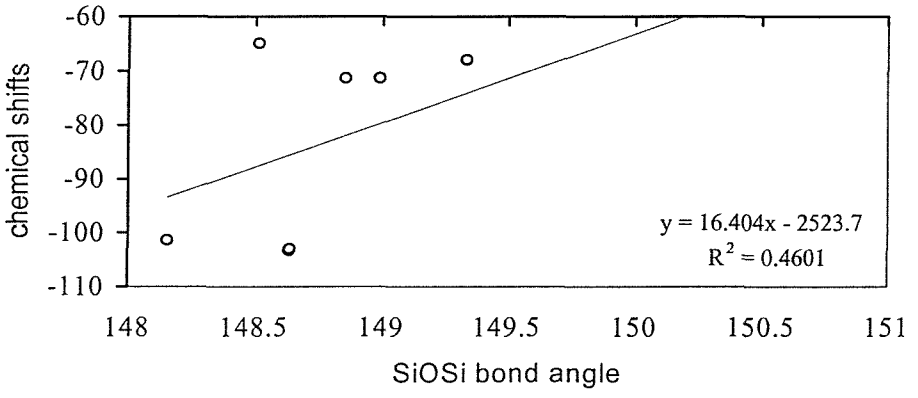

Figure 4.15: Results for correlation between the ^{29}Si NMR chemical shifts and geometric parameters of Si_8 cages.

4.3 Conclusion

The cage structures of silsesquioxanes are as flexible as other silica-oxygen compound and this flexibility is attributed to the ease of deformation of the Si-O-Si angle and the Si-O bonds as testified by the variety of conformation observed with various R groups (Si_8) and substituents (Si_7) at the cage.

1. The range within which individual Si-O and Si..Si atomic distances and Si-O-Si and O-Si-O bond angles vary for silsesquioxane published with R values less or equal 0.10 using X-ray diffraction are as follows;

a). **Si_8 cages**

1.51 Å < d(Si-O) < 1.72 Å*

3.06 Å < d(Si..Si) < 3.16 Å

107° < O-Si-O < 110°

140° < Si-O-Si < 156°

b).**Si_7 cages**

1.57 Å < d(Si-O) < 1.66 Å

3.0 Å < d(Si..Si) < 3.24 Å

101° < O-Si-O < 114°

135° < Si-O-Si < 172°

2. Linear correlation was observed between Si..Si nonbonding distances and Si-O-Si angles both in Si_8 and in Si_7 cages.

3. Attempts to correlate the ^{29}Si NMR chemical shift with any geometric parameters of silsesquioxanes failed to establish good correlation.

4.4 References

1. M. Karplus, *J. Am. Chem. Soc.*, 1963, **85**, 2871.

2. F. H. Allen, S. Bellard, M. D. Brice, B. A. Cartwright, A. Doubleday, H. Higgs, T. Hummelink, B. G. Hummelink-Peters, O. Kennard, W. D. S. Motherwell, J. R. Rodgers and D. G. Watson, *Acta Crystallogr.*, 1979, **B35**, 2331 and reference therein.

3. P. Murray-Rust and J. P. Glusker, *J. Am. Chem. Soc.*, 1984, **106**, 1018.

4. P. Murray-Rust and S. Motherwell, *Acta Crystallogr.*, 1978, **B34**, 2518.

5. F. H. Allen, O. Kennard and R. Taylor, *Acc. Chem. Res.*, 1983, **16**, 146.

6. J. A. K. Howard, R. C. B. Copley, J. W. Yao and F. H. Allen, *Chem. Commun*, 1998, 2175.

7. F. J. Feher and T. A. Budzichowski, *Polyhedron*, 1995, **14**, 3239; M. G. Voronkov and V. I. Lavrent'yev, *Topics in Current Chemistry*, 1982, **102**, 199; P.G. Harrison, *J. Organometal. Chem.*, 1997, **542**, 141.

8. See for example, D. W. Meek and T. J. Mazane, *Acc. Chem. Res.*,1981, **14**, 266., and references therein.

9. F. H. Allen and S. Fortier, *Acta Crystallogr.*, 1993, **B49**, 1021.

10. F. H. Allen, P. R. Raithby, G. P. Shield and R. Taylor, *Chem. Commun.*, 1998, 1043.

11. J. Grimshaw, *PhD. Thesis*, Southampton University, 1999.

12. W. Ries, I. Bernal and M. Quast, T. A. Albright, *Inorg. Chim.Acta.*, 1984, **83**, 5.

13. N. V. Podberezskaya, I. A. Baidina, V. I. Alexeev, S. V. Borisov, T. N. Martynova, *Zh. Strukt. Khim.*, 1981, **22**, 116.

14. V. W. Day, W. G. Klemperer, V. V. Mainz, D. M. Millar, *J. Am. Chem. Soc.*, 1985, **107**, 8262.

15. M. Rattay, D. Fenske, P. Jutzi, *Organomet.*, 1998, **17**, 2930.

16. M. A. Said, H. W. Roesky, C. Rennekamp, M. Andruh, H. G. Schmidt and M. Noltemeyer, *Angew.Chem.,Int.Ed.Engl.*,1999, **38**, 661.

17. R. Tacke, A. Lopez-Mras, W. S. Sheldrick, A. Sebald, *Z. Anorg. Allg. Chem.*, 1993, **619**, 347.

18. G. Calzaferri, R. Imhof and K. W. Tornroos, *J. Chem. Soc., Dalton Trans.*, 1994, 3123.

19. K. Larsson, *Ark. Kemi*, 1960, **16**, 203.

20. G. Koellner and U. Muller, *Acta Crystallogr., (Cr. Str. Comm.)*,1989, **C45**, 1106.

21. V. E. Shklover, Yu. T. Struchkov, N. N. Makarova and K. A. Andrianov, *Zh. Strukt. Khim.*, 1978, **19**, 1107.

22. M. A. Hossain, M. B. Hursthouse and K. M. A. Malik, *Acta Crystallogr.*, 1979, **B35**, 2258.

23. G. Calzaferri, R. Imhof and K. W. Tornroos, *J. Chem. Soc., Dalton Trans.*, 1993, 3741.

24. S. Lucke, K. Stoppek-Langner, B. Krebs and M. Lage, *Z. Anorg. Allg. Chem.*,1997, **623**, 1243.

25. G. Calzaferri, C. Marcolli, R. Imhof and K. W. Tornroos, *J. Chem. Soc., Dalton Trans.*, 1996, 3313.

26. F. J. Feher and T. A. Budzichowski, *J. Organomet. Chem.*, 1989, **373**, 153.

27. I. A. Baidina, N. V. Podberezskaya, V. I. Alexeev, T. N. Martynova, S. V. Borisov and A. N. Kanev, *Zh. Strukt. Khim.*, 1979, **20**, 648.

28. C. Bonhomme, P. Toledano, J. Maquet, J. Livage and L. Bonhomme-Coury, *J. Chem. Soc., Dalton Trans.*, 1997, 1617.

29. U. Dittmar, B. J. Hendan, U. Florke and H. C. Marsmann, *J. Organomet. Chem.*, 1995, **489**,185.

30. F. T. Edelmann, Y. K. Gun'ko, S. Giessmann and F. Olbrich, K. Jacob, *Inorg. Chem.*, 1999, **38**, 2109.

31. F. J. Feher, S. L. Gonzales and J. W. Ziller, *Inorg. Chem.*, 1988, **27**, 3440.

32. R. Duchateau, H. C. L. Abbenhuis, R. A. van Santen, A. Meetsma, S. K. -H. Thiele and M. F. H. van Tol, *Organomet.*, 1998, **17**, 5663.

33. F. J. Feher and R. L. Blanski, *Chem. Commun.*,1990, 1614.

34. H. C. L. Abbenhuis, A. D. Burrows, H. Kooijman, M. Lutz, M. T. Palmer, R. A. van Santen and A. L. Spek, *Chem. Commun.*, 1998, 2627.

35. F. J. Feher and D. A. Newman, *J. Am. Chem. Soc.* ,1990, **112**, 1931.

36. F. J. Feher and J. F. Walzer, *Inorg. Chem.*, 1991, **30**, 1689.

37. T. Maschmeyer, M. C. Klunduk, C. M. Martin, D. S. Shephard, J. M. Thomas and B. F. G. Johnson, *Chem. Commun.*, 1997, 1847.

38. F. J. Feher, S. H. Phillips and J. W. Ziller,1997, *J. Am. Chem. Soc.*, **119**, 3397.

39. F. J. Feher and S. H. Phillips, J. W. Ziller, *Chem. Commun.* ,1997, 829.

40. F. J. Feher and J. F. Walzer, *Inorg. Chem.*, 1990, **29**, 1604.

41. F. J. Feher, D. A. Newman and J. F. Walzer, *J. Am. Chem. Soc.*,,1989, **111**, 1741.

42. T. A. Budzichowski, S. T. Chacon, M. H. Chisholm, F. J. Feher and W. Streib, *J. Am. Chem. Soc.*, 1991, **113**, 689.

43. F. J. Feher, T. A. Budzichowski, K. Rahimian and J. W. Ziller, *J. Am. Chem. Soc.*, 1992, **114**, 3859.

44. F. J. Feher, K. Rahimian, T. A. Budzichowski, J. W. Ziller, *Organomet*, 1995, **14**, 3920.

45. F. J. Feher, *J. Am. Chem. Soc.*, 1986,**108**, 3850.

46. M. H. Chisholm, T. A. Budzichowski, F. J. Feher, J. W. Ziller, *Polyhedron*, 1992, **11**, 1575.

47. W. A. Herrmann, R. Anwander, V. Dufaud and W. Scherer, *Angew. Chem., Int. Ed. Engl.*, 1994, **33**, 1285.

48. F. J. Feher and T. A. Budzichowski and J. W. Ziller, *Inorg. Chem.*, 1997, **36**, 4082.

49. F. J. Feher and T. A. Budzichowski, K. J. Weller, *J. Am. Chem. Soc.*, 1989, **111**, 7288.

50. F. J. Feher and T. A. Budzichowski, *Organomet.*, 1991, **10**, 812.

51. E. Lipmaa, M. Mägi, A. Samoson, G. Engelhardt and A. R. Grimmer, *J. Am. Chem. Soc.*, 1980, **102**, 4889, G. Engelhardt, U. Lohse, E. Lipmaa, M. Tarmak and M. Mägi, *Z. Anorg. Allg. Chem.*, 1981, **482**, 49.

52. P. H. Wei, *Z. Kristallogr.*, 1935, **92**, 355; J. V. Smith, *Acta Crystallogr.*, 1954, **7**, 479.

53. W. Noll, *Angew. Chem. Int. Ed.*, 1963, **2**, 73.

54. G. E. Brown, G. V. Gibbs and P. H. Ribbe, *Amer. Mineral.*, 1969, **54**, 1044.

55. F. Liebau, *Acta Crystallogr.*, 1984, **40A**, C254.

56. H. Gies, *Z. Kristallogr.*, 1984, **167**, 73.; 1983, **164**, 247.

57. H. Gerke and H. Gies, *Z. Kristallogr.*, 1984, 166, 11

58. W. H. Zachariasen and H. A. Plettinger, *Acta. Crystallogr.*, 1965, **18**, 710.

59. R. E. Gibbs., *Proc. Roy. Soc.*, 1926, **113A**, 351.

60. G. I. Golodets, *Heterogeneous Catalytic Reactions Involving Molecular Oxygen*, Elsevier, New York, 1983.

61. F. Liebau, *Structural Chemistry of Silicates*, Springer-Verlag, New York, 1985, p.185.

63. G. E. Brown, G. V. Gibbs and P. H. Ribbe, *Amer. Min.*, 1969, **54**, 1044

64. D. Taylor, *Mineral. Mag.*, 1972, **38**, 629.

65. C. Glidewell, *Inorg. Chim. Acta.*, 1975, **12**, 219.

66. D. W. J. Cruicshanks, *J. Chem. Soc.*, 1961, 5486.

67. J. V. Smith and C. S. Blackwell, *Nature*, 1983, **303**, 223.

68. C. L. Frye and W. T. Collins, *J. Am. Chem. Soc.*, 1970, **92**, 5586.

69. M. T. Weller, S. E. Dann, G. M. Johnson and P. J. Mead in *Progress in Zeolites and Microporous Materials*, H. Chon, S. K. Ihm and Y. S. Uh, Eds., vol 105, Elzevier,1997.

Chapter 5

POSS as the model for silica surface

Chapter Five: POSS as the model for silica surface

5.0 Introduction

Surface hydroxyl groups are the active sites of important heterogeneous catalyst supports such as silica and related solids. The surface chemistry of pure silica is due primarily to the presence of hydroxyl groups on the surface. Undoubtedly, the isolated hydroxyl group of silica, ≡SiOH, is the most studied and best characterised of all the surface objects.[1] The O-H stretching mode ν(O-H) falls at 3747 cm^{-1}, a value believed to be slightly dependent of temperature.[2,3]

One of the approaches in modelling surface hydroxyl group is the cluster approach or a full periodic approach.[4] Before the advent of density functional theory, a minimal size cluster such as H_3SiOH was normally chosen[5] as the simplest model of the isolated hydroxyl group on the silica surface. Even such a limited cluster size can satisfactorily reproduce the frequency of the O-H stretch, together with its anharmonicity. Examination of the data concerning the interaction with small molecules such as H_2O, NH_3 and CO shows that silanol is less acidic than the real hydroxyl group of silica, nonetheless silanol still serves quite well as a model.[6] Interaction of the silanediol molecule, $SiH_2(OH)_2$ with H_2O and NH_3, has also been reported.[4]

Another familiar approach is by adopting a cagelike structure, in particular, in similarity with hydridosilsesquioxanes, $H_8Si_8O_{12}$. The suitability of this structure in mimicking vibrational features[1] and NMR features,[7] both free and when interacting with H_2O of isolated hydroxyl group, ≡SiOH, has been reported. The interaction with NH_3 has also been reported.[8] Because of their defined cage like structures, silsesquioxanes complexes are considered suitable for mimicking silica surfaces.[9] This structures can also be considered as a part of zeolites as well, resembling for instance, the zeolite double-four-ring (D4R).[10]

Several reports in the literature however, have suggested that the type of surface group which participates most effectively in adsorption or reaction with silica surface was the strongly hydrogen bonded surface hydroxyls,[11] which are characterised by a broad band in the infra red region at around 3500 cm^{-1}. Trisilanol, $[Cy_7Si_7O_9(OH)_3]$, and other incompletely condensed POSSs,[9] represent some of the best possible models for this purpose. Besides, experimental results also suggest that the most reactive sites for silica surface may be those possessing three (or more) adjacent siloxy groups.[12]

The salient feature of this group of model compound is the structural similarity between trisilanol and the known SiO_2 polymorphs. A view down the C_3 axis of the vacant vertex of trisilanol bears a close resemblance to the potential co-ordination sites available of β-cristobalite (111) form of SiO_2. Thus, this class of compounds in a way is useful to model the silica surface. Moreover, by virtue of this similarity, it would serve as an excellent model system for many heterogeneous silica supported catalysts. In addition, it could also be used to model the modified silica surfaces as well.

There have been many theoretical studies of the molecular and electronic structures of silsesquioxanes and its precursors. Again, the use of H atoms as the R group, is prominent. Another frequent R group is the OH group.[13] The study of an incompeletely condensed POSS model on the other hand, is new. Experimentally, model systems for studying SiO_2 supported catalytic systems are normally based upon metallasilsesquioxane complexes and $-c\text{-}C_5H_9$, $c\text{-}C_6H_{11}$ and $c\text{-}C_7H_{13}$ as R groups.[14] In this study we had chosen to adopt H as the R group. While the use of OH might be preferable to using H as the "capping group", this substitute would result in systems that are simply too large to be conveniently examined using available computational resources at the desired level of theory.

In the present work, a quantum chemical approach is used to predict the IR vibrational frequencies of the surface hydroxyl groups and surface methoxy species. The structures studied in this work are given in Figure 5.1. The aim is to find out if this small SiO_2 framework is capable of hydrogen bonding because a useful model of silica surface should be capable of hydrogen bonding.

$H_7Si_7O_9$ $(OH)_2(OCH_3)$, **II** and $H_7Si_7O_9(OH)_3$, **III** are hypothetical models of incompletely condensed POSSs. Despite a large volume of work with silsesquioxanes since their discovery in 1946, there are only few examples of incompletely condensed POSSs. Exploration of these systems especially with simpler and well-resolved NMR spectra such as $H_7Si_7O_9(OH)_3$ (and $Me_7Si_7O_9(OH)_3$) would be very desirable although at the moment hindered by lack of efficient and high yield synthetic route of $H_8Si_8O_{12}$.[15] $H_8Si_8O_{12}$ increasing industrial importances as silica coatings for application in the environmental protection, as an interlayer dielectric for integrated circuit,[16] as photoresist[17] and in material technology for SiO_2 film deposition[18] also make it attractive to study.

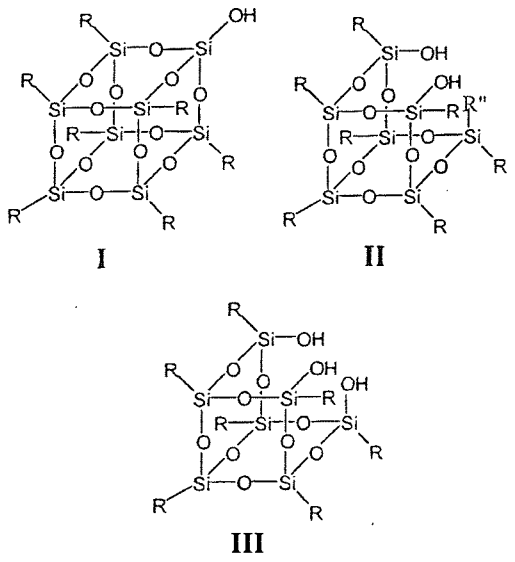

Figure 5.1: Model surface hydroxyl group , R=H, R"=OCH_3

The study of surface methoxy group is of a great interest for catalysis, being suggested as the key intermediates in various reactions of methylation and methanol conversion by various oxides. At room temperature, methanol is physically adsorbed to a surface hydroxyl group, but at higher temperature, chemisorption occurs through the formation of $SiOCH_3$ groups.[19]

Two different forms of chemisorbed methanol on SiO_2 were suggested in the literature. One is believed to occur through esterification of surface hydroxyl group[20]

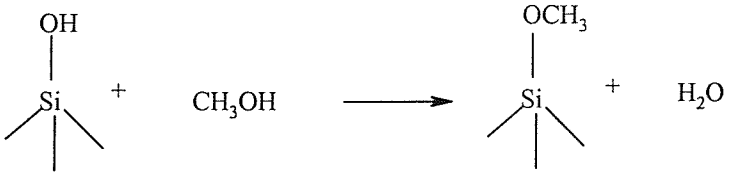

and the other is considered to be formed by methanol dissociating on the strained SiOSi bridge.[21]

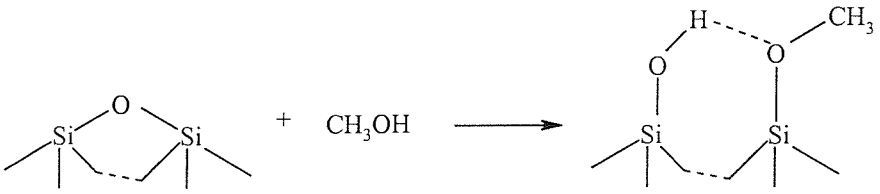

In a recent study, Gates and Papile[22] had treated the MgO with methanol and used the $SiOCH_3$ species as a probe molecule to understand the metal-metal oxide interaction.

$$CH_3I \xrightarrow{Cu/SiO_2\ (673K)} CH_3\text{-}Cu + I\text{-}Cu$$

$$CH_3I \xrightarrow{Cu/SiO_2\ (473K)} CH_3\text{-}Cu + I\text{-}Cu \quad + Si\text{-}OCH_3$$

(5.1)

Spillover of methoxy group onto the supported silica surface forming the $SiOCH_3$ species has also been observed. In the study of the reactions of methyl fragments from methyl iodide dissociation on Cu/SiO_2, Driessen and Grassian,[23,24] reported the formation of $SiOCH_3$ group, [Equation 5.1]. IR data suggested that methyl groups migrate or spillover onto the silica support where they react with the surface hydroxyl group to form $SiOCH_3$. Connor and Falconer[25] have discussed the spillover phenomenon for both atoms and molecular fragments as well as proposed mechanisms for spillover. The importance of spillover in heterogeneous catalysis was also discussed in the paper.

5.1 Computational Details

For the calibration purpose, computations were performed at the HF and the DFT levels adopting the hybrid Becke3 exchange functional and Lee-Yang and Parr correlation functionals,[26,27] (B3LYP) on $H_8Si_8O_{12}$, with O_h point group. Two basis sets were adopted;

i). The standard 6-31G basis set on Si, O, C and H atoms with *d* polarisation functions on silicon and oxygen atoms, and *p* polarisation functions on hydrogen atoms.

ii). The DZP[28] basis set Si, O, and H atoms.

This approach was adopted with the aim of comparing the accuracy of the adopted basis sets, the 6-31G** against the DZP, which is used frequently in the literature.

was first used to generate various stable structures by scanning the low energy portion of PES. This is represented as a function of three dihedral angles; ∠HCOSi (from 0.0 to 360), ∠HOSiH (from 0.0 to 180.0) and ∠COSiH (from 0.0 to 60.0) each with a 30.0 ° increment.

A geometry for the lowest energy conformer generated by the PM3 model was next used as a trial geometry to initiate optimization at the Becke3LYP level. The confirmation test for this lowest energy conformer consists a new round of geometry optimization starting with geometry of the new conformer. If subsequent optimization has the same structure or new structures of higher energy, the search was completed; otherwise the resulting lowest energy was subjected to the same confirmatory test again.

The final lowest energy conformer was then taken to be the most stable Becke3LYP/6-31G** structure for **II.** The verification of the final structure as a minimum on the PES was made by a vibrational frequency calculation that yielded all positive frequencies.

All calculations in this work onward was performed using the Becke-3-LYP level of calculation and the 6-31G* basis set, which were deemed to provide an acceptable compromise between the computational effort required and accuracy of calculated parameters.

Geometry optimizations were performed using the appropriate symmetry group for the others: C_s for $Si_8O_9H_7(OH)$, C_3 for $H_7Si_7O_9$ $(OH)_3$ and the lowest energy conformer, C_1 for $H_7Si_7O_9$ $(OH)_2$ (OCH_3). The calculation of vibrational frequency using the DFT method is facilitated by the availability of the analytical second derivative techniques.

All calculations were performed on Gaussian98 program[30] using a Dell Pentium with a 450 MHz processor computer.

Upon completion of **III**, similar work has also been reported,[31] which will also be discussed alongside with this work.

```
Si1   0    a    -a    -a
Si2   0    a     a    -a
Si3   0    a     a     a
Si4   0   -a     a     a
Si5   0   -a    -a     a
Si6   0   -a    -a    -a
Si7   0   -a     a    -a
O8    0    b    -b     0.
O9    0    b     0.    b
O10   0    b     b     0.
O11   0    b     0.   -b
O12   0    0.   -b    -b
O13   0   -b     0.   -b
O14   0    0.    b    -b
O15   0   -b     b     0.
O16   0    0.    b     b
O17   0   -b     0.    b
O18   0    0.   -b     b
O19   0   -b    -b     0.
H20   0    c    -c    -c
H21   0    c     c    -c
H22   0    c     c     c
H23   0   -c     c     c
H24   0   -c    -c     c
H25   0   -c    -c    -c
H26   0   -c     c    -c
H27   8    d1    1     a1   20    db
H28   9    d1    3     a1   22    db
C29  18    d2    5     a2   24    da
H30  29    d3   18     a1    5    dc
H31  29    d3   18     a1   30    120.0
H32  29    d3   18     a1   31    120.0
       Variables:
a= 1.5555
b=1.85
c=2.3055
d1=0.942122
d2=1.4
d3=1.2
a1=109.47122
a2=114.0
da=120.0
db=0.0 S 6 30.0
dc=0.0 S 2 90.0
```

Table 5.1: Input for the co-ordinates involved in the $H_7Si_7(OH)_2(OCH_3)$, **II**, PES study

5.2 Results and Discussion

5.2.1 Calibration results

A summary of the results for geometry optimization on $Si_8O_{12}H_8$ is given in Table 5.2. For $Si_8O_{12}H_8$, it is possible to compare the calculated geometric data with the experimental results, allowing us to compare the level of accuracy of the calculated values with the experimental data.

Table 5.2: Bond length (in Å) and SiOSi angle (in °) of $H_8Si_8O_{12}$,[32] values in parenthesis are from Törnroos et al[33]

Parameters	Theoretical Methods				Expt.
	HF/6-31G**	HF/DZP	B3lyp/6-31G**	B3lyp/DZP	
Si-O	1.6265	1.6225	1.6443	1.6418	1.659(1.6195)
Si-H	1.453	1.4487	1.4645	1.4581	1.475
O-Si-O	108.97	108.67	109.63	109.39	106.6(109.5)
O-Si-H	108.97	110.26	109.31	109.54	112.2
Si-O-Si	149.40	149.98	148.09	148.56	153.9(147.55)

Several theoretical studies involving this system have also been reported using various basis sets, such as 3-21G*, 6-31G**, DZP, and DZP/TZP(O).[34] As illustrated in Table 5.3, the accuracy of the calculated geometrical data depends very much on the basis set and the method used.

Table 5.3: Si-O distance (in Å) and Si-O-Si angle (in °) for $H_8Si_8O_{12}$, calculated using various basis sets.[34]

Method/ Basis set	HF 3-21G*	HF 6-31G**	HF DZP/TZP(O)	Expt
Si-O	1.644	1.63	1.626	1.619
SiOSi		149.0	150.0	147.5

It should be noted here that the theoretical results were based on the gas phase. At high temperatures and low pressures, intermolecular effects are considered to be minimal. The geometry and the properties of a molecule in crystalline state are different from the respective gas phase. Moreover, the interactions between pairs of molecules, are also affected by the crystalline environment, so the slight variations in the values are expected.

Comparison of the calculated geometry with the experimental values shows that in both sets of calculations, the 6-31G basis set and the DZP basis set give results which are almost within the same range of accuracy. The HF method however, predicted the geometrical data more accurately when compared to the B3LYP method. The Si-O bond was found to be overestimated by about 0.0243 Å and 0.0218 Å using the 6-31G* basis set and the DZP basis set respectively.

The vibrational frequencies of $H_8Si_8O_{12}$ have been investigated in detail by Calzaferri *et. al.*[35,36] The calculated vibrational frequencies using the DZP and the 6-31G** basis sets also seem to indicate that they are almost equal in accuracy, as shown in Figure 5.2 and 5.3. This result also indicates that the 6-31G** basis set would serve as accurate as the DZP basis set. However, in terms of computational cost, the 6-31G** basis set is a better compromise, especially in the study of large systems.

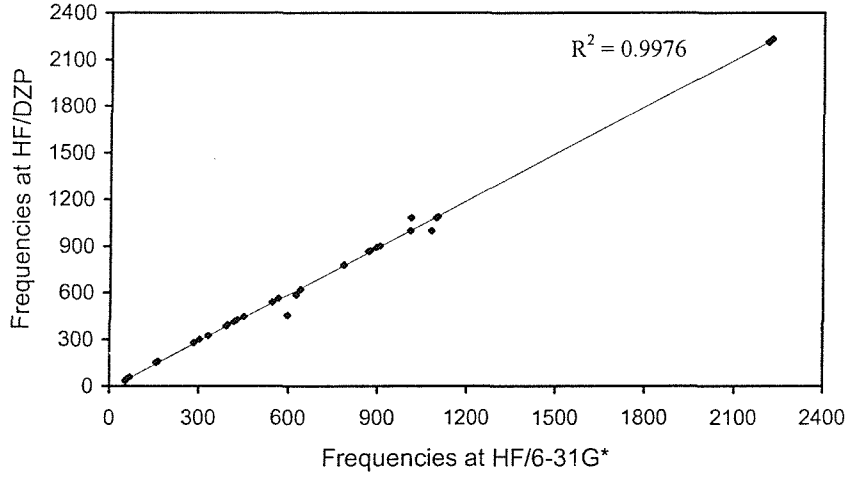

Figure 5.2: Comparing the vibrational frequencies of $H_8Si_8O_{12}$ at HF level

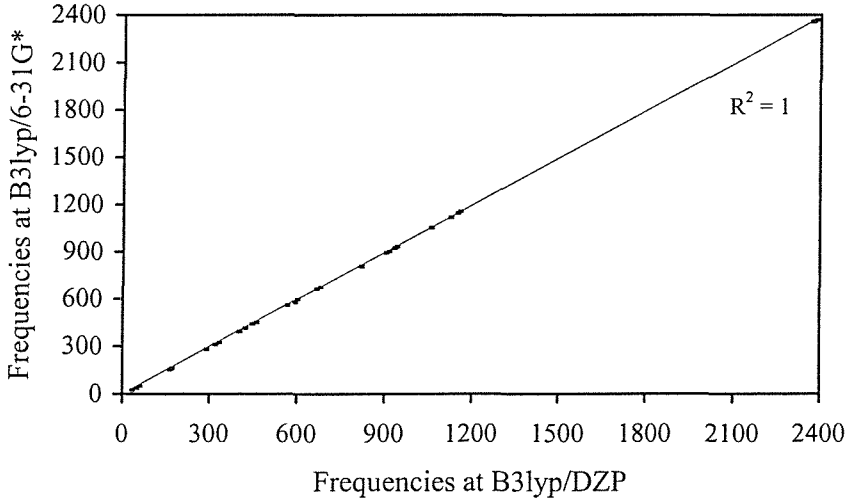

Figure 5.3: Comparing the frequencies of $H_8Si_8O_{12}$ at B3lyp level

The ability of the HF and B3LYP methods using the DZP and 6-31G** basis sets against experimental vibrational frequencies was presented in Table 5.4. All the HF level calculated frequencies however, were scaled to 0.89 as suggested.[37]

Table 5.4: IR active vibrational frequencies (in cm^{-1}) of $Si_8O_{12}H_8$. Modes assignments and vibration types were based on the work Calzaferri *et. al.*[37]

Mode	Theoretical				Experimental	
	HF/631G**	HF/DZP	B3LYP/631G**	B3LYP/DZP	In CCl_4	Type of vibration
T1u	2492.8	2483.3	2361	2372	2277	ν (Si-H)
T1u	1221.7	1230.5	1155.5	1154.5	1141	ν_{as}(Si-O-Si)
T1u	972.5	971.0	893.3	899.6	881	δ(O-Si-H)
T1u	604.6	610.6	559.3	563.5	566	ν(Si-O-Si)
T1u	499.4	504.6	450.2	457.9	465	ν(Si-O-Si)
T1u	439.2	445.9	392.0	398.7	399	δ(O-Si-O)

In general, we found that the accuracies as high as 0.02 Å, 1°-2° and of about 5% off the exact vibrational frequencies, can be expected from this theoretical approach. The fact that the 6-31G** basis set used in the present work is smaller than the DZP basis set (392 basis functions), the use of the 6-31G basis set plus polarization functions on Si, O and H atoms (372 basis functions) would be advantageous, given the overall similarity of the calculated geometry and the vibrational frequencies between the two basis sets.

The HF method provides slightly better accuracy for structural data, but DFT-Becke3LYP method has been reported to yield more reliable energies, and for larger systems, it is the only ab initio technique that can be realistically applied. [38]

A comparison of the CPU timing needed for a single point calculation on several molecules investigated in this work is given in Table 5.5. This work was originated from our initial attempt to study metal-support interactions using theoretical method, with the metal centre being rhodium *gem* dicarbonyl. For comparison on system involving the transition metal, we also reported the timing for $Cy_7Si_7O_{11}(OTMS)(CrO_2)$[39], **A** with Cy_7 groups being replaced by H atoms and the ECP basis set by Wadt and Hay[40] was applied on the Cr atom.

The problem size is measured here in terms of the total number of the basis functions (N) involved in a calculation which itself depends on the system size and the basis set chosen. Timing usually varies depending on the type of the computer on which the computation is performed. All jobs reported were run on a powerful Dell Pentium Pro 250.0 MGB RAM computer, no other job running at the same time as the environment where the job is performed may slow or affect the exact timing.

Table 5.5: ‡ Relative to CPU timing

Structures	$H_7Si_7(OH)_3$ **III**	$H_7Si_7(OH)_2(OCH_3)$ **II**	$Cy_7Si_7O_{11}(OTMS)(CrO_2)$[39]
No. of basis functions	363	388	484
CPU timing(hr:min:sec)	00:43:15	5:16:15	30:56:32
Relative CPU timing‡	1	417	2,498

While structures **II** and **III** are small compared to the available experimental data, to some even this study could be seen as very ambitious. To illustrate this point, we compare the relative CPU timing between structure **III** single point calculation with that of methanol (50 basis functions) and silanol (54 basis functions), Figure 5.5.

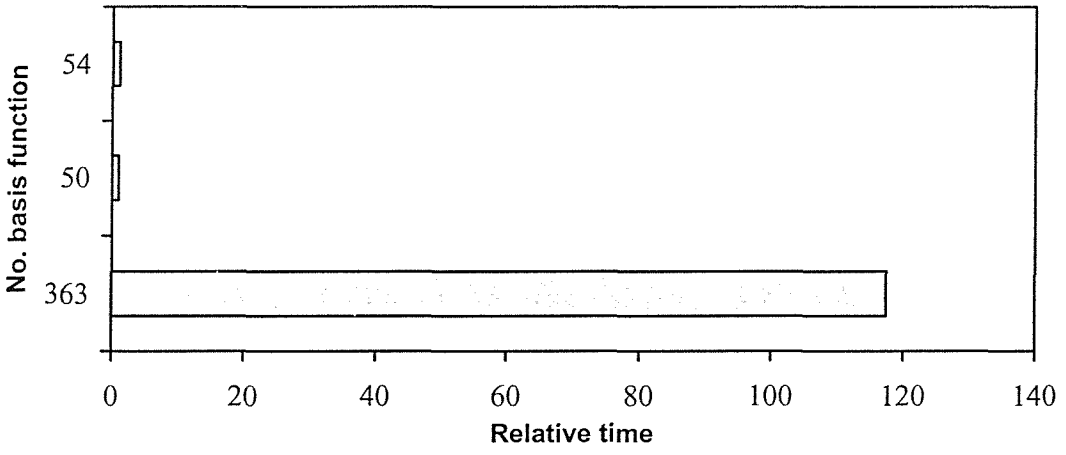

Figure 5.5: Comparison between the basis functions and CPU timing for $H_7Si_7(OH)_3$, **III**, methanol, MeOH, and silanol, SiOH

As can be seen, the CPU time increases rapidly with the problem size. While the substituents involved in this study are on a smaller scale compared to the transition metal complexes usually involve in the real catalytic processes or in the incompletely condensed POSS's, at the moment, the study of such system is limited due to the restricted computer resources.

5.2.2 Potential energy surface study

The result of the PES study on **II** using both the PM3 and the Becke3LYP methods were represented by Figure 5.6 and Figure 5.7. This combination studies indicate that **II** has the lowest energy was when H-Si-O-H dihedral angle is (150.0,120.0°), the H-C-O-Si between 60-90° and the C-O-Si-H dihedral angle is 30.0°.

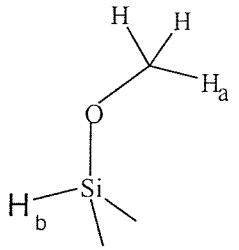

It should be kept in mind however, the structure found in this study does not necessarily represent a global minima, although attempt has been made to avoid local minima structure. The use of the PM3 method and its accuracy in the study of the silica system has been reported earlier for example by Blazkowski and van Santen[41] and Ozturk.[42]

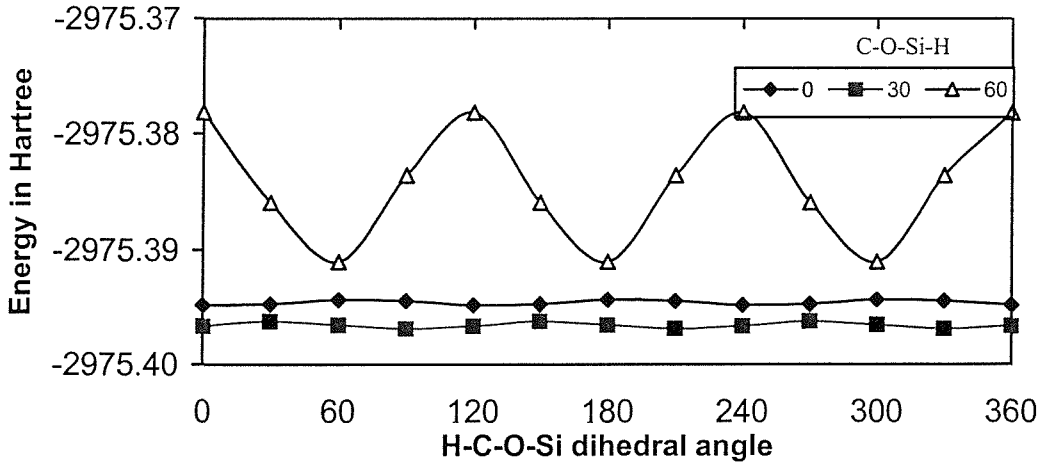

Figure 5.6: Potential Energy surface for $H_7Si_7O_9(OH)_2(OCH_3)$ as a function of H-C-O-Si and C-O-Si-H dihedral angles using the B3LYP method

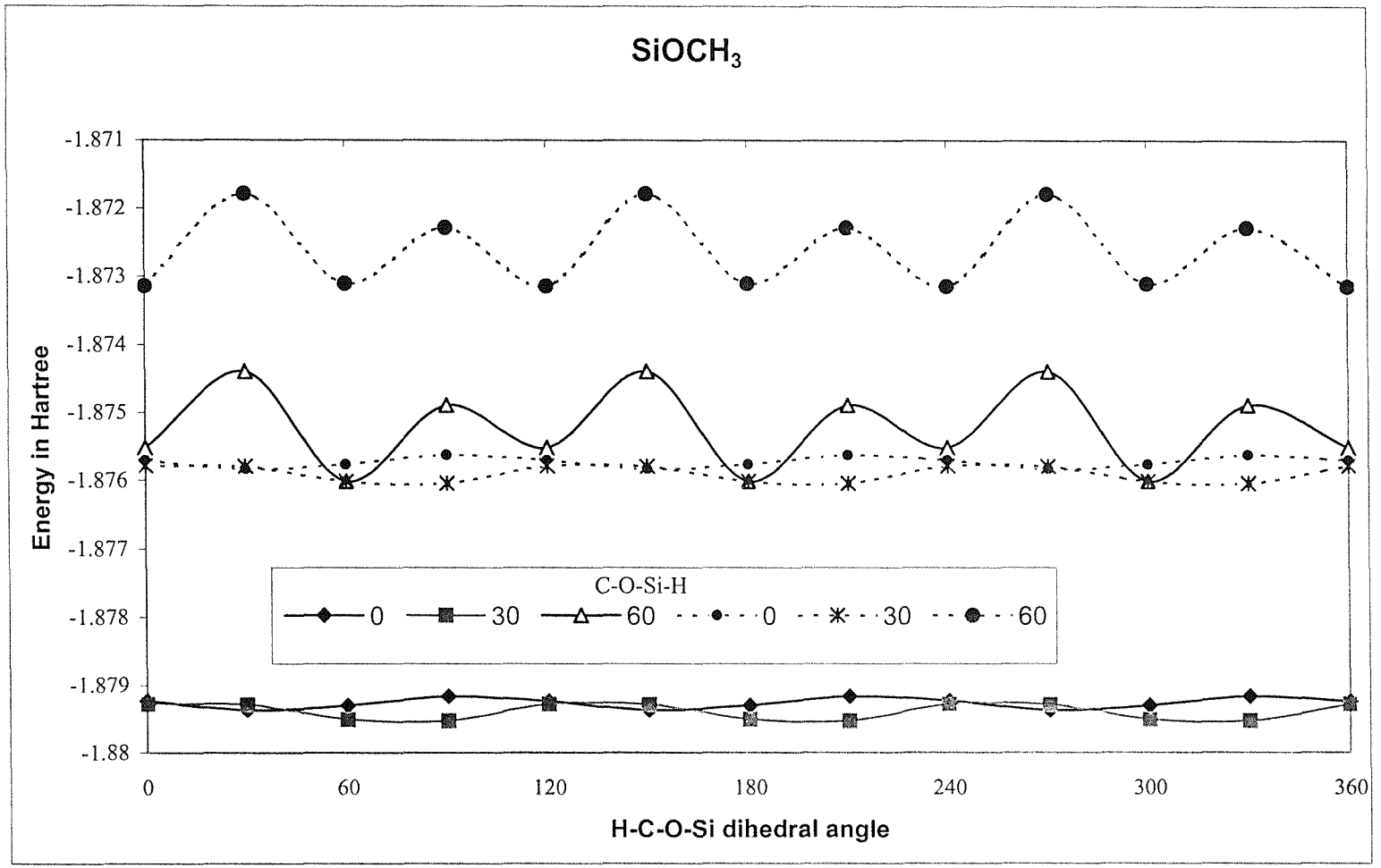

Figure 5.7 : Result of a PES study at PM3 level of II, solid line –∠HOSiH=150,120.0°, broken line- –∠HOSiH=120,120.0° as function of H-C-O-Si and C-O-Si-H dihedral angles

Table 5.6: Geometric parameters calculated using B3LYP calculation for structure I, adopting 6-31G* basis. Distances in Å, angles in °.

Si(1)-O(9)	1.629	Si(1)-O(10)-Si(4)	146.000
Si(1)-O(10)	1.642	Si(7)-O(14)-Si(8)	146.957
Si(1)-O(19)	1.642	Si(3)-O(11)-Si(4)	151.276
Si(1)-O(21)	1.632	Si(3)-O(15)-Si(8)	147.041
Si(2)-O(9)	1.639	Si(5)-O(16)-Si(8)	150.178
Si(2)-O(12)	1.645	Si(4)-O(17)-Si(5)	146.810
Si(2)-O(13)	1.645	Si(5)-O(18)-Si(6)	146.590
Si(3)-O(11)	1.643	Si(1)-O(19)-Si(6)	146.291
Si(3)-O(12)	1.644	Si(6)-O(20)-Si(7)	151.197
Si(3)-O(15)	1.644	Si(1)-O(21)-H(29)	116.959
Si(4)-O(10)	1.643		
Si(4)-O(11)	1.642		
Si(4)-O(17)	1.644		
Si(5)-O(16)	1.642		
Si(5)-O(17)	1.644		
Si(5)-O(18)	1.644		
Si(6)-O(18)	1.645		
Si(6)-O(19)	1.642		
Si(6)-O(20)	1.642		
Si(7)-O(13)	1.644		
Si(7)-O(14)	1.644		
Si(7)-O(20)	1.643		
Si(8)-O(14)	1.644		
Si(8)-O(15)	1.644		
Si(8)-O(16)	1.643		
Si(2)-H(22)	1.463		
Si(3)-H(23)	1.464		
Si(4)-H(24)	1.464		
Si(5)-H(25)	1.464		
Si(6)-H(26)	1.464		
Si(7)-H(27)	1.464		
Si(8)-H(28)	1.464		
O(21)-H(29)	0.963		
Si(2)-O(12)-Si(3)	146.053		
Si(2)-O(13)-Si(7)	146.263		
Si(1)-O(9)-Si(2)	152.335		

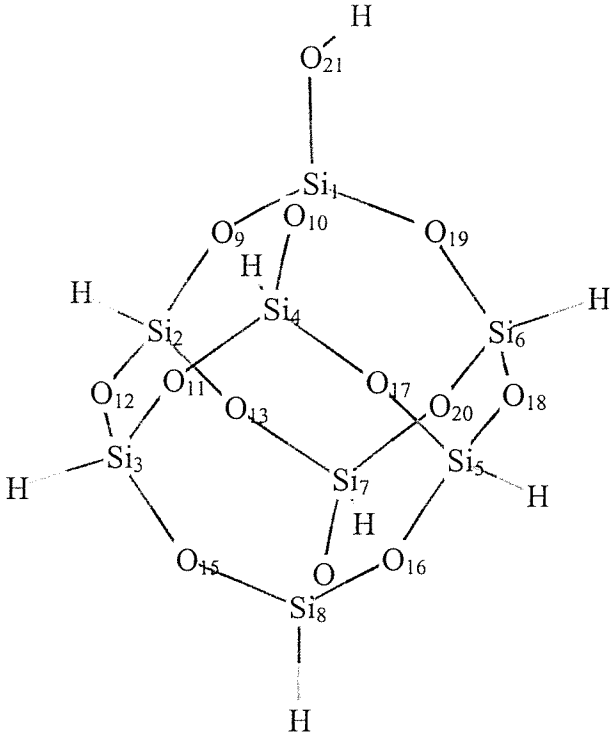

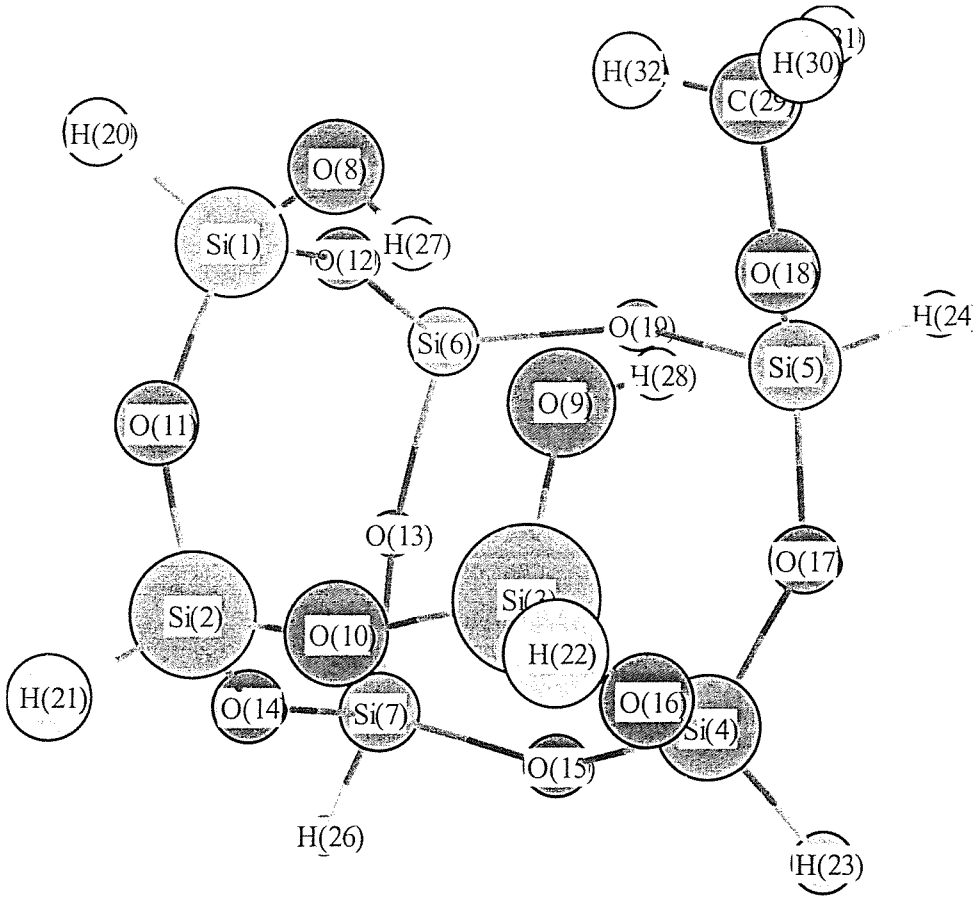

Figure 5.8: Model structure of $H_7Si_7O_9(OH)_2OCH_3$, **II**

Table 5.7: Optimized geometrical parameters of $H_7Si_7(OH)_2OCH_3$ at B3LYP/6-31G** level. Distance in **Å**, angles in °. Refer Figure 5.8 for numbering assignment.

Si(1)-O(8)	1.634	O(11)-Si(2)-O(14)	110.105
Si(1)-O(11)	1.653	O(9)-Si(3)-O(10)	107.998
Si(1)-O(12)	1.653	O(9)-Si(3)-O(16)	108.951
Si(2)-O(10)	1.648	O(9)-Si(3)-H(22)	111.857
Si(2)-O(11)	1.637	O(10)-Si(3)-O(16)	111.112
Si(2)-O(14)	1.647	O(15)-Si(4)-O(16)	110.315
Si(3)-O(9)	1.657	O(15)-Si(4)-O(17)	109.514
Si(3)-O(10)	1.641	O(16)-Si(4)-O(17)	109.091
Si(3)-O(16)	1.648	O(17)-Si(5)-O(18)	105.223
Si(4)-O(15)	1.640	O(17)-Si(5)-O(19)	112.018
Si(4)-O(16)	1.642	O(18)-Si(5)-O(19)	110.444
Si(4)-O(17)	1.648	O(12)-Si(6)-O(13)	110.675
Si(5)-O(17)	1.635	O(12)-Si(6)-O(19)	109.043
Si(5)-O(18)	1.668	O(13)-Si(6)-O(19)	109.304
Si(5)-O(19)	1.637	O(13)-Si(7)-O(14)	110.065
Si(6)-O(12)	1.629	O(13)-Si(7)-O(15)	109.349
Si(6)-O(13)	1.644	O(13)-Si(7)-H(26)	109.197
Si(6)-O(19)	1.650	O(14)-Si(7)-O(15)	109.764
Si(7)-O(13)	1.644	Si(1)-O(8)-H(27)	115.791
Si(7)-O(14)	1.640	Si(3)-O(9)-H(28)	118.713
Si(7)-O(15)	1.646	Si(2)-O(10)-Si(3)	145.803
O(8)-H(27)	0.979	Si(1)-O(11)-Si(2)	147.578
O(9)-H(28)	0.984	Si(1)-O(12)-Si(6)	159.560
O(18)-C(29)	1.440	Si(6)-O(13)-Si(7)	147.049
C(29)-H(30)	1.092	Si(2)-O(14)-Si(7)	147.425
C(29)-H(31)	1.095	Si(4)-O(15)-Si(7)	148.403
C(29)-H(32)	1.093	Si(3)-O(16)-Si(4)	146.726
O(8)-Si(1)-O(11)	111.866	Si(4)-O(17)-Si(5)	148.294
O(8)-Si(1)-O(12)	110.787	Si(5)-O(18)-C(29)	122.093
O(11)-Si(1)-O(12)	107.750	Si(5)-O(19)-Si(6)	150.382
O(10)-Si(2)-O(11)	110.267	O(18)-C(29)-H	107.648
O(10)-Si(2)-O(14)	109.154	H(30)-C(29)-H_{av}	108.591

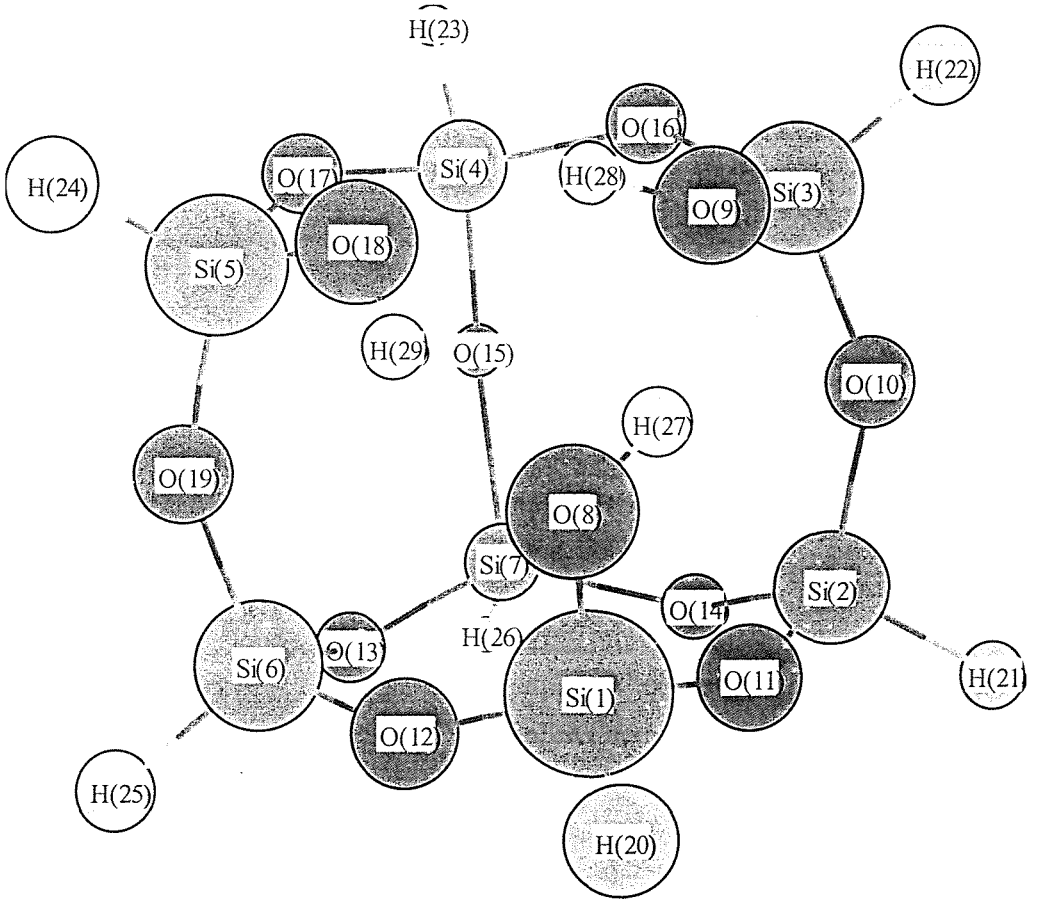

Atoms	Inner frame	Outer frame
Si	1.0651	1.0332
O	–0.6307	–0.6657
H	H –0.1097, -0.105	0.3600

Figure 5.9: Structure of optimized $H_7Si_7O_9(OH)_3$ and Mulliken charge distribution

Table 5.8: Selected geometrical parameters of $H_7Si_7O_9(OH)_3$ **III** optimized at B3lyp/6-31G** level. Distance in Å, angles in °. Refer Figure 5.8 for numbering assignment.

Si(1)-O(8)	1.658	O(9)-Si(3)-O(10)	108.407
Si(1)-O(11)	1.645	O(9)-Si(3)-O(16)	109.024
Si(1)-O(12)	1.643	O(10)-Si(3)-O(16)	110.706
Si(2)-O(10)	1.643	O(15)-Si(4)-O(16)	109.937
Si(2)-O(11)	1.644	O(15)-Si(4)-O(17)	109.558
Si(2)-O(14)	1.643	O(16)-Si(4)-O(17)	109.538
Si(3)-O(9)	1.658	O(17)-Si(5)-O(18)	108.407
Si(3)-O(10)	1.643	O(17)-Si(5)-O(19)	110.705
Si(3)-O(16)	1.645	O(18)-Si(5)-O(19)	109.024
Si(4)-O(15)	1.643	O(12)-Si(6)-O(13)	109.561
Si(4)-O(16)	1.644	O(12)-Si(6)-O(19)	109.542
Si(4)-O(17)	1.643	O(13)-Si(6)-O(19)	109.937
Si(5)-O(17)	1.643	O(13)-Si(7)-O(14)	109.661
Si(5)-O(18)	1.658	O(13)-Si(7)-O(15)	109.662
Si(5)-O(19)	1.645	O(14)-Si(7)-O(15)	109.661
Si(6)-O(12)	1.643	Si(1)-O(8)-H(27)	116.059
Si(6)-O(13)	1.643	Si(3)-O(9)-H(28)	116.053
Si(6)-O(19)	1.644	Si(5)-O(18)-H(29)	116.052
Si(7)-O(13)	1.643	Si(2)-O(10)-Si(3)	148.018
Si(7)-O(14)	1.643	Si(1)-O(11)-Si(2)	149.165
Si(7)-O(15)	1.643	Si(1)-O(12)-Si(6)	148.013
O(8)-H(27)	0.980	Si(6)-O(13)-Si(7)	148.204
O(9)-H(28)	0.980	Si(2)-O(14)-Si(7)	148.204
O(18)-H(29)	0.980	Si(4)-O(15)-Si(7)	148.207
O(8)-Si(1)-O(11)	109.026	Si(3)-O(16)-Si(4)	149.169
O(8)-Si(1)-O(12)	108.409	Si(4)-O(17)-Si(5)	148.018
O(11)-Si(1)-O(12)	110.705	Si(5)-O(19)-Si(6)	149.165
O(10)-Si(2)-O(11)	109.540		
O(10)-Si(2)-O(14)	109.561		
O(11)-Si(2)-O(14)	109.937		

5.2.3 Optimized geometric parameters

Selected optimized geometries of **I, II** and **III** are given in Table 5.6-5.8. Optimized structures of **II** and **III** are presented in Figure 5.8 and 5.9 respectively. The structure of **II** and **III** shows that there is a possibility of hydrogen bonding. This possibility will be discussed separately in the following section.

The B3LYP level is known to overestimate the Si-O and OH bonds, but the trend predicted is consistent with the result for $H_8Si_8O_{12}$ discussed earlier. The geometry optimization on the hypothetical structures of **I-III** at the B3LYP level resulted in an average Si-O distance of 1.645 Å, which is very similar with the Si-O distance in $H_8Si_8O_{12}$ at the same level of treatment.

All three Si-O bonds, attached directly to the OH bonds in **III**, have slightly longer bond length, 1.657 Å, than the rest of the Si-O bonds in the Si-O framework. In **II**, an elongation of Si-O bond directly attached to the methyl group to 1.668 Å was also observed. One of the SiO(H) bond distance is similar to the terminal SiO bond in **III**, while the other is shorter, 1.634 Å. Further bond elongation was observed for C-O bond. The C-O distance is predicted to be 1.44 Å, a slight increase of ~0.03 Å for the C-O distance in the methanol at the same level of treatment.

The Si-H distances in **I, II** and **III**, on the other hand, differ only marginally nor does the CH_3O substituent onto the system seems to change it.

The calculated O-H distance for **I,** 0.963 Å is slightly larger than the experimental value of O-H distance in H_2O, 0.9548 Å[43]. However, this value is smaller than the distance reported by Pereira et al, on series of silica based clusters, which lies between 0.97-1.03 Å[38] The OH distances in both structure **II** and **III**, increases at ~ +0.02 Å.

The Si-O-Si bond angle within the cage is between 148°-149°, which is in agreement with the typical SiO framework. The SiOH bond angles were predicted to be roughly 116.0 ° for both structure **I** and **III**. Two SiOH bond angles were observed for **II**, one is almost 116° and the other one is slightly wider, 118.8°, Table 5.7. The same level of study on silanol, H_3SiOH predicted the angle to be 116.7°. Peri reported an experimental SiOH bond angle on silica was about 113°.[44]

The Si-O-C bond angle was predicted to be 122.1°, slightly smaller than the typical Si-O-C bond angle at the ab initio level of calculation using the 3-21G* basis

set, 124.8° and 123.2° for $(CH_3)_2SiHOCH_3$ and $CH_3SiH_2OCH_3$ respectively but in the correct range.[1]

5.2.4 Hydrogen bonded system

The lengthening and shortening of bonds observed in **II** and **III** which have been discussed earlier can be attributed to the hydrogen bonding and the acceptor/donor relationship within the system.[45] Figure 5.10 shows the possible arrangement of hydrogen bonding of **II** and its Mulliken population charge. The summary of the nonbonding parameters for **II** and **III** is given in Table 5.9.

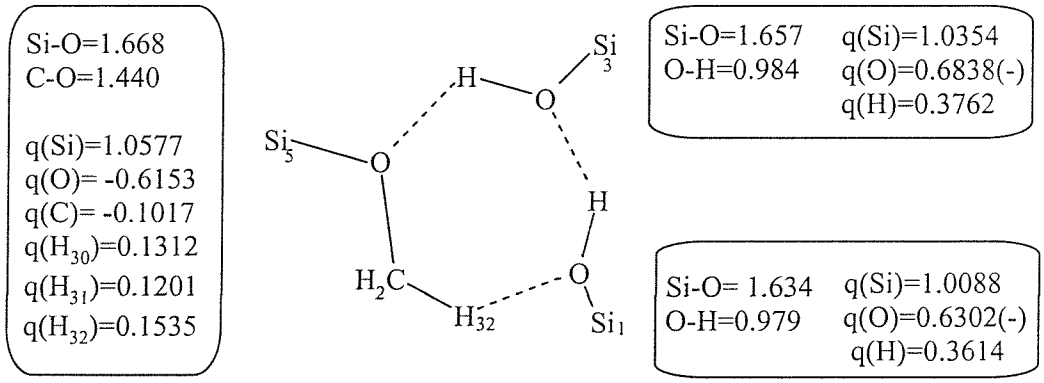

Figure 5.10: Possible hydrogen bonding for structure **II**, and its Mulliken charge distribution, also refer Figure 5.8, distances in Å, charges in a.u.

A long SiO bond of the other neighboring SiOH group, 1.657 Å on the other hand, suggested that the $SiOCH_3$ also acts as a proton acceptor too towards a nearby SiOH group, in agreement with experimental result which suggested $SiOCH_3$ to be involved in two fold hydrogen bonding mechanism.[46]

The CH...O distance, in **II**, is 2.755 Å and the angle is 139.3°. There are many examples of nonbonded interactions of oxygen and CH group in the literature. In nearly all cases, the C-H bond is adjacent to either an electron withdrawing group or some other activating groups (i.e. CN, CO, S and halogen) which serve to influence heavily on the polarization of the CH bond. A weak hydrogen bonding between the

CH group and the oxygen has been attributed to have the role in determining the molecular packing and the conformation in the crystal.[47]

Intramolecular CH..O interactions have also been observed and are believed to be very important in determining the conformational preferences.[48]

A search of the Cambridge Crystallographic Database has been carried out by Taylor and Kennard.[49] Using recognized values for the van der Waals radii of the CH group and the oxygen,[50] they found 59 CH..O contacts of distance at least 0.3 Å less than the sum of the van der Waals radii with CH..O angles greater than 90°. The investigators concluded that the short CH..O contacts, both inter and intramolecular, occurred quite frequently and were likely due to an electrostatic stabilisation, resulting in an attractive rather than a repulsive interaction and could be reasonably described as hydrogen bonding.

These authors also reported that short C-H...C and C-H...H contacts were found to be extremely rare. It was established that (C-H) atoms have a statistically significant tendency (>99.9%) to form short intermolecular contacts to oxygen rather than carbon or hydrogen. [55]

The (H)O...O(H) distances in **II** are 2.785 and 2.729 Å. **III** has three equivalent HO...OH distances of 2.79 Å. These short O..O distances indicate possible of hydrogen bonding for both **II** and **III**. Experimentally, trisilanol is known to crystallize as a strongly hydrogen bonded dimer in the space group of $P\bar{1}$.[9,51] Although the hydrogen bonding protons could not be located in the final difference map, the highly symmetrical nature of the bonding is suggestive of a hydrogen bonding interaction like the one shown in Figure 5.12. The ORTEP plot from a single crystal crystal X-ray diffraction study of trisilanol is shown in Figure 5.11.

Feher *et al* had reported the O..O distances are around 4.03 Å.[43] Inter molecular O..O distances of 2.63-2.64 Å on the other hand, were observed in a dimer system. However, as a monomer, at O..O distance of 4.0 Å, hydrogen bonding is less likely to occur.

Both this work and the recent literature report predicted that as a monomer this hypothetical model of trisilanol would exist as a hydrogen bonded molecule. This work may seem to contradict the experimental result, but it is important to remember that the system study in this work is not only in gas phase but also is a monomer.

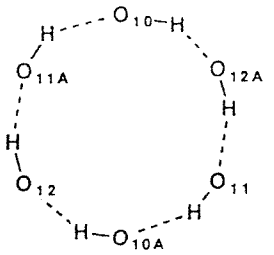

Figure 5.11: Representation of the most probable hydrogen bonding arrangement of trisilanol

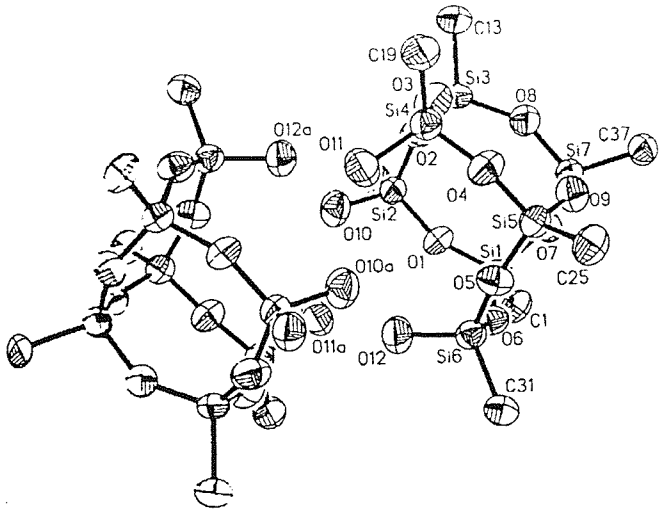

Figure 5.12: ORTEP plot of trisilanol. The molecule crystallises as a hydrogen bonded dimer in the space group $P\bar{1}$

The OH...H distance of 1.889 Å is larger than the mean for O···H distances reported by Ceccarelli and co-workers[52] based on a survey of neutron diffraction geometries of 74 OH···O bonds, 1.818 Å. However, this result is in agreement with Krijnen *et. al.*[31] who reported the OH...H distance of 1.89 Å on a similar model structure **III**, using the DFT-BLYP method and the DZVP2 basis set.

The calculated OH..O angle of **II** was 164.1°. The bonding with OCH_3, i.e. OH..O(C) yielded 164.3°. Ceccarelli and co-workers had reported the mean OH..H angle of 167.1°. The calculated OH..O angles of **III**, however, were found to be 148.1°. These values however, are still in the normal range of hydrogen bonding angles, that is greater than 90.0° and in agreement with the result by Pereira *et al* who reported OH..O angles between 134.8° and 147.2°. Furthermore, Bene and Pople[53] reported the HO..H bond angle of 122°, in a study of water dimer.

Table 5.9: Average nonbonding distances (in Å) and bond angles (in °) for **II** and **III**

Parameters	Theoretical	
	II	**III**
	This work	This work
$O_8..O_9$	2.785	2.79
$O_9..O_{18}$	2.729	2.79
$O_{18}..O_8$	3.909	2.79
$(C)H_{31}..O_8$	2.755	-
OH..O(H)	164.1	148.1(all three)
OH..O(C)	163.2	-
(C)H..O	139.3	-

5.2.5 Charge distribution/transfer

An additional property of considerable interest is the charge distribution as derived from a Mulliken population analysis (see Section 2.5.3). Important charges for [SiOH] and [$SiOCH_3$] groups for **II** and **III** are given in Figure 5.9 and 5.10 respectively.

If we consider that the more positive charge indicates an electron donating group and less means electron accepting, then the most obvious possibility is that $Si_3O_9H_{28}$ is an electron acceptor. Based on electron deficiency in O_{18}, we could say that the $SiOCH_3$ group is an electron donor, which is consistent with the known fact that the methoxy group is an electron donating group. This is also consistent with longer Si-O and C-O bonds observed.

While electron donating, i.e. more positive charges, may result in a weaker bonding, so a longer bond length is observed (as in the $SiOCH_3$ group), the relation in the two SiOH groups contradicts this fact, Figure 5.10. Shorter bond lengths have more positive charges instead and vice versa, are observed for the two SiOH groups.

Another possible explanation would be the SiOH groups act both as donor and acceptor at the same time, a phenomena usually associated as co- operativity effect.

The low charge on Si_1 is quite unusual, but in overall, we could say that the Si_1OH group is the least perturbed of the three terminal groups and perhaps consistent with a weaker hydrogen bonding. (Note: $O_8..O_9$ is 2.789 Å while $O_9..O_{18}$ is 2.729 Å). Apparently, there is an electron donation from the methoxy group through H_{32} to O_8, however, this transfer may be too small to cause any significant increase in total charge for O atom.

For structure **III**, all the three SiOH groups have equivalent charges, Si (1.0333), O (-0.6657) and H (0.3600), which perhaps illustrates and is consistent with the equal hydrogen bonding strength.

Finally, it is important to remember that Mulliken population analysis is arbitrary, while it certainly is the most widely model employed , the Mulliken charge partitioning is also the most criticized.[54]

5.2.6 Vibrational frequency analysis

5.2.6.1 ν(OH) bands

The calculated OH frequencies for **I-III**, are presented in Table 5.11. There is no experimental data on structure **I** but theoretical work on these species has been reported. The ν(OH) was found at 3896 cm^{-1} which is slightly lower than value reported by Ugliengo and co-workers, 3925 cm^{-1}. The harmonic estimate for the experimental isolated ν(OH) for a silica surface was predicted to be 3927 cm^{-1}. Krijnen *et al* , on the other hand, reported a value of 3697 cm^{-1} on **I** using BLYP/DZVP2. It is also important to mention that the latter made no mention of anharmonic values or scaling factor.

However, these authors also proved that the ν(OH) frequencies of **I**, can be attributed to the 3700 cm^{-1} band (isolated) in the zeolite microporous structure while ν(OH) of **III** was assigned to the 3500 cm^{-1} band (hydrogen bonded), based on a combination study of DFT of the above and FTIR data of dealuminated mordenite, a type of dealuminated zeolites. This work also shows that the DFT-B3LYP method is capable to differentiate between the two types of ν(OH)s, isolated and hydrogen bonded. The $\Delta\nu$(OH) bands of **I** and **III**, 299 cm^{-1} are in good agreement with the experimental data of the isolated and hydrogen bonded hydroxyl groups, ~250 cm^{-1}.

Theoretical calculation on **II** predicted the presence of two bands at 3339.9 and 3458.0 cm^{-1} attributed to the H-bonded stretching frequencies. This result is also

in agreement with the infrared data of $Cy_7Si_7O_9(OH)_2(OSnMe_3)$ and $Cy_7Si_7O_9(OH)_2(OTMS)$, recorded in KBr disk [55] which shows a H-bonded OH stretching frequencies at 3450 and 3422 cm^{-1} respectively.

For structure **III**, Krijnen et al reported three bands assigned to the ν(OH) bands at 3403, 3396 and 3331 cm^{-1}. This work however, predicted only a single band at 3460 cm^{-1} attributed to the equivalent environment. This difference may not be able to be proved because hydrogen bonded ν(OH) peak(s) are very broad, so these peaks may not observable at all, experimentally. The single band is consistent with cyclic hydrogen bonding system described by Maes and Smets.[56]

Table 5.11: ν(OH) frequencies and related frequencies for structures **I** to **III**

Structures	ν(OH) (cm^{-1})	Intensity (km/Mole)	O..O distance (Å)	OH distance (Å)
I	3746.6(3896)	106	-	0.963
II	3338.9(3473)	794.8	2.729	0.984
	3458.0(3597)	535.7	2.785	0.979
III	3460.0(3600)	674	2.79	0.980

- scaled at 0.9614, values in parenthesis are the original calculated v(OH)

A sharp increase in intensity of OH bands was also observed in the **II** and **III** compared to **I**. In experimental data, this sharp increase in intensity means very broad absorption band due to hydrogen bonded OH group(s). The two peaks of different intensity in **II**, were most probably due to varying hydrogen bonding strength. The shorter O..O distance in **II** is also consistent with the lower ν(OH) bands, Table 5.11.

5.2.6.2 $\nu(SiOCH_3)$ bands

Table 5.12 shows the vibrational assignment of $SiOCH_3$ bands compared to the reported experimental literature values. The comparison is also made with methanol as experimental data suggested that the $\nu(CH_3)$ of the isolated $SiOCH_3$ surface is about the same as that of $\nu(CH_3)$ of methanol.[23] Pelmenschikov *et al*

Table 5.12: Calculated $\nu(CH_3)$ bands vs. experimental data

	$H_7Si_7O_9(OH)_2(OCH_3)$, **II** B3LYP/6-31G**		Methanol Experimental[1]	Methanol B3LYP/6-1G**		$SiOCH_3$ Spillover[57]	$SiOCH_3$ CH_3OH-SiO_2[23]
	Calc	Scaled		Calc	Scaled		
CH assym stretch	3147	3025	3000	3122	3001	2985	3000
CH assym stretch	3124	3003	2960	3034	2916	2954	2958
CH symm stretch	3042.5	2925	2844	2988	2872	2852	2858
CH_3 deformation	1502 1510 1525	1444, 1452 1466	1477 1455 1477	1499 1508 1527	1441 1450 1468	1462	1464

reported[46] a shift to higher frequencies by about 20 cm^{-1} when compared to the $\nu(CH_3)$ of isolated $SiOCH_3$, [Table 5.12].

Interestingly, experimental data suggested that the $\nu(CH_3)$ bands of the hydrogen bonded $SiOCH_3$, should be shifted towards higher frequencies compared to the isolated $SiOCH_3$ methoxy group by about 20 cm^{-1}. This is believed to be due to the withdrawal of the electrons charge from the CH_3 group.[50] The result of this calculation yielded a shift towards higher wavenumber 24 cm^{-1}, which is consistent with the charge transfer discussed earlier. The predicted bands at 3003 and 2925 cm^{-1} can not be confirmed as they are undistinguishable experimentally due to the broadening of this band.

5.2.7 The method

The utilization of Becke3LYP exchange correlation functions employed in this study has been extensively used in the study of hydrogen bonded clusters. This method has also been tested against HF, MP2 and MP4 methods. (See for instance the work by Nova and Sossa[58], Hagemeister[59] and Mó *et al.*[60]). These authors found that the B3LYP functional predicts H-bonding geometries that are in good agreement with MP2 method which is known for its ability to deal with hydrogen bonding.

The correlated methods, such as MP2 or higher, provide good agreement with experimental result at considerably high computational cost and this restricted their usefulness to a rather small system. DFT method however, provides an alternative to this and significantly shortens the classical procedures and renders a reasonable compromise between accuracy and computational effort.[61] The HF approximation usually reported to inaccurately predict the geometry of hydrogen bonded structure.

5.3 Conclusion

The salient feature of trisilanol is its structural similarity with the known SiO_2 polymorphs. Despite this similarity, experimental data of trisilanol shows it is not capable of hydrogen bonding (intramolecularly), while useful model of silica surface should be capable of hydrogen bonding.

Under the condition tested, i.e. monomer, this theoretical study reported that smaller hypothetical trisilanol is indeed capable of hydrogen bonding. Evidence of hydrogen bonding is supported by

- short O..O distances and OH..H angles are within suggested parameters for hydrogen bonding,
- increase in intensity, which indicate broadness of the bands, a significant mark of hydrogen bonding
- charge distribution
- and lower shift in the ν(OH) frequencies both in the hypothetical trisilanol and that of model methoxylated silica surface.

The method and basis set used, B3LYP/6-31G**, have been tested reliable in predicting hydrogen bonding in numerous literature reports.

The work contained in this chapter helps confirm that trisilanol could be an excellent model of silica surfaces, in addition to offering three active OH sites. However, this work gives valuable insight into the difficulties and factors to consider for future analysis in using trisilanol as the model for silica surfaces.

5.4 References

1. B. Civallerri, E. Garrone and P. Ugliengo, *Chem. Phys. Lett.*, 1998, **294**, 103.

2. P. R. Ryason and B. G. Russell, *J. Phys. Chem.*, 1975, **79**, 1276.

3. L. M. Kustov, V. Y. Borovkov and V. B. Kazansky, *J. Catal.*, 1981, **72**, 149.

4. J. Sauer, P. Ugliengo, E. Garrone and V. R. Saunders, *Chem. Rev.*, 1994, **90**, 2095 and references therein.

5. P. Ugliengo, E. Garrone, *J. Mol. Catal.*, 1989, **54**, 439.

6. J. Sauer, *J. Phys. Chem.*, 1987, **91**, 2315; P. Ugliengo, V. R. Saunders and E. Garrone, *J. Phys. Chem.*, 1989, **93**, 5210; P. Ugliengo, V. R. Saunders and E. Garrone, *Surf. Sci.*, 1989, **224**, 498; P. Ugliengo, V. R. Saunders and E. Garrone , *Chem. Phys. Lett.*, 1990, **169**, 501.

7. B. Civalleri, E. Garrone and P. Ugliengo, *Chem. Phys. Lett.*, 1999, **299**, 443.

8. B. Civalleri, E. Garrone and P. Ugliengo, *Langmuir*, 1999, **15**, 5829.

9. F. J. Feher, D. A. Newman, and F. J. Walzer, *J. Am. Chem. Soc.*, 1989, **111**, 1741.

10. P. G. Harrison, *J. Organometal. Chem.*, 1997, **542**, 141.

11. L. R. Synder and J. W. Ward, *J. Phys. Chem.*, 1968, **70**, 3971; V. Y. Davydov, A. V. Kiselev, L. T. Zhuravlev, *Trans. Faraday Soc.*, 1964, **60**, 2254; D. W. Sindorf and G. E. Maciel, *J. Phys. Chem.*, 1982, **86**, 5208.

12.F. J. Feher, D. A. Newman, *J. Am. Chem. Soc.*, 1990, **112**, 1936.

13. See for example, J. Sauer and J. R. Hill, *Chem. Phys. Lett.*, 1994, **218**, 333.

14. F. J. Feher and D. A. Newman, *Polyhedron*, 1995, **14**, 3241.

15. F .J. Feher and T. A. Budzichowski, *J. Organometal. Chem.*, 1989, **373**, 153.

16. G. Chandra, *Mater. Res. Soc., Symp. Proc.*, 1991, **203**, 97.

17. H. Tosaka, K. Yamaguchi, M. Orihara, N. Ide and K. Otaki, *Jap. Patent*, 1987,**87**, 24,265; *Chem Abstr.*, 1987, **107**: 124570.

18. S. B. Desu, C. H. Peng, T. Shi, and P. Agaskar, *J. Electrochem. Soc.*, 1992, **139**, 2682; M. D. Newman, S. B. Desu, and C. H. Peng, *Chem. Mater.*, 1993, **5**, 1636.

19. K. K. Unger, *Porous Silica*, 2nd ed., Elsevier, Oxford, 1979.

20. E. Borello, A. Zecchina, C. Morterra, *J. Phys. Chem.*, 1967, **71**, 2938; H. P. Boehm, H. Knözinger in *Catalysis- Science and Technology*, J. P. Anderson and M. Bourdart (Eds.) Springer, Berlin, 1983, vol. 4, p. 39.

21. R. S. McDonald, *J. Phys. Chem.*, 1958, **62**, 1175.

22. C. J. Papile and B. C. Gates, *Langmuir*, 1992, **8**,74.

23. M. D. Driessen and V. H. Grassian, *J. Catal.*, 1996, **161**, 810; M. D. Driessen and V. H. Grassian, *Langmuir*, 1995, **11**, 4213. M. D. Driessen and V. H. Grassian, *J. Am. Chem. Soc*, 1997, **119**, 1697.

25. W. C. Connor Jr. and J. L. Falconer, *Chem. Rev.*, 1995, **95**, 765.

26. A. D. Becke, *Phys. Rev. A*, 1988, **38**, 3098 ; A. D. Becke, *J. Chem. Phys*, 1993, **48**, 5648 ; A. D. Becke, *J. Phys. Chem,* 1993, **98,** 1372.

27. C. Lee, W. Yang, R. G. Parr, *Phys. Rev. B*, 1988, **37**, 785.

28. T. H. Dunning Jr., *J. Chem Phys.,* 1989, **90**, 1007.

29. J. J. P. Stewart, *J. Comput. Chem.,* 1989, **10**, 209.

30. Gaussian 98 (Revision A.7), M. J. Frisch, G. W. Trucks, H. B. Schlegel,G. E. Scuseria, M. A. Robb, J. R. Cheeseman, V. G. Zakrzewski, J. A. Montgomery, R. E. Stratmann, J. C. Burant, S. Dapprich, J. M. Millam, A. D. Daniels, K. N. Kudin, M. C. Strain, O. Farkas, J. Tomasi, V. Barone, M. Cossi, R. Cammi, B. Mennucci, C. Pomelli, C. Adamo, S. Clifford, J. Ochterski, G. A. Petersson, P. Y. Ayala, Q. Cui, K. Morokuma, D. K. Malick, A. D. Rabuck, K. Raghavachari, J. B. Foresman, J. Cioslowski, J. V. Ortiz, B. B. Stefanov, G. Liu, A. Liashenko, P. Piskorz, I. Komaromi, R. Gomperts, R. L. Martin, D. J. Fox, T. Keith, M. A. Al-Laham, C. Y. Peng, A. Nanayakkara, C. Gonzalez, M. Challacombe, P. M. W. Gill, B. G. Johnson, W. Chen, M. W. Wong, J. L. Andres, M. Head-Gordon, E. S. Replogle and J. A. Pople, Gaussian, Inc., Pittsburgh PA, 1998.

31. S. Krijnen, R. J. Harmsen, H. C. L. Abbenhuis, J. H. C. Van Hoof and R. A. van Santen, *Chem. Commun.*, 1999, 501.

32. K. Larson, *Ark. Kemi.*, 1960, **16**, 215.

33. T. P. E. Auf der Heyde, H-B Bürgi, H. Bürgi and K. Törnroos, *Chimia*, 1991, **45**, 38.

34. J. R. Hill and J. Sauer, *J. Phys. Chem.*, 1994, **98**, 1238.

35. P. Bornhauser, G. Calzaferri, *Spectrochim. Acta*, 1990, **46A**, 1045..

36. C. Marcolli, P. Lainé, P. Bornhauser, G. Calzaferri, and J. Tomkinson, *J. Phys. Chem. B*, 1997, **101**, 1177.

37. J. B. Foresman and Æ. Frisch in *Exploring Chemistry with Electronic Structure Methods*, 2nd ed., Gaussian Inc., Pittsburgh, 1996.

38. J. C. G. Pereira, C. R. A. Catlow, and G. D. Price, *J. Phys. Chem. A.*, 1999, **103**, 3252.

39. F. J. Feher and R. L. Blanski, *Chem. Commun.*,1990, 1614.

40. P. J. Hay and W. R. Wadt, *J. Chem. Phys.*, 1985, **82**, 270,284,299.

41. S. R. Blazkowski, R. A. van Santen, *J. Phys. Chem.*, 1995, **99**, 11728

42. S. Ozturk, I. Onal, and S. Senkan, *Ind. Eng. Chem. Res.*, 2000, **39**, 250.

43. G. W. C. Kaye, and T. H. Laby, Eds, *Tables of Physical and Chemical Constants*, 14th ed, Longman , London, 1973.

44. J. B. Peri, *J. Phys. Chem.*, 1966, **70**, 2937.

45. P. Ugliengo, A. Bleiber, E. Garrone, J. Sauer and A. M. Ferrari, *Chem. Phys. Lett.*, 1992, **191**, 537.

46. A. G. Pelmenschikov, G. Morosi, A. Gamba, *in Proceedings of the 9th International Conference*, Montreal, 1992, R. von Ballmoos, J. B. Higgins, M. M. J. Tracey, Eds., Butterworth-Heinemann, London, 1993, p. 537.

47. see for example J. Sarma and G. Desiraju, *Acc. Chem. Res.*, 1986, **19**, 222.

48. S. Zushi, Y. Kodama, K. Nishibata, K. Umemura, M. Nishio, J. Uzawa and M. Hirota, *Bull. Chem. Soc. Jpn.*, 1980, **53**, 3631 and references therein.

49. R. Taylor, O. Kennard, *J. Am. Chem. Soc.*, 1982, **104**, 5063.

50. A. Bondi, *J. Phys. Chem.*, 1964, **68**, 441.

51. J. F. Brown Jr. and L. H. Vogt Jr., *J. Am. Chem. Soc.*, 1965, **87**, 4313.

52. C.Ceccarelli, G.A.Jeffrey, R.Taylor, *J.Mol. Struct.*, 1981, **70**, 255.

53. J. E. Del Bene, J. A. Pople, *J. Chem. Phys.*, 1970, **52**, 4858.

54. K. B. Wiberg and J. J. Wendoloski, *J. Phys. Chem.*, 1984, **88**,586.

55. J. G. Grimshaw, *PhD Thesis*, Southampton University, 1999.

56. G. Maes and J. Smets, *J. Phys. Chem.*, 1993, **97**, 1818.

57. M. D. Driessen and V. H. Grassian, *Langmuir*, 1995, **11**, 4213.

58. J. J. Nova and C. Sossa, *J. Phys. Chem.*, 1995, **99**, 15837.

59. F. C. Hagemeister, C. J. Gruenloh and T. S. Zwier, *J. Phys. Chem.*, 1998, **102**, 82.

60. O. Mó, M. Yánez, J. Elguero, *J. Chem. Phys.*, 1997, **107**, 3592.

61. M. Lozynski, D. Ruzinska Roszak and H. G. Mack, *J. Phys. Chem. A.*, 1998, **102**, 2899.